DEVELOPMENT OF WELLBORE SIMULATOR FOR BETTER UNDERSTANDING OIL WELL CEMENT BEHAVIOR AND GAS MIGRATION DURING EARLY GELATION

by

Zichang Li

B.S., Tsinghua University, Beijing, China, 2008

M.S., Tsinghua University, Beijing, China, 2010

Submitted to the Graduate Faculty of

Swanson School of Engineering in partial fulfillment

of the requirements for the degree of

Doctor of Philosophy

University of Pittsburgh

2015

UNIVERSITY OF PITTSBURGH

SWANSON SCHOOL OF ENGINEERING

This dissertation was presented

by

Zichang Li

It was defended on

July 8th, 2015

and approved by

Anthony T. Iannacchione, Ph.D., Associate Professor, Department of Civil and Environmental Engineering, University of Pittsburgh

John C. Brigham, Ph.D., Assistant Professor, Department of Civil and Environmental Engineering, University of Pittsburgh

Barbara G. Kutchko, Ph.D., Senior Research Scientist, National Energy Technology Laboratory, U.S. Department of Energy

Dissertation Director: Julie M. Vandenbossche, Ph.D., Associate Professor, Department of Civil and Environmental Engineering, University of Pittsburgh

DEVELOPMENT OF WELLBORE SIMULATOR FOR BETTER UNDERSTANDING OIL WELL CEMENT BEHAVIOR AND GAS MIGRATION DURING EARLY GELATION

Zichang Li, Ph.D.

University of Pittsburgh, 2015

Gases can migrate into the cemented annulus of a wellbore during early hydration when hydrostatic pressure within the cement slurry declines. Different means to describe hydrostatic pressure reduction have been proposed and reported in the literature. Among them, static gel strength (SGS) is the most-widely accepted concept in describing the strength development of hydrating cement. The classic shear stress theory proposed by Sabins et al. (1982) employs SGS to quantify the hydrostatic pressure reduction. API Standard 65-2 provides a standard for determining the transition time using the concept of SGS. Current industry practice is to reduce the transition time, thereby lowering the potential for invading gas introducing migration pathways in the cemented annulus. This approach, while certainly helpful in reducing the risk of gas migration, does not eliminate its occurrence. A better means to characterize cement matrix strength using fundamental concepts for replacing SGS is desired.

In this study, an enhanced wellbore simulation chamber (WSC) is developed to simulate hydrostatic pressure reduction in the cemented annulus and possible gas invasion under representative borehole conditions. In addition to the device itself, specific casting and testing protocols have been developed, which detail the procedures required for proper operation of the apparatus. The WSC makes adjustments to the existing cement hydration analyzers by providing

representative wellbore conditions, which accounts for rock formation, real-scale wellbore section, and varying overburden pressure.

The results from the simulations ran using the WSC are quite revealing. The wellbore cross-sections from the WSC simulations show the porous cement that resulted in localized regions from pressurized fluids as well as gas channeling during cement gelation. The effects of different factors on hydrostatic pressure reduction are also investigated, including: formation permeability, initial overburden pressure, wellbore temperature, water-cement ratio, cement composition, and $CaCl_2$-based accelerator. Experimental results verify that shortening transition time cannot change the occurrence of gas migration, as the microstructural development for the same slurry may be identical although the hydration occurs at different rate. The introduction of fundamental concepts in analysis provides the opportunity to parameterize slurry designs and other important factors associated with wellbore conditions.

TABLE OF CONTENTS

LIST OF TABLES

LIST OF FIGURES

NOMENCLATURE

Symbol	Explanation
Ambient T.	Ambient temperature
API	American Petroleum Institute
BWOC	by weight of cement
C_2S	dicalcium silicate
C_3A	tricalcium aluminate
C_3S	tricalcium silicate
C_4AF	tetracalicium alumino-ferrite
$CaCl_2$	calcium chloride
$CaCl_2$•2H2O	calcium chloride dihydrate
CHA	cement hydration analyzer
CHP	critical hydration period
Cmt T.	cement slurry temperature
CSGS	critical static gel strength
CWSS	critical wall shear stress
ESEM	environmental scanning electron microscope
EIA	U.S. Energy Information Administration
FPF	flow potential factor

KCl	potassium chloride
NaCl	sodium chloride
SCP	sustained casing pressure
SEM	scanning electron microscope
SGS	static gel strength
OBP	overburden pressure
OPC	ordinary Portland cement
OSGS	optimal static gel strength
OWC	oil well cement
PA DEP	Pennsylvania Department of Environmental Protection
$P_c(\alpha)$	capillary porosity at degree of hydration of α
Pore P.	pore pressure
ppg	pound per gallon
PSD	particle size distribution
SCM	supplementary cementitious materials
SRN	slurry response number
w/c ratio	water-cement ratio
WSC	wellbore simulation chamber
α	degree of hydration

ACKNOWLEDGEMENTS

I would like to first express my appreciation and sincere gratitude to my research supervisor Professor Julie M. Vandenbossche for her consistent support through my PhD study at the University of Pittsburgh. Her invaluable guidance and inspiration helped me grow confidence and develop both academically and personally. My thanks also owe to other faculty members on my committee, Professor Anthony T. Iannacchione, Professor John C. Brigham as well as Dr. Barbara G. Kutchko from NETL, Department of Energy. Without the inspiration, encouragement, and guidance from them, it would not have been possible for me to accomplish this dissertation.

I would like to thank my family for their constant love, understanding and support in my life. My parents have always been a great encouragement for this great achievement. In particular, I would like to thank my wife and her family for making my life colorful and enjoyable in Pittsburgh.

I would like to thank Professor Donald Janssen from the University of Washington, Seattle for providing the experimental devices and the idea to develop a simulator for this study. I would like to acknowledge the input of Mr. Charles C. Hager for his tips and assistance in the laboratory. Special thanks are owed to my fellow graduate student, Mr. Alexander S. Vuotto, and undergraduate student, Mr. Nathan D. Bech, who devoted their time in helping conduct the laboratory experiment. I also would like to extend my appreciation to my other fellow graduate

students for making my research life much easier, including Mr. Matthew J. Grasinger, Ms. Nicole Dufalla, Dr. Feng Mu, Dr. Manik Barman, Mr. Kevin Alland, Mr. Steven G. Sachs, and Mr. John DeSantis.

Special thanks are also due to the Department of Civil and Environmental Engineering at the University of Pittsburgh, including Faculty, Staff, Technicians, Secretaries, and Personnel, who contributed directly or indirectly to the accomplishments of this work. The Swanson School of Engineering (SSOE) Center for Energy, University of Pittsburgh is acknowledged for their continued support of this research effort.

Last, but not lease, I gratefully acknowledge financial support from the Department of Energy (NETL Regional University Alliance). Specific acknowledgments are also owed to Mr. Seth Pelepko and Mr. Eugene Pine from the Pennsylvania Department of Environmental Protection as well as Shell, Halliburton, Schlumberger, Lafarge, U.S. Steel for natural gas well pad tours, insightful meetings, and the donation of materials.

I DEDICATE THIS DISSERTATION TO MY FAMILY MEMBERS.

1.0 INTRODUCTION

1.1 BACKGROUND AND MOTIVAITION

Gases can migrate into the cemented annulus of a wellbore during early hydration when hydrostatic pressure within the cement slurry declines below that of a formation gas or fluid (Bonett and Pafitis 1996). Different means to describe hydrostatic pressure reduction have been proposed and reported in literature (Harton et al. 1983; Sutton et al. 1984a, 1984b; Bannister and Lawson 1985; Sykes and Logan 1987; Jones and Carpenter 1991; Zhou and Wojtanowicz 2000). Among them, the classic shear stress theory is most-widely accepted to explain the mechanism of hydrostatic pressure reduction in the cement column (Sutton et al. 1984a, 1984b). In the classic shear stress theory, hydrostatic pressure reduction was derived as a function of static gel strength (SGS), which describes the strength development of hydrating cement (Mueller 2002). However, experimental results (Zhang 2002; Zhu et al. 2012) demonstrate that no simple relationship between SGS and hydrostatic pressure reduction can be found. Approaches, derived from the concept of SGS, such as flow potential factor (FPF) (Sutton et al. 1984a, 1984b), critical wall shear stress (CWSS) (Stiles 1997) and slurry response number (SRN) (Sutton and Ravi 1989; Harris et al. 1990), have contributed to better understanding mechanisms of gas migration and means to minimize it. Unfortunately, these approaches do not accurately predict gas migration.

While SGS was originally adopted to describe the shear stress at cement-formation and cement-casing interfaces, it has also been used to estimate the shear resistance required to deform slurry during the hydration period. Prior to early hydration, the hydrostatic pressure will overcome the formation gas pressure and prevent gases from invading the cement column. As hydration progresses, the cement develops sufficient rigidity to withstand the gas invasion. This critical hydration period is defined as the *transition time* (Sabins et al. 1982; Mueller 2002). API Standard 65-2 provides guidelines for determining the transition time using the concept of SGS (API 2010a). Current industry practice is to minimize the transition time, thereby lowering the potential for invading gas that may introduce migration pathways within the cemented annulus. This approach, while certainly helpful in reducing the risk for gas migration, does not eliminate its occurrence. Characteristics of the transition time end-points depend on slurry properties and downhole conditions. Moreover, SGS is not able to characterize the gas-tight property of a cement slurry (Beirute and Cheung 1990).

When cement slurry gels, the mechanical properties are governed by its growing solid fraction (hydration products). The gel can deform under shear loading, but gases and other fluids will need to break, or fracture, the bond between solids and push them aside for pathways to form within the cement matrix domain at this point. To fully understand this process, the bond strength between solid particles and the compressibility of the cement matrix are needed. The bond strength between solid hydration products and compressibility of the solid matrix are mechanical properties based on the changing rigidity of the cement during the gelation stage. However, SGS does not address these important properties, and therefore, SGS is limited in its ability to predict gas migration potential. A better means to characterize the development of cement matrix strength using fundamental concepts and variables for replacing SGS is desired.

1.2 RESEARCH OBJECTIVE AND SCOPE

An enhanced wellbore simulation chamber (WSC) is developed under the present study to achieve a better understanding of the physical behavior of cement slurries subjected to the wellbore conditions. This includes the hydrostatic pressure reduction in the cement column, and to investigate the important mechanisms that affect the mechanical properties of the cement, as well as the mechanisms of gas migration under imbalanced pressure conditions. The improvements over commercial cement hydration analyzers (CHAs) includes: 1.) simulation of rock formation, 2.) real-scale wellbore section, 3.) varying effective overburden pressure representing the depth of interest, and 4.) wellbore permeability measurement under simulated in-situ conditions.

The present study also undertakes the task of verifying the hypothesis of using fundamental properties of cement hydration to characterize the bulk property of cement slurries in the borehole. Degree of hydration is introduced to describe the hydrostatic pressure reduction in the cemented annulus during early hydration. Capillary porosity is used to analyze the void volume development in the cement matrix domain with respect to degree of hydration. The knowledge thus gained could ultimately allow the development of parameterizing slurry designs and borehole conditions for quantifying hydrostatic pressure reduction when the cement gels in the wellbore, leading both to economic and ecological benefits.

The specific objectives of this study are provided below:

(1) Evaluate state-of-art practices for evaluating the potential for gas migration and develop theoretical foundation and research needs;

(2) Develop an enhanced wellbore simulation apparatus for performing an experimental study;

(3) Simulate cement hydration under representative wellbore conditions;

(4) Simulate the physical process of gas invasion and the topology of defected cemented annulus under pressurized gases and other fluids;

(5) Investigate the effects of different cement and wellbore factors on the hydrostatic pressure reduction;

(6) Experimentally verify the feasibility of using fundamental concepts to characterize the evolution of hydrostatic pressure reduction in the cemented annulus during critical hydration period.

1.3 ORGANIZATION OF DISSERTATION

This dissertation has been divided into five chapters. The concise description of the contents of each chapter is provided below.

In Chapter 2, the basic concept of controlling transition time and other approaches developed to evaluate the potential for gas migration are discussed. This chapter provides a review on the gas-control theories and identifies future research directions and technology development needs.

Chapter 3 is divided into two parts. The first part summarizes the history of the CHAs used to characterize the cement behavior in the wellbore and investigate the mechanisms of gas migration and hydrostatic pressure reduction in the cemented annulus. The second part presents a detailed description of the newly-developed laboratory-scale WSC, including the device design, the protocol developed for casting the artificial formation lining the wellbore and the operational procedure for the WSC. WSC results from calibration tests verify the capability of

the WSC in simulating cement behavior under the representative wellbore conditions and the advantages of the WSC over the existing CHAs.

In Chapter 4, the results of WSC experiments are discussed. The physical phenomena of gas migration during cement gelation are investigated. The effects of different factors on slurry pore pressure are also studied, including: formation permeability, initial overburden pressure, wellbore temperature, water-cement (w/c) ratio, cement composition, and $CaCl_2$-based accelerator. The WSC results experimentally verify the hypothesis of characterizing the bulk properties of hydrating cement using fundamental concepts, such as degree of hydration.

Chapter 5 presents the main conclusions drawn from the present study. A few recommendations for future research have also been formulated.

2.0 THEORY-BASED REVIEW OF LIMITATIONS WITH STATIC GEL STRENGTH IN CEMENT MATRIX CHARACTERIZATION

The concept of controlling transition time and other approaches developed to evaluate the potential for gas migration help improve the slurry design and cementing practice, but cannot eliminate gas migration. Cement gel can deform under shear loading, but gases and other fluids will need to break, or fracture, the bond between solids and push them aside for pathways to form within the cement matrix domain during early hydration. To fully understand this process, the bond strength between solid particles and the compressibility of the cement matrix are needed. SGS does not address these important properties, and therefore, is limited in its ability to predict gas migration potential. This chapter summarizes research activities associated with an investigation into SGS and provides a discussion on the limitations of SGS for characterizing slurry properties with respect to preventing gas migration.

2.1 INTRODUCTION

Casing support and zonal isolation are the two principal objectives of primary cementing (Bonett and Pafitis 1996). However, achieving zonal isolation usually poses the greatest challenge, as it is difficult to predict when the potential for formation gas to migrate into cement sheath exists. “Gas migration,” “gas invasion,” “annular gas flow,” “gas leakage” and “gas channeling” are all

synonymous terms used to describe gas entry into cemented annular spaces. Historical practice strongly suggests that gas migration, vent flows, etc., prior to, during or after cementing, can have serious consequences, such as severe injuries and environmental pollution (Goodwin and Crook 1992; Jackson and Murphey 1993; Wojtanowicz et al. 2001; Bellabarba et al. 2008; Kutchko 2008; Harrison 1985). Recently, gas migration occurrences have attracted more public attention due to the rapid onshore exploitation of shale gas. In addition, incidents continue to occur even with significant improvements in well construction practices. Examples include the fresh water contamination in Wyoming (EPA 2011), and stray gas migration in Pennsylvania (PA DEP 2009; Reese et al. 2014). A recent Canadian study (Dusseault et al. 2014) shows that environmental issues associated with wellbore gas migration have been found throughout Canada as well. In particular, signs of stray gas exist in 75% of the gas wells in the Western Canada Sedimentary Basin (Rowe and Muehlenbachs 1999; Muehlenbachs 2012; Tilley and Muehlenbachs 2013). Statistical data shows that 25% of failures of primary cement jobs are the result of gas migration (Gonzalo 2001). Drilling practices in Northeast Pennsylvania indicate that stray gas primarily comes from non-target gas-bearing formations, not reservoirs. Figure 2.1 shows the presence of gas-bearing formations throughout the depth of a few selected wells.

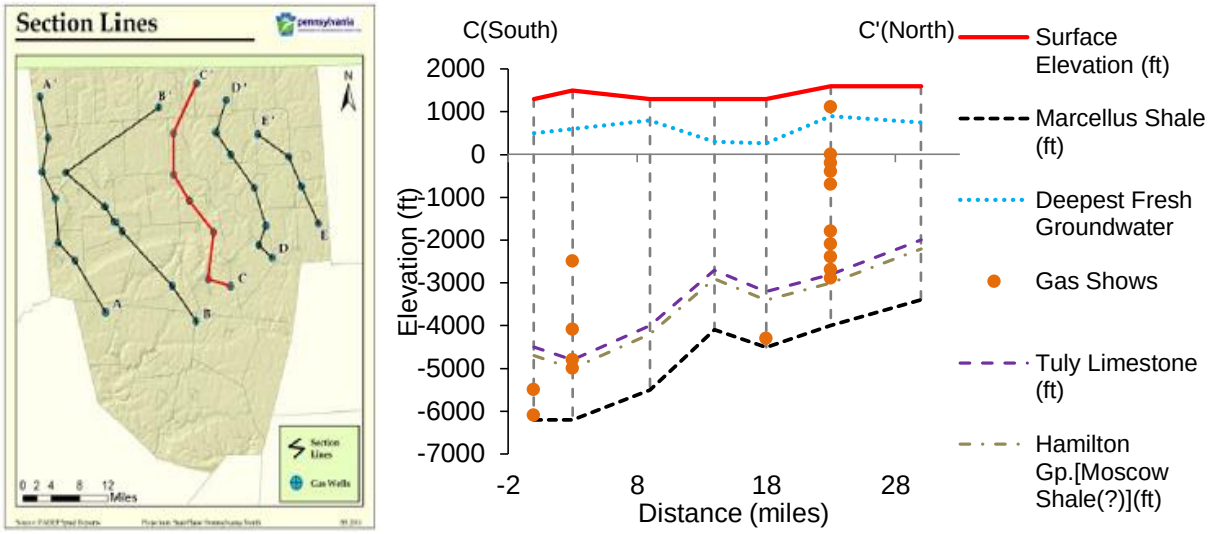

Figure 2.1. Occurrence of shallow gas sands in Bradford County, PA (adapted from PA DEP).

Typically "primary" gas migration occurs within a few hours, or at most some days after cement placement. The mechanisms of gas migration and the means to prevent it have been a topic of interest since the 1960s. While gas migration was first believed to occur exclusively through the weakness of the casing-cement and cement-formation interfaces, Carter and Slagle (1970) documented that gases can also penetrate the cement matrix during early hydration. Since then, more research has been focused on the early gelation stage of cement hydration. Figure 2.2 shows cement sheaths from laboratory tests exhibiting the effects of gas invasion during cement gelation (Crook and Heathman 1998). As seen in the figure, significant irregularly-shaped gas channels formed within the cement. Several scenarios have been studied regarding the means by which gases invade the cemented annulus during setting and hardening. These studies attribute the cause of gas migration to ineffective hydrostatic head, fluid loss during cementing, and differential pressure occurrence between the cement and formation, which precede the cement setting. The pressure difference between effective hydrostatic pressure and formation gas pressure allows gases to migrate into the gel pores of the cement matrix. During

cement gelling and prior to complete hardening, the conventional cement slurry loses its ability to transmit hydrostatic pressure to the formation. It has been observed that the slurry pore pressure actually declines shortly after cement placement (Cooke et al. 1983).

Figure 2.2. Test cores of cement subjected to gas migration (Crook and Heathman 1998).

Different theories to explain the mechanisms of hydrostatic pressure reduction have been proposed, including: 1.) localized bridging due to fluid loss (Bannister and Lawson 1985), 2.) sedimentation of cement suspensions due to slurry instability (Harton et al. 1983; Bannister and Lawson 1985), 3.) volume reduction due to fluid loss and chemical shrinkage (Sykes and Logan 1987; Jones and Carpenter 1991; Zhou and Wojtanowicz 2000), and 4.) supporting of cement due to bond at interfaces (Sutton et al. 1984a, 1984b). The classic gas migration theory is the most-widely accepted theory, which accounts for both self-support and volume reduction of the cement. After slurry placement, the initial overburden pressure in the cement column is designed to be higher than the formation gas pressure. Although fluid loss and chemical shrinkage occur, the slurry can move downward and compensate for the volume reduction. If the cement slurry is

flowable, the hydrostatic pressure will not drop significantly. As hydration progresses, the interactions between the cement column and the annular surfaces develop and chemical shrinkage and/or fluid loss continues. Due to the supporting effect of the borehole wall on the cement column, the tendency to move downward gradually decreases. Therefore, the effective hydrostatic pressure starts to drop. The hydrostatic pressure continues to drop until some *critical time* when the hydrostatic pressure is less than the formation gas pressure. If the cement has not developed sufficient strength to withstand the gas pressure, pressurized formation gases will invade the hydrating cement and create gas channels. Gas invasion may not cease until *final time* when the cement develops enough cohesive strength to prevent the entry and flow of gases and other fluids through the cement column. The period between *critical time* and *final time* is defined as the *transition time* (Mueller 2002). Experimental work has verified that gases do not penetrate the cement matrix as long as the slurry pore pressure remains above the formation gas pressure (Cheung and Beirute 1985). This process is illustrated in Figure 2.3.

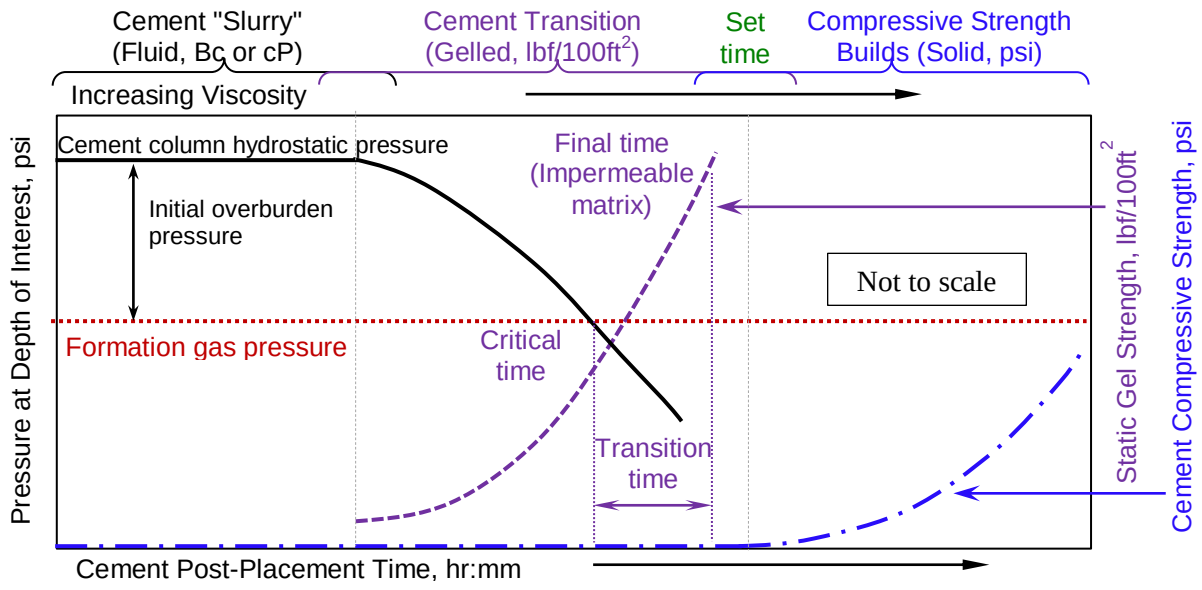

Figure 2.3. Pressure and strength evolution (adapted from Halliburton and BJ Services).

In order to quantify the hydrostatic pressure reduction, SGS was introduced in the classic shear stress theory to describe the shear stress at the casing-cement and cement-formation interfaces. In this way, the hydrostatic pressure reduction can be expressed as a function of SGS. In API Standard 65-2, SGS is specified for determining the transition time (API 2010a). Currently, the petroleum industry attempts to minimize the risk of gas migration by insuring that the SGS-based transition time is as short as possible.

The concept of controlling transition time and other approaches developed to evaluate the potential for gas migration can only provide a qualitative estimate. They help improve the slurry design and cementing practice, but cannot eliminate gas migration. In addition, SGS is not sufficient to predict when a cement slurry becomes gas-tight. In this chapter, research activities associated with SGS are summarized and its application for evaluating the potential for gas migration is evaluated. These evaluations show that SGS fails to adequately describe the observed hydrostatic pressure reduction. A discussion is also provided regarding the limitations of SGS for characterizing slurry properties with respect to preventing gas migration.

2.2 STATIC GEL STRENGTH THEORY

The first attempt to explain the gas communication by means other than leakage at interfaces was made by Carter and Slagle (1970). Since then, a great deal of effort has been invested in this topic and can be divided into three categories: 1.) mechanisms of hydrostatic pressure reduction, 2.) methods to calculate effective hydrostatic pressure, and 3.) ways to prevent hydrostatic pressure reduction. It is recognized that the main factor preventing gas from entering the cement is the hydrostatic pressure generated by the cement column and the drilling mud above it.

Hydrostatic pressure must be greater than formation pore pressure to prevent gas invasion and less than fracturing pressure of the formation to avoid lost circulation and/or fluid loss. Different mechanisms of hydrostatic pressure reduction have been proposed. Among them, the most-widely used model, derived from the classic shear stress theory, was proposed by Sabins et al. (Sutton et al. 1984a, 1984b).

2.2.1 Determination of hydrostatic pressure reduction

2.2.1.1 Classic shear stress theory

A physical model of the classic shear stress theory is shown in Figure 2.4. In this model, the cement column is assumed to be a single-phase homogeneous material, which is loaded by gravity, wall shear stress, pressure applied from the cement column above, and pressure from the cement column below. The entire cement column will move once shear failure occurs at the interfaces. The force-balanced equation for an increment of cement section (ΔL) can be written as (Sutton et al. 1984a, 1984b):

$$\tau\pi(OD + ID) \cdot \Delta L = \frac{\pi(OD^2 - ID^2)(P_1 - P_2 + \Delta L \cdot \rho_c \cdot g)}{4} \tag{2.1}$$

where,

τ = shear stress, or SGS;

P_1 = pressure applied on the cement section from the top;

P_2 = pressure applied on the cement section from the bottom;

ρ_c = density of cement slurry;

OD = borehole diameter;

ID = casing outside diameter;

ΔL = cement section length;

g = gravitational acceleration.

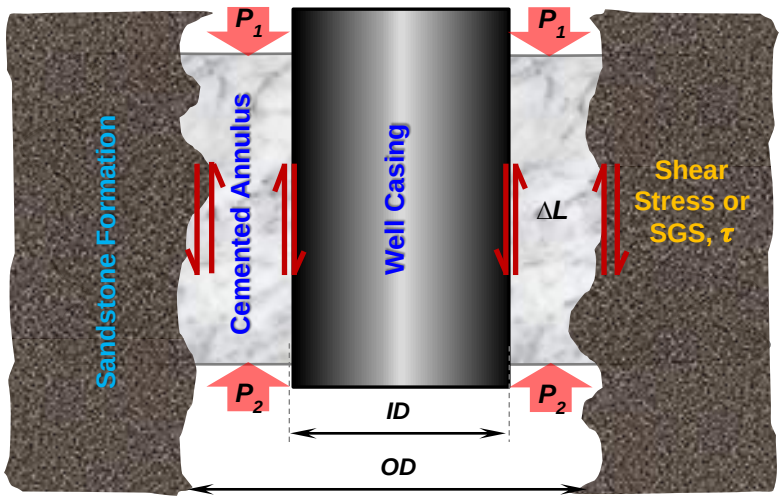

Figure 2.4. Sketch of pressure reduction in hydrating cement column.

By integrating from the top of the cement to the depth of interest, Equation (2.1) can be written as:

$$\int_0^L \tau \cdot dL = \left(\frac{OD - ID}{4}\right) \cdot \left[[P_0 - P(L,t)] + g \int_0^L \rho_c \cdot dL\right] \tag{2.2}$$

where,

P_0 = hydrostatic pressure applied on top surface of cement column, typically generated from drilling mud (P_m), wash (P_{wa}), spacer columns (P_{sp}), and surface pressure(SP). That is, $P_0 = (P_m + P_{wa} + P_{sp} + SP)$;

$P(L,t)$ = effective pore pressure at depth L and time t;

L = cement column length, considered from the top of cement to the depth of interest.

Assuming that the properties of the entire cement column are identical, Equation (2.2) can be simplified as:

$$\tau = \frac{(OD - ID) \cdot [\rho_c \cdot gL + P_0 - P(L,t)]}{4L} \tag{2.3a}$$

Therefore, the effective hydrostatic pressure at depth H and time t can be rewritten as:

$$P(L,t) = P_0 + \rho_c \cdot gL - \frac{4L}{OD - ID} \cdot \tau \tag{2.3b}$$

The original intention of Equation (2.3b) was to explain the hydrostatic pressure reduction during cement gelation. It captures the essential mechanism of hydrostatic pressure reduction and serves as a tool to quantify the hydrostatic pressure during cement gelation.

After the aforementioned model was developed, researchers tried to predict the hydrostatic pressure reduction using this model but were unsuccessful. According to Equation (2.3b), the relationship between the pressure reduction and the SGS is linear, as shown in Figure 2.5. Experimental results contradict this assumption. As seen in Figure 2.6, the hydrostatic pressure reduction is not necessarily proportional to the SGS development. While the classic shear stress theory reflects the interaction between cement and borehole, it is not sufficient to predict the hydrostatic pressure reduction accurately.

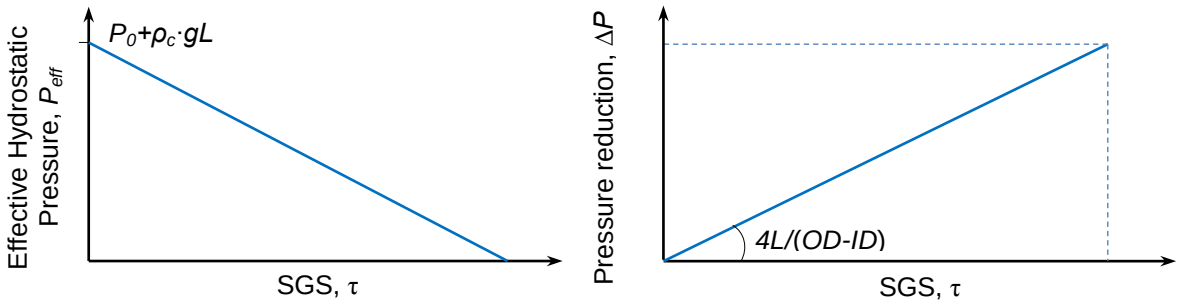

(a) Effective hydrostatic pressure vs. SGS (b) Pressure reduction vs. SGS

Figure 2.5. Relationship between hydrostatic pressure and SGS.

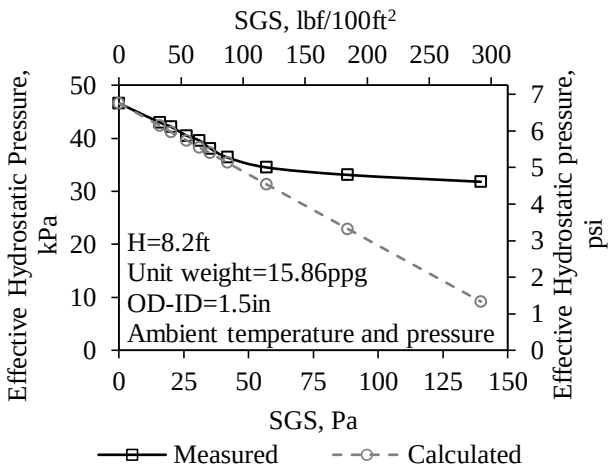

(a) Measured vs. calculated results (adapted from Zhang 2002)

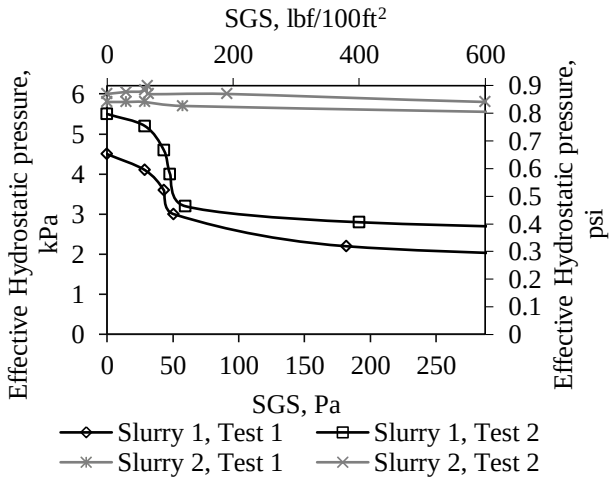

(b) Results of two different slurry designs (adapted from Zhu et al. 2012)

Figure 2.6. Effective hydrostatic pressure with respect to SGS.

When the model based on classic shear stress theory was developed, the physical meaning of shear stress and factors causing pressure reduction were not fully understood, thereby affecting the accuracy of the developed relationship. First, the cement slurry is a solid-fluid coupled media, particularly in the early gelation stage of cement hydration. It is inappropriate to assume that the cement slurry is a single-phase homogeneous material. Second, the mechanism of hydrostatic pressure reduction may change with the development of cement hydration. The microstructure of the cement matrix and its evolution are not considered in this model. The cement composition and additives will significantly influence the slurry mechanical properties and its hydration. In addition, the model does not consider the effect of slurry instability and inclined annuli.

2.2.1.2 Revised model

Volume reduction was identified as another critical factor affecting hydrostatic pressure reduction. The internal volume of cement slurry decreases due to chemical shrinkage and fluid

loss (Tinsley 1980). By assuming no volume change during the early hydration stage, the existence of a linear relationship in Equation (2.3) is contradicted. Later, it was recognized that the borehole and the casing will deform due to the pressure change (Jones and Carpenter 1991; Zhou and Wojtanowicz 2000). According to Boyle-Mariotte's law, the effective hydrostatic pressure will decrease due to volume reduction. The basic relationship between pressure change and volume changes is presented below (Zhou and Wojtanowicz 2000):

$$\Delta p = (\Delta v_{loss} + \Delta v_{sh} - \Delta v_T - \Delta v_{wh} - \Delta v_{csg})/(V_0 \cdot c) \quad (2.4)$$

where, $\Delta v_{loss}, \Delta v_{sh}, \Delta v_T, \Delta v_{wh}, and\ \Delta v_{csg}$ denote volume changes due to fluid loss, chemical shrinkage, temperature change, wellbore deformation, and casing deformation, respectively.

The volume reduction method captures the physical changes in the borehole. Nevertheless, in-situ conditions are so complicated that the pressure reduction is difficult to accurately predict. Many of the influential factors are difficult to quantify and have to be assumed. Moreover, the theory assumes a static state for the cement slurry. This would overlook the deformation of the cement column and the volume change in the cement matrix. As a result, this theory is more applicable to the later hydration stage rather than the early gelation stage of cement hydration.

In order to consider both slurry rheological properties and volume reduction, Chenevert and Jin (1989) studied the effects of time-dependent variables on SGS, including temperature and pressure in the cement column, and slurry composition and set time of the cement. By integrating from the top to the depth of interest, a revised expression of effective hydrostatic pressure can be written as (Chenevert and Jin 1989; Prohaska et al. 1993):

$$P(L,t) = P_0 + g \cdot \int_0^L \frac{\rho_c}{1 - S(L,t)} \cdot dL - \frac{4}{OD - ID} \int_0^L \tau(\gamma, t) \cdot dL \qquad (2.5)$$

where,

$\gamma =$ shear strain;

$S(L,t) =$ shrinkage of cement slurry at depth L and time t.

Equation (2.5) is more comprehensive and theoretically accurate than Equation (2.3b). Not only is the variation of SGS in the wellbore considered, but also volume changes with respect to the time and depth. However, this model is fundamentally based on the classic shear stress theory, which shares the same limitations previously discussed. After the cement is placed, the hydrostatic pressure is constant as the cement deforms to some extent to compensate for the volume reduction caused by fluid loss and chemical shrinkage. The friction, or bond, at the interfaces tries to support the cement matrix. When the slurry at or near the interfaces is not able to deform, it is inappropriate to determine the static friction using the force-balanced equation, as the actual shear stress at the interface will be less than the back-calculated SGS from Equation (2.3). The reason is that the friction component is determined by other variables in the statically-indeterminate system. Additionally, enhanced additives are typically blended in the slurry design to control gas migration, which makes it inappropriate to predict the hydrostatic pressure reduction using Equation (2.3). For instance, a fluid loss additive can help maintain a high hydrostatic pressure even in the presence of the SGS development, as shown in Figure 2.6b. Therefore, the theoretical relationship using the concept of SGS is not capable of evaluating the potential for gas migration.

2.2.2 Practical approaches

A desire for design criteria to be applied in the field triggered the petroleum industry to develop approaches to assist operators in predicting the potential for gas migration. Several of the more common approaches are presented below.

2.2.2.1 FPF (Halliburton, 1984)

As Equation (2.3) captures the phenomena of hydrostatic pressure reduction in the early hydration stage, researchers tried to evaluate the feasibility of using this model for predicting gas migration. By using the classic shear stress theory, Sutton et al. (1984b) developed a gas FPF to predict the potential for gas migration. FPF, sometimes called Gas Flow Potential (GFP), is defined as:

$$FPF = MPR/OBP \tag{2.6}$$

where,

OBP = initial OverBalance Pressure, as:

$$OBP = \rho_c \cdot gL + P_0 - P_f \tag{2.7}$$

P_f = formation gas pressure;

MPR = Maximum Pressure Reduction at a given SGS value. MPR can be obtained by substituting Equation (2.3) (for English units):

$$MPR = \rho_c \cdot gL + P_0 - P(L,t) = \tau \cdot 4L/(OD - ID) = SGS/300 \times L/D \tag{2.8}$$

where,

D = Difference between hole diameter and casing diameter ($OD - ID$), in;

300 = Conversion factor, lbf/in;

SGS = Static Gel Strength, or τ, lbf/100ft^2.

The assumption of the FPF theory is that gases will not penetrate the cement slurry if the effective hydrostatic pressure is higher than the formation gas pressure. Equation (2.6) is in fact a modification of the standard shear stress equation presented in Equation (2.3b). According to Equations (2.3) and (2.6), FPF should equal 1 when the effective hydrostatic pressure equals the formation gas pressure. The SGS at the time when the effective hydrostatic pressure is zero can also be determined using Equation (2.3a) for a typical slurry design, as shown below.

$$SGS = [\rho_c \cdot gL + P_0 - P(L,t)] \cdot \frac{OD - ID}{4L} = [\rho_c \cdot gL + 0 - 0] \cdot \frac{OD - ID}{4L}$$
$$= (\rho_c \cdot g) \cdot \frac{OD - ID}{4} = \left[(15.6ppg * 0.052) * \left(\frac{2.5in}{4} * \frac{1.0ft}{12in}\right)\right] psi \quad (2.9)$$
$$= 0.0423\ psi = 608\ lbf/100ft^2$$

However, Equation (2.3b) may overestimate the hydrostatic pressure reduction. Experiments indicate that residual effective hydrostatic pressure exists even after the cement's final set, as shown in Figure 2.6. This can be explained using boundary flow theory, as shown in Figure 2.7. With the development of cement hydration, chemical shrinkage occurs and cement slurry is capable of moving downward due to gravitational forces. As the interface bond increases, slurry particles near the borehole wall will adhere to the surface. The central portion of the slurry is still able to move downward relatively freely, maintaining the effective hydrostatic pressure. The movement of cement slurry is governed by the principles of laminar flow and the shear deformation described in Equation (2.3).

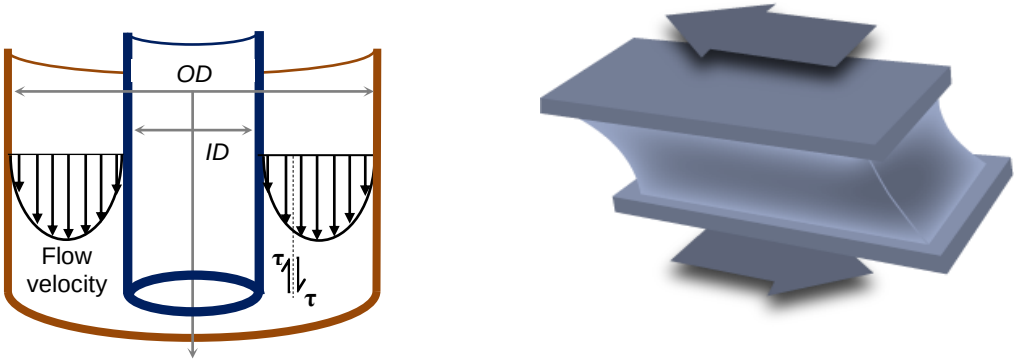

(a) Boundary layer flow (b) Resistance to shear deformation

Figure 2.7. Boundary flow theory and shear bond strength.

Due to the lack of effective methods to accurately predict gas migration, criteria for defining gas migration potential have been established using empirical field observations. SGS at the end of transition time was experimentally determined to be 522 lbf/100ft^2 (250 Pa) by Sabins et al. (1982). A SGS of 500 lbf/100ft^2 is commonly used to calculate the FPF. Based on field experience, the results of FPF are divided into three categories: severe, moderate and minor. Unfortunately, the development of these rules remains unpublished (Nelson 1990).

Generally, FPF is a unit-less value used to predict the severity for encountering gas migration. FPF lacks a physical meaning, and the use of FPF is a qualitative approach with the empirical criteria for this approach established using relatively limited field experience.

2.2.2.2 CWSS (Schlumberger, 1996)

In order to provide a meaningful variable in evaluating the potential for gas migration, Schlumberger introduced another tool to evaluate the potential for gas migration. Wall shear stress is defined as *static friction* which occurs at the interfaces between the cement and the casing or formation. Therefore, CWSS represents the shear stress at the interfaces when the

effective hydrostatic pressure is equal to the formation gas pressure (Bonett and Pafitis 1996; Stiles 1997). The original formula is shown as:

$$CWSS = 0.25\left[P_m + P_{wa} + P_{sp} + P_{sl} + SP - P_f\right] \times (OD - ID)/L \quad (2.10a)$$

which can be simplified as:

$$CWSS = OBP \times D/(4L) \quad (2.10b)$$

Critical hydration period (CHP) is another term for the transition time, which is described as the time period between CWSS and the development of an impermeable cement matrix that gases can no longer enter or migrate through. In the CWSS approach, the risk of gas migration can be reduced by shortening the CHP, as shown in Figure 2.8. A means to reduce the CHP is to increase CWSS. A relatively high CWSS will result in a relatively lower risk for gas migration.

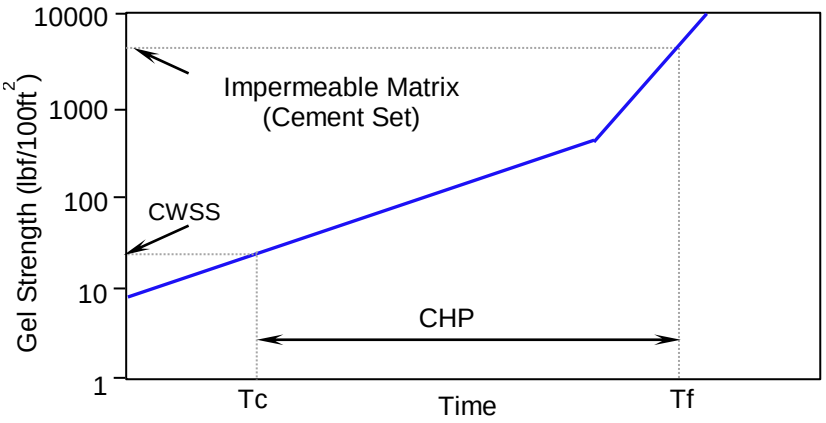

Figure 2.8. CHP in the CWSS approach (adapted from Brandt et al. 1998).

In essence, the theoretical foundation of CWSS is the same to that of the FPF. While the FPF method is used to calculate the effective pressure by using SGS, the CWSS method is used to determine the shear stress by using the maximum allowable pressure reduction. The

relationship between FPF and CWSS can be derived from Equations (2.3), (2.6) and (2.10), and shown as:

$$FPF = SGS/CWSS \tag{2.11}$$

A comparison between FPF and CWSS is presented in Table 2.1. Although CWSS provides more levels of classification, both of them can only provide a qualitative severity level for encountering gas migration. Similar to the FPF, the empirical criteria for the CWSS method were established based on limited field experience. In addition, CWSS denotes the mechanical properties at the interfaces, which is not an intrinsic property of cement slurry.

Table 2.1. Comparison between FPF and CWSS.

Approach	Severity Rating				
FPF*	Severe		Moderate		Minor
	> 8	(8)	4 - 8	(4)	< 4
CWSS*	Very critical		Critical	Moderate	Low	Very low
	25Pa (50lbf/100ft^2)		75Pa (150lbf/100ft^2)	150Pa (300lbf/100ft^2)	250Pa (500lbf/100ft^2)	

Note: * Values are orders of magnitude, which is based on limited experience.

2.2.2.3 SRN (Halliburton, 1989)

Two necessary conditions are required for gas invasion into settable slurry (Bonett and Pafitis 1996): 1.) a driving force to initiate the gas flow, and 2.) space within the cemented annulus for gas to occupy. The stability of the cement slurry is critical to maintaining the effective hydrostatic pressure during cement hydration. Fluid loss will dramatically decrease the hydrostatic pressure, which will also provide space for gas to occupy. In order to consider the fluid loss during cement hydration in predicting the potential for gas migration, the SRN method

was proposed. SRN is defined as a ratio of the SGS development rate to the rate of fluid loss at the time when SGS develops at a maximum rate of change (Sutton and Ravi 1989; Harris et al. 1990), and can be written as:

$$SRN = \frac{\frac{d(SGS)}{dt} / SGS_{\max rate}}{\frac{dl}{dt} / (V/A)} \tag{2.12}$$

where,

$d(SGS)/dt =$ maximum rate of change of SGS;

$SGS_{\max rate} =$ SGS at time of maximum rate of change;

$dl/dt =$ rate of fluid loss at time of SGS_{max};

$V =$ Volume of annular space per unit length;

$A =$ Area of formation face per unit length.

SRN is a significant improvement over the Slurry Performance Factor (SPF) developed by Schlumberger (Rae et al. 1989). The critical time determined by the SRN method corresponds to the onset of a rapid increase in SGS. Fluid loss represents volumetric reduction of the slurry and the rate of fluid loss declines over time. At the critical time, the rate of fluid loss should be very small (high values of SRN). Otherwise, pressure at the bottom of cement slurry could rapidly decline, causing gas migration.

The SRN method was recently correlated with the conventional measure of gas migration potential, the FPF. This constitutes the first "quantitative" model for the annular wellbore seal integrity (Harris et al. 1990). Figure 2.9 and Equation (2.13) show the criteria for slurry design using the SRN-FPF approach.

$$SRN = 26.3 + (47.4 \times FPF) - (2.7 \times FPF^2), for\ 1 < FPF < 9 \quad (2.13.1)$$

$$SRN = -8.1 + (27.3 \times FPF) - (0.98 \times FPF^2), for\ 1 < FPF < 15 \quad (2.13.2)$$

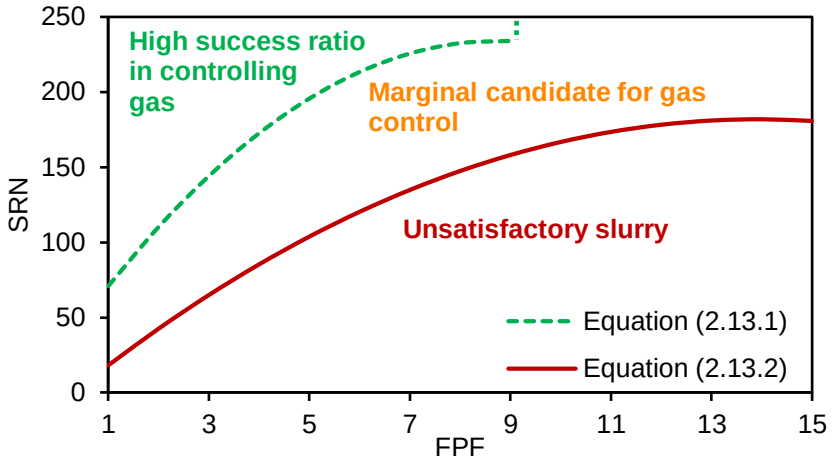

Figure 2.9. SRN ranges.

The SRN method intends to determine the critical time when the maximum rate of pressure reduction will occur. Volume reduction and self-support are both taken into account. However, typical values of $SGS_{\max rate}$ take place when the SGS is approximately 100 to 200 lbf/100ft^2. As the slurry is still flowable, the rate of pressure reduction at the critical time determined by SRN may not be the maximum. Also, since the FPF is used to quantify the failure criteria, the SRN method is also based on empirical criteria established using relatively limited field experience.

2.2.2.4 Discussions

The aforementioned approaches capture the essential factors affecting hydrostatic pressure reduction. They provide guidelines on improving slurry design and construction practice (Levine et al. 1979). For example, new cement designs, such as right angle set (RAS) cement,

surfactant agents, expansive cement, impermeable agents and latex particles, have been developed and implemented based on their performance. Casing design optimization, multi-stage cementing (Shiflet et al. 2005; Labibzadeh et al. 2010) and cement pulsation treatment (Wojtanowicz et al. 2002) have been employed in practice.

However, the accuracy of these approaches is still a concern as it is very difficult to quantify the efficiency of cement displacement. Moreover, the approaches are based on the classic shear stress theory, and therefore shares the same limitations discussed in Section 2.2.1.1. From Table 2.1 and Figure 2.9, the aforementioned approaches are fundamentally of the same philosophy. The criteria are not slurry properties but calculated values (Stiles 1997; Gonzalo et al 2001), which only provide a qualitative estimation of the potential for gas migration. Currently, these approaches are mainly used for designing slurries with favorable properties, such as optimal density, minimal fluid loss and short transition time. They also provide guidance for casing string design. Calibrated using field experience, the approaches have been able to assist operators in mitigating bottomhole gas migration. However, recent gas migration occurrences from onshore unconventional shale gas plays have caused the petroleum industry to re-evaluate them. While the approaches indicate a "minor" potential for gas migration, shallow stray gas migration and interzonal communication are underestimated by all of these approaches (PA DEP 2009; EPA 2011; Dusseault et al. 2014).

2.2.3 Measuring transition time

Due to the absence of an effective means to determine gas migration occurrence, the petroleum industry tries to reduce the risk of gas migration by shortening the transition time, and the critical hydration period during the gelation stage (Roges et al. 2004). After the relationship between

SGS and hydrostatic pressure was established through the application of classic shear stress theory, the petroleum industry tried to employ this model by focusing research efforts on methods to determine SGS and criteria for its application.

In API Standard 65-2, the concept of SGS is referenced to determine the transition time, which is defined as the period between the time when critical static gel strength (CSGS) and optimal static gel strength (OSGS) are achieved. When cement achieves CSGS, the slurry is no longer capable of transmitting hydrostatic pressure that overbalances the formation pore pressure. CSGS can be calculated when the formation pore pressure is known by using Equation (2.3a). When sufficient information is not available to confidently calculate CSGS, a value of 100 lbf/100ft^2 may be used (API 2010b). In addition, 500 lbf/100ft^2 is specified as OSGS, at which the slurry has developed enough cohesive strength to prevent the entry and flow of gas and reservoir fluids through the cement (Kolstad et al. 2004). The faster the OSGS is achieved, the less likely it is that the cement will transmit gas. OSGS is specified as 500 lbf/100ft^2. It should be noted that the paper published by Sabins, et al. (1982) is the only available peer-reviewed document in which 100 and 500 lbf/100ft^2 were justified as acceptable criteria, regardless of different slurry designs and application conditions. Moreover, Stevart and Schouten (1988) showed that gel strength considerably below 500 lbf/100ft^2 could inhibit gas percolation, but most gas migration was conclusively shown to occur after the cement's initial set.

The API has been evaluating different types of SGS test devices in order to develop standard measurement methods. In API RP 10B-6 (or ISO 10426-6), three different testing apparatuses for determining SGS are recommended, including: 1.) rotating-type, 2.) intermittent rotation-type, and 3.) ultrasonic-type SGS devices. Well-known commercial SGS devices

include the MACS II® by Fann (2011), the SGSM by OFITE (2014a), the Rotating Paddle Consistometer by CTE (2014a), and the SGSA by Chandler Engineering (2014a).

2.2.3.1 Mechanical measurement

Even though the equipment designs for measuring SGS attempt to maintain a quasi-static state for cement slurries, results vary from different rotating speeds, measurement time intervals, and device types. Figure 2.10 shows the paddle and the vane used to shear the slurry in the SGS devices. Figure 2.11 and Figure 2.12 present the typical patterns of the SGS measurements using the two different devices, respectively. It should be noted that 100 and 500 lbf/100ft^2 were developed using the paddle design shown in Figure 2.10a. Although an extremely-low shear rate is used, the slurry is repeatedly destructed along the shearing front. For the rotating-type SGS device in Figure 2.10a, a standard rotating speed of 0.2 degree/minute (MACS II) indicates a 3.0 micrometer/sec shearing speed at the edge of the paddle, which is the same scale of cement particle size (an average cement particle size is approximate 20 micrometers). Therefore, the rotating-type SGS device is a continuously destructive test. The rotating speed of the paddle will significantly affect the measured results. By reducing the rotating speed of the paddle, the measured SGS will continuously get closer to the true SGS of the slurry. When it comes to the intermittent rotation-type SGS device, the shearing front is created once the shearing movement occurs. The measured SGS mainly depends on the static time period for cement flocculating. The later the test starts, the higher the SGS. The shearing front is the cylindrical surface generated by the vane, which is the area used to calculate the SGS. The rotating-type device creates a similar shearing front to that created by the intermittent rotation-type device, even though the shape of the stirring paddle is different, as shown in Figure 2.10b. The flocculation of hydration products at the shearing front suffers the cycles of construction, damage and

reconstruction. Therefore, neither the rotating-type nor the intermittent rotation-type device qualifies for non-destructive testing, as a weak shearing front is created from the repeated microstructural destruction.

(a) Paddle in rotating-type device (Fann 2011)

(b) Six-blade vane in intermittent rotation-type device (OFITE 2014a)

Figure 2.10. Paddle designs of SGS devices.

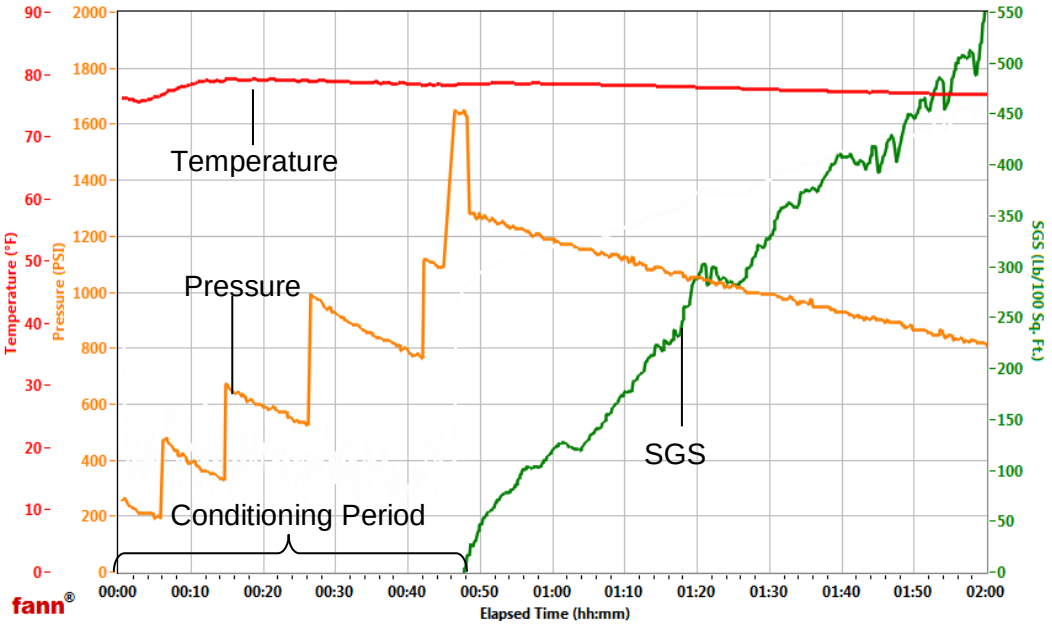

Figure 2.11. Typical SGS measurement using rotating-type device.

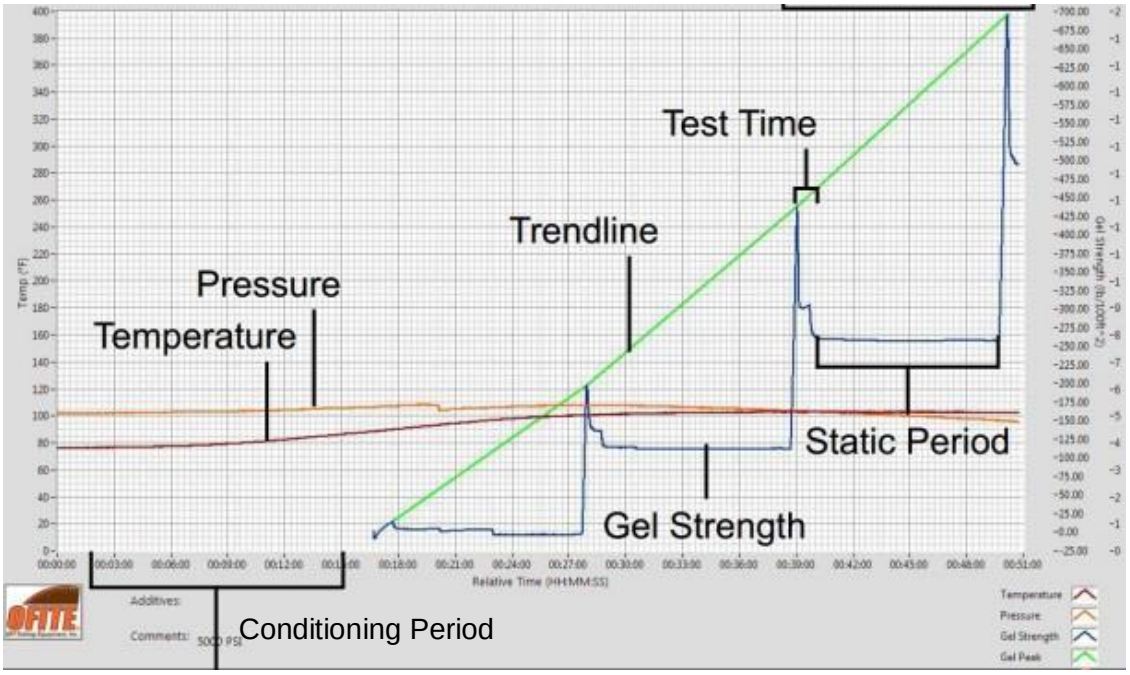

Figure 2.12. Typical SGS measurement using intermittent rotation-type device (OFITE 2014a).

An example of destructive testing is shown in Figure 2.13 where the delay in the formation of gel strength is related to the number of destructive measurement points. The repeatedly destructed tests were conducted by shearing the same slurry sample every 10 minutes, while the single destructed tests were performed on the slurries that set quiescently from the beginning until the testing time. As seen in the figure, the repeated destruction dramatically decreases the gel strength of the slurry. Figure 2.14 shows the morphology of hydration products. After 2 hours of stirring in the viscometer, the typical morphology of hydration products does not change but crystals align the shear direction (indicated by arrows), to develop a preferred orientation.

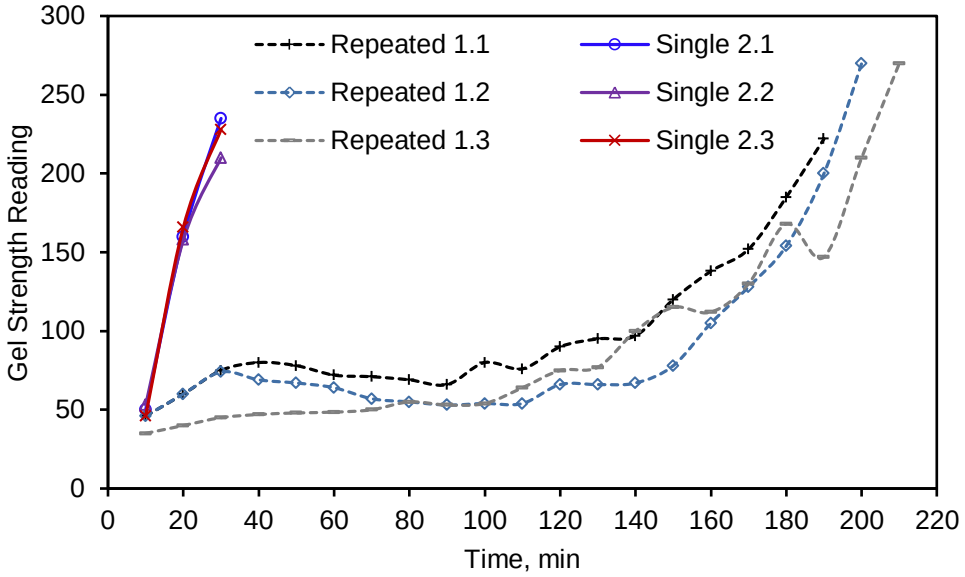

Note: Repeated Destruction (Three repetitions: 1.1, 1.2, 1.3) vs. Single Destruction (Three repetitions: 2.1, 2.2, 2.3)

Figure 2.13. Gel strength development comparison (Zhang 2002).

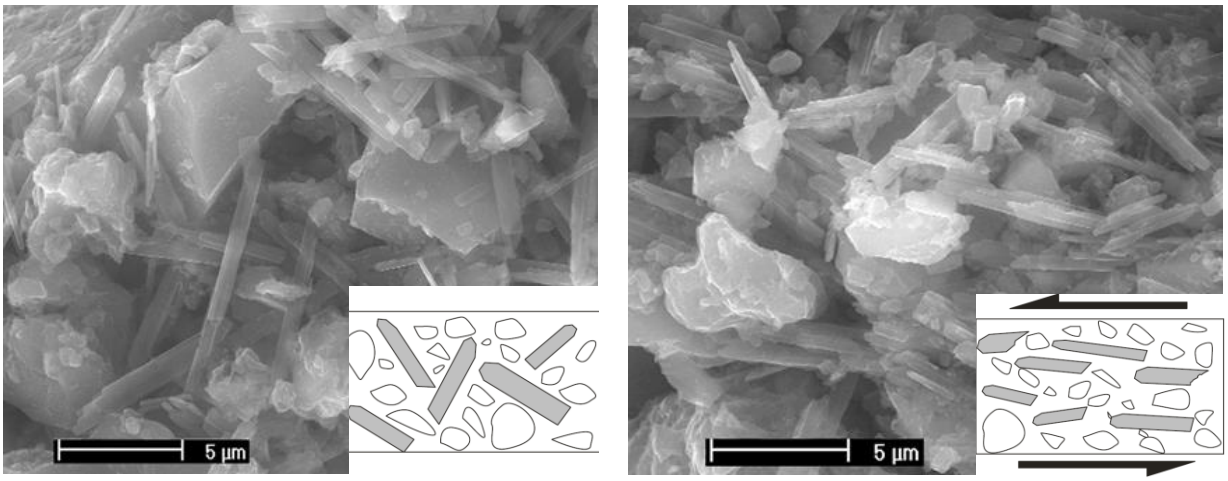

(a) Cement hydrated without agitation: random orientation

(b) Cement paste after 2 hours of shearing in the viscometer: preferred orientation

Figure 2.14. ESEM Image of cement after 2 hours of hydration (Rößler et al. 2008).

2.2.3.2 Nondestructive measurement

Due to the copyright of patents, the method using ultrasonic technology to determine SGS is not described in API RP 10B-6 (2010b). Details of an acoustic device for determining the SGS of a cement slurry can be found in Patent Application US5992223A (Sabins and Maki 1999). The

SGSA provided by Chandler Engineering is an ultrasonic cement analyzer. According to Patent Application US599223A, ultrasonic devices do not always provide accurate SGS measurements, as shown in Figure 2.15. Cement properties are inferred by measuring the change in the energy level of an ultrasonic signal transmitted through the cement specimen as it gels and are labeled as "computed gel strength" in Figure 2.15. Clearly, the relationship has to be accurately calibrated between SGS development and longitudinal ultrasonic wave properties (i.e. velocity and attenuation). As seen in Figure 2.15b, although the predictions of SGS development are relatively accurate with the ultrasonic testing, the results for the transition time (from 100 to 500 lbf/100ft^2) have large discrepancies when compared with that of the measured SGS, which may be caused by the presence of latexes. Air bubbles also significantly affect the ultrasonic velocity. Therefore, slurries containing additives, i.e. increased levels of latexes or air bubbles, may require an adjustment of the coefficients in the computational models.

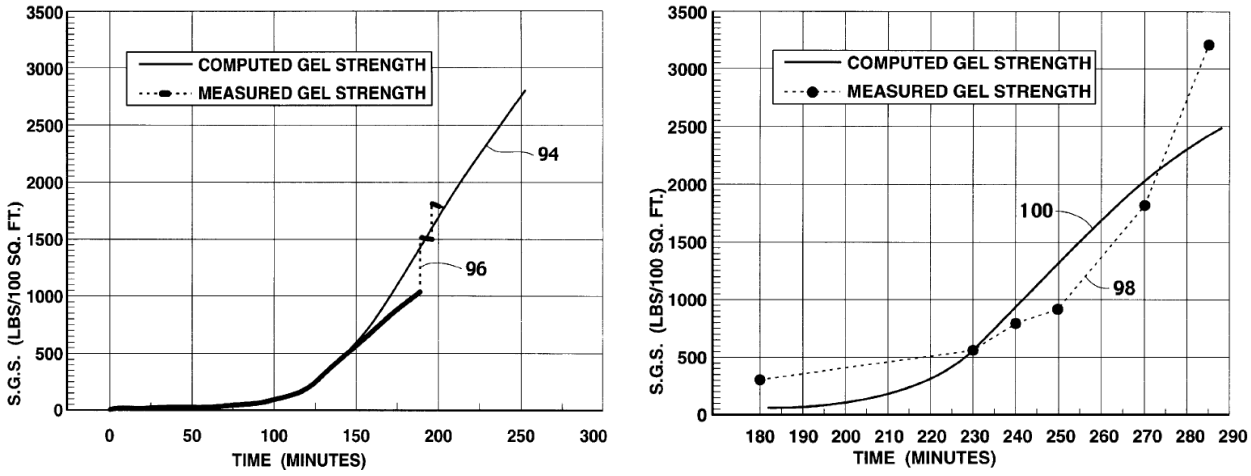

(a) Neat cement (b) Latex cement

Figure 2.15. Evaluation of SGS measurement using ultrasonic device (Sabins and Maki 1999).

The literature indicates that the ultrasonic testing can be used to determine the initial set of cement. Zhang et al. (2010) studied the effect of the w/c ratio, temperature and chemical additives on early hydration of API Class H cement. As shown in Figure 2.16, the ultrasonic wave velocity remains constant (approximately 1500 m/s, which is equivalent to the wave velocity through water) until cement slurries gain the initial setting strength defined in ASTM C191 (2013).

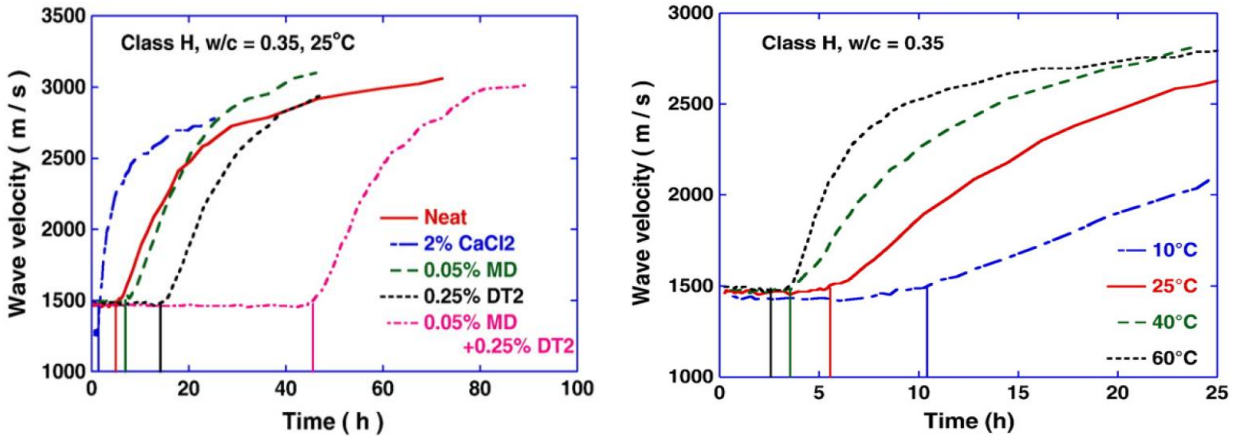

(a) Cement with different additives (b) Neat cement cured at 10, 25, 40 and 60 ℃

Note: solid straight lines indicating the initial setting time determined by Vicat test

Figure 2.16. Ultrasonic wave velocity versus time curves (Zhang et al. 2010).

Other non-destructive methods to monitor cement hydration include: 1.) non-electrode resistivity measurement, and 2.) dielectric constant measurement. Similar to ultrasonic measurement devices, these non-destructive methods can capture the slurry phase changes. The amplitude of the measurement depends on the components and their quantities. Therefore, it is difficult to develop a general relationship between the SGS and the electrical resistivity or the dielectric permittivity during the early hydration stage.

2.3 CEMENT MATRIX CHARACTERIZATION

2.3.1 Using SGS to quantify cement rigidity

The term "gel", which is commonly used within the petroleum industry, differs significantly from the definition applied in polymer science. It is used to describe cement thixotropic properties. Gel strength is measured by shearing slurry samples at a very low shear rate after the samples are allowed to set quiescently for a period of time. The peak shear stress during the start of rotation at a shear rate of $5.11s^{-1}$ is recorded as the gel strength. API RP 10B-2 (2013) standardizes the 10-second and 10-minute gel strength, although measurements after 30 minutes or 16 hours may also be made. Note that the CWSS method employs the gel strength, as shown in Figure 2.8. Different from gel strength, SGS is defined as the shear stress derived from force required to initiate flow of a fluid. The concepts and methods for cement characterization are actually adopted from the viscosity concept for liquid materials. However, the cement slurry is not a liquid, but a phase-changing solid-fluid coupled media.

As discussed in Section 2.2.1.1, the concept of SGS was originally employed to describe the static shear stress at interfaces. After cement placement, a very thin cement layer will adhere to the rough surface of the casing and the formation. As the cement continues gelling, shear deformation occurs within cement slurry and should follow the boundary layer flow theory, as shown in Figure 2.7. Therefore, SGS describes cement resistance to deformation by shear stress. Adopted from fluid dynamics, SGS does reflect the cement strength as it increases with rigidity development of the cement matrix. However, the interaction between the formation gas and the cement matrix is not purely shearing. Gases and other fluids have to break through the cement

matrix and generate a path by pushing bonded solids apart. This requires that the normal bond strength be overcome and the cement matrix be compressed, as shown in Figure 2.17.

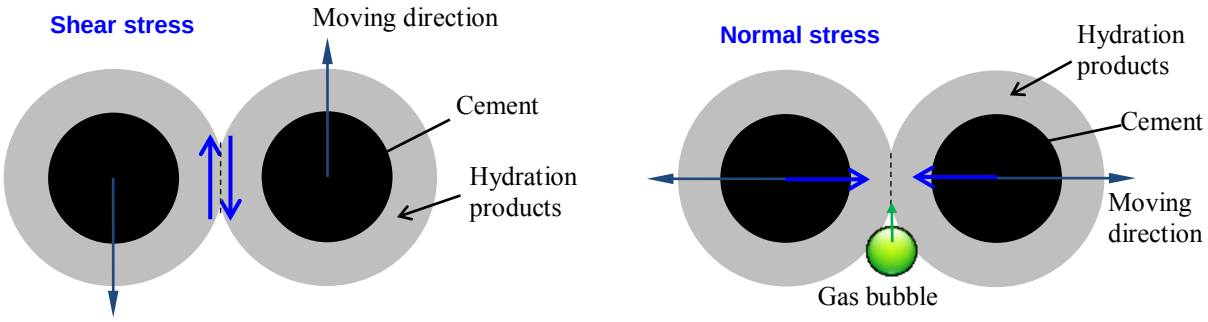

(a) Shear bond strength (b) Normal bond strength

Figure 2.17. Shear bond strength and normal bond strength.

Neither the compressibility of the cement matrix, nor the normal bond strength between the particles, has a direct relationship with the shear bond strength within the cement layers. Being a bulk mechanical property, SGS includes the interface bond or cohesion between particles; however, it is impossible to distinguish the normal strength between particles from the shear strength within the cement layers using SGS solely. In addition, SGS cannot describe the compressibility of the cement matrix as SGS alone is not sufficient to reflect either shear thinning or shear thickening. Therefore, SGS is an "apparent" parameter describing the bulk mechanical character of the cement matrix. Neither the normal bond strength between solids nor the compressibility of the cement matrix can be distinguished from shear bond strength using only SGS.

2.3.2 Slurry performance enhancements

Different additives are commonly blended to adjust slurry properties and achieve desirable results. For example, it has been demonstrated that latexes and particle size distributions can improve the gas-tight properties of cement slurry. However, neither the SGS nor the model for hydrostatic pressure reduction is able to capture the effectiveness of these additives in preventing gas migration.

2.3.2.1 Latexes

The mechanisms of latexes in helping with resistance to gas migration have been discussed for a considerable length of time (Jones and Carpenter 1991). A sensitivity study was carried out to evaluate the effects of latex, dispersant and w/c ratio (Rocha et al. 2013). Table 2.2 shows the results of SGS development and gas migration occurrences. Slurries with adequate concentrations of latex were resistant to gas migration, despite their shrinkage and SGS history. Early in the hydration process, latex particles are suspended separately in the cement slurry. They will flocculate and coalesce as films or membranes within the cement matrix during early gelation stage of cement hydration. As the latex is a deformable polymer, the SGS does not significantly increase. The latex films serve as the crystallization nucleus for hydration products promoting growth. Therefore, CSGS is achieved more rapidly when latex is added. Figure 2.18a shows that hydration products coagulate on latex flocculants. However, embedded latex flocculants decrease the "permeability" of cement matrix when cement starts to gel. In more basic slurry designs, such as groups with 0.09% dispersant, the latex can extend the transition time. The adhesive and cohesive properties of latex help to resist the cement from being torn apart. Figure 2.18b shows the adhesion effect of latex in the cement matrix.

Table 2.2. Effect of latex on SGS development and gas-tight property (adapted from Rocha et al. 2013).

Dispersant, BWOC	0.09%				0.46%			
w/c ratio, BWOC	0.4		0.44		0.4		0.44	
Latex, BWOC	0%	8.14%	0%	8.14%	0%	8.14%	0%	8.14%
Time, minute (CSGS)	203	91	217	137	252	220	288	241
Time, minute (OSGS)	286	319	296	399	347	262	359	319
Transition time, min	83	228	79	262	95	42	71	78
Gas tight	No	Yes	No	Yes	No	Yes	No	Yes

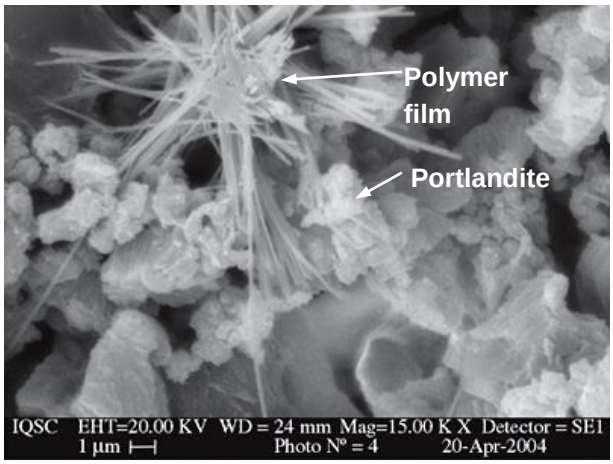

(a) Adherence between polymer film and Portlandite (Gomes et al. 2005)

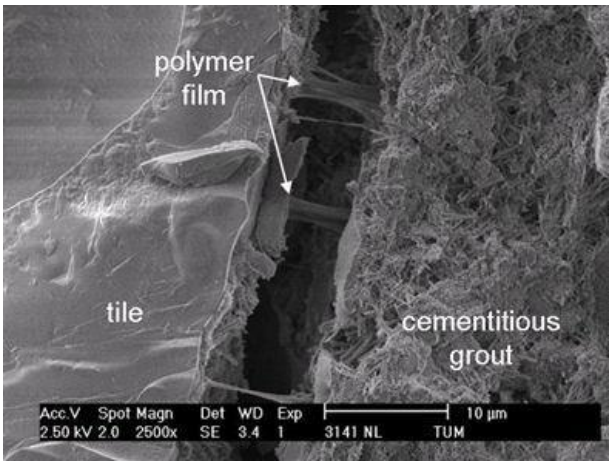

(b) Adhesion of a sintered tile on cement mortar by latex film bridging (28 days hardening) (Plank 2014)

Figure 2.18. SEM graphs of latex in cement matrix.

Compared to the micrometer (10^{-6}m) magnitude of the size of cement particles, nanometer-scale (10^{-9}m) latexes can form a colloid-dispersion system between cement particles, which reduces the permeability of cement matrix. When latex flocculates, it performs like a barrier, which can also bridge hydration products. The adhesive and cohesive properties of latex improve the bond between solids and the elasticity of the cement matrix (Bonett and Pafitis 1996). Unfortunately, SGS is unable to capture the dramatic enhancement of the ductility due to the bridging effect of latexes. As the shearing movement is extremely low in the mechanical

SGS measurement devices discussed in Section 2.2.3.1, the latex film is not expanded and reinforcement cannot be shown. Therefore, SGS is not able to distinguish the normal interaction from the shearing property. Neither the barrier effect nor the lower permeability can be captured by SGS.

2.3.2.2 Particle size distribution

Another means to enhance slurry performance with respect to gas migration prevention is optimization of the particle size distribution (PSD) (Boisnault et al. 1999). When the PSD is optimized, solid particles can be well compacted. Therefore, less water is needed and the fluid loss can be reduced. Another advantage is that a well-graded slurry is less compressible than a poorly graded slurry. As shown in Figure 2.17, gases have to push solids apart in order to form a channel. By filling space between bigger solids with smaller particles, the solid fraction is larger and gaps are smaller, as shown in Figure 2.19. In a well-graded slurry sample, solid particles are compacted and in close contact with surrounding particles. This will also decrease the permeability of the cement matrix.

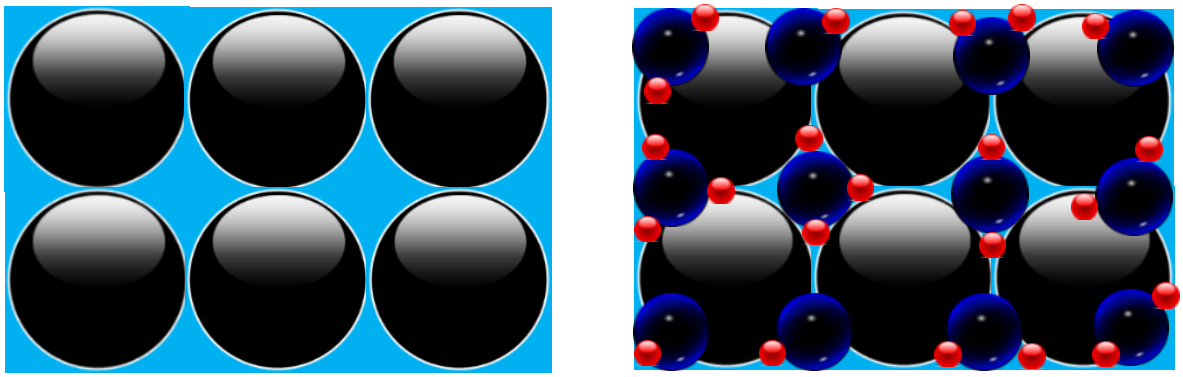

(a) Conventional cement slurries (b) Particle size optimization slurries

Figure 2.19. Compressibility of cement matrix.

It is notable that SGS may not necessarily be high in a well-graded slurry. In order to demonstrate the effect of cement particle size on the cement matrix strength development, coarse cement particles are assumed to be twice as large as fine cement particles. With an identical w/c ratio, the contact area will be the same for the same hydration stage, as shown in Figure 2.20. The SGS may be equal, as the contract area is the same. However, the finer matrix provides much smaller voids and, therefore, a less permeable matrix.

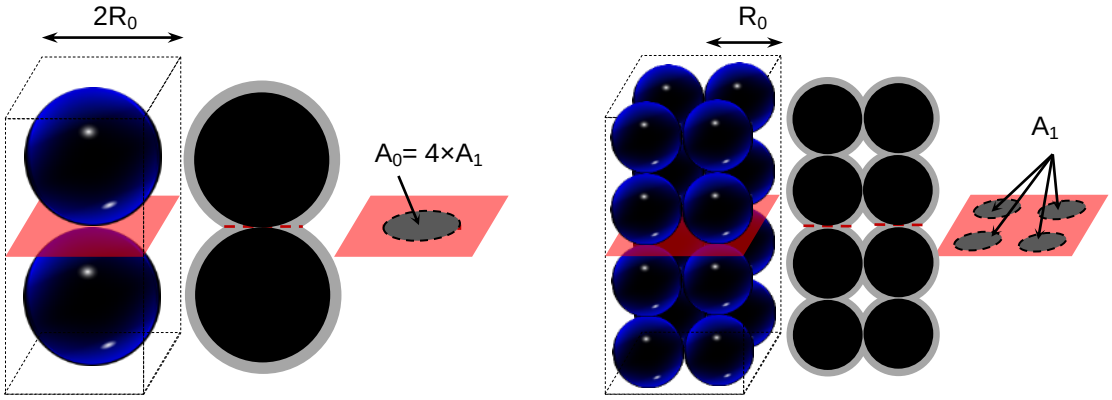

(a) Coarse cement particles (b) Fine cement particles

Figure 2.20. The same contact area at the same hydration stage.

2.3.3 Microstructural development

As discussed in Sections 2.3.1 and 0, SGS is an "apparent" property reflective of the strength development of cement slurry. Compressibility, permeability and normal bond strength of a cement matrix cannot be distinguished from shear bond strength by using solely SGS. In order to predict the gas-tight properties of cement, a better approach is to characterize cement microstructural development.

2.3.3.1 Solid-fluid coupled media

The microstructural development of cement is illustrated in Figure 2.21. When cement is mixed with water, the cement particles disperse in the water, forming a suspension. As cement particles are small and the interaction between particles is weak, the mixture maintains a high fluidity. However, when the w/c ratio is lowered or the interaction between cement solids increases due to hydration, a network is generated by the particles interacting with each other. Cohesive strength develops between solids as the volumetric fraction of solids increases. The bond and friction between particles strengthen when the hydration products on solids start to overlap with each other. An initial load is required to overcome the resistance to deform the cement matrix, which is commonly referred to as the "yield point" of the slurry. When the slurry starts deforming, the measured plastic viscosity indicates the effect of the cohesion and the friction between solids. The bond will be reconstructed when the slurry is left undisturbed.

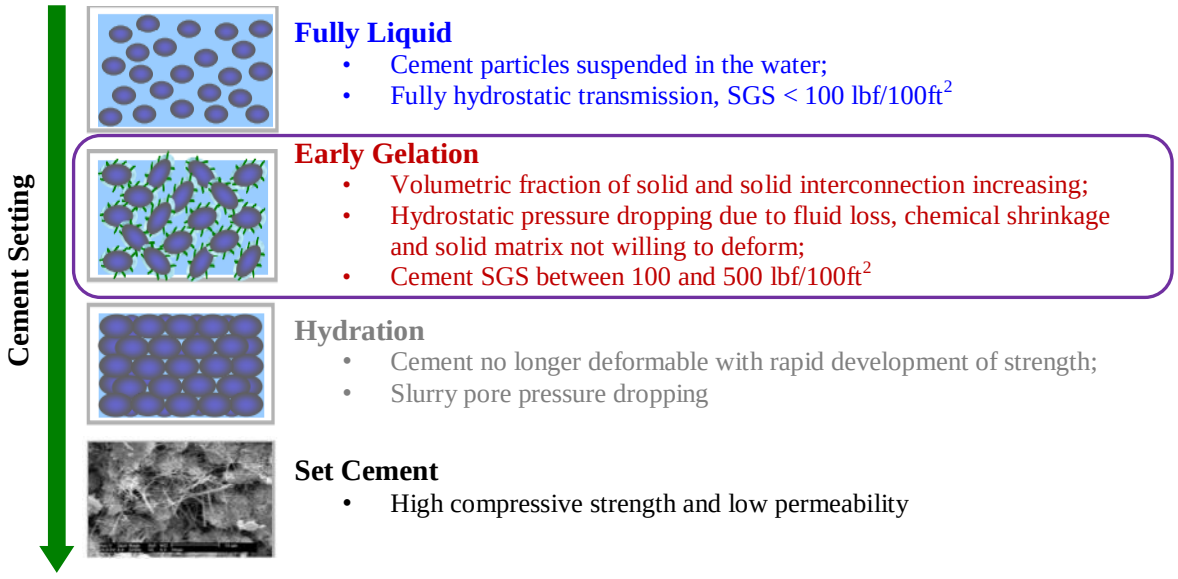

Figure 2.21. Microstructural development of cement (adapted from Kellingray 2007).

While fluid and solid mechanisms can be used to analyze the behavior of the slurry when it is either entirely liquid or solid, the transition gelation state is much more complicated to assess. As mentioned in Section 2.2.1.1, the cement slurry is actually a solid-fluid coupled media. By assuming a mixture of cement particles suspended in water, the effects of different additives can be easily demonstrated. For example, a dispersant agent can be added to the slurry design to increase the fluidity of the cement slurry. Figure 2.22 presents the viscosity results for a neat slurry as well as the same mix blended with a dispersant agent. As seen in the figure, a dispersant agent decreases the yield stress of the slurry and has little effect on the plastic viscosity. This decrease in yield stress occurs because the dispersant agent reduces the solid interaction and weakens the apparent network within the cement matrix. After the cement slurry begins to deform, the shearing occurs within the cement. The particle friction of cement slurry is similar and will, therefore, govern the plastic viscosity. The opposite is true when a thixotropic agent is used.

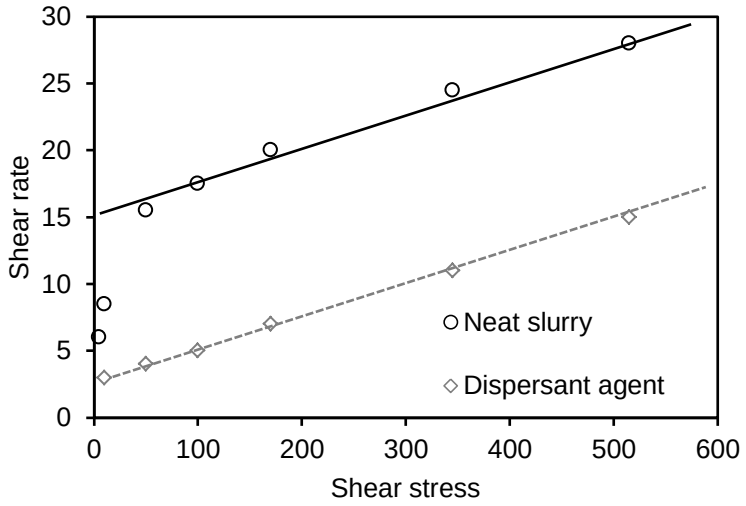

Note: Neat slurry – neat Class H slurry mixed at 15.8 ppg; Dispersant agent – same formulation mixed with 0.1 gal/sk of lignosulfonate dispersant

Figure 2.22. Effect of dispersant agent on slurry viscosity (Nelson 1990).

2.3.3.2 Principal properties

The microstructure of the cement slurry determines its properties. In order to capture the development of cement physical properties, fundamental concepts and variables should be used to characterize the chemical evolution of cement hydration and the micromorphology of the cement matrix.

Cement hydration is a chemical reaction in which the major compounds in cement form chemical bonds with water molecules and become hydrates or hydration products. Compositions of a slurry vary in components and their quantities. Curing conditions can affect strength development and hydration products. Nevertheless, the fraction of Portland cement clinker (including interground gypsum) that has fully reacted with water can always be employed to describe the hydration stage for a slurry design. In Section 2.3.3.1, hydration kinetics is discussed from the view of microstructural development. The cement microstructural development may be identical for cement when the fraction of cement clinker reacted with water is the same. This can be the case according to the findings by Zhang et al. (2010). As shown in Figure 2.16, although the initial set time is different for the same slurry designs blended with different chemical additives, the percent of cement clinker fully reacted with water are identical at the initial set. By using the percentage of cement clinker reacted with water to describe the cement hydration, the effects of other variables can be distinguished. For instance, the w/c ratio affects the physical properties of cement slurry significantly. Figure 2.23 presents a random distribution of cement particles. By comparing Figure 2.23a and Figure 2.23b, the effect of the w/c ratio is illustrated using the microstructural development of the cement matrix. When the w/c ratio is high, the cement particles are suspended in the water with little contact with other particles. As the distance between particles increases, the interactions are lower, and therefore a

high fluidity is observed. More hydration products must form in order to fill the space between particles. Therefore, a high w/c ratio design needs to achieve a higher reaction stage to develop the same cement matrix strength as compared to that of a low w/c ratio design.

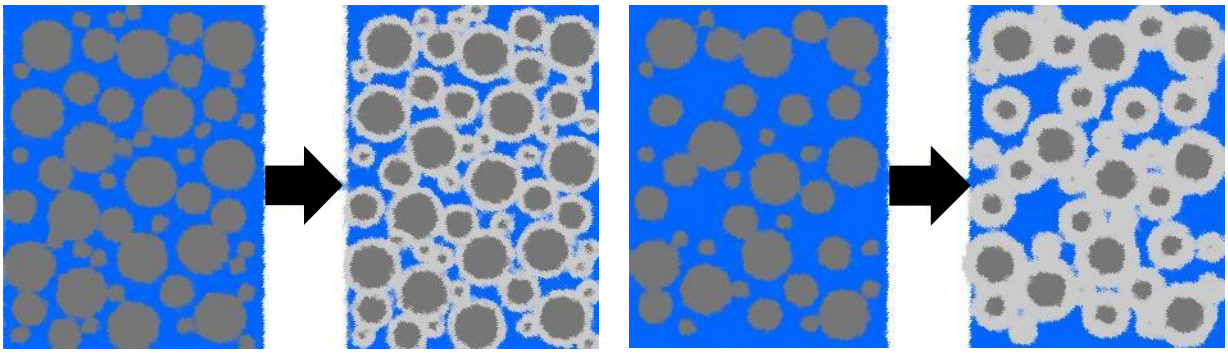

(a) Low w/c ratio (b) High w/c ratio

Figure 2.23. Effect of w/c ratio on cement matrix development (Zhang et al. 2010).

The interaction between solids can be described using the shear and normal bond strengths, as shown in Figure 2.17. The cement particles have a variety of angular shapes and the particle sizes are typically from 1 to 100 micrometers. Nevertheless, the rigidity of the cement slurry depends on the strength of the flocculated structure of cement matrix, more specifically the bridging strength of solids. In a stabilized slurry design, cement particles are suspended in the solution in a homogeneous state. The distance between particles can be determined when the w/c ratio is known. As cement hydrates, the volumetric fraction of solids increases and a flocculated structure is generated by the solid matrix connected by the hydration products, as shown in Figure 2.21. The shear bond strength and the normal bond strength between solids develop and keep increasing when more hydration products between different solid particles overlap each other. The compressibility of the cement matrix can be estimated when the volumetric fraction of solids and the strength between solids are known.

By knowing cement components and other additives and their physical properties, the volumetric fraction of solids and the percolation of cement matrix can be predicted with respect to the stage of cement hydration. The rigidity of the cement matrix can be characterized using the shear and normal bond strengths between solids. Finally, cement matrix properties can be reliably characterized at the microstructural scale instead of using laboratory tests designed to quantify an "apparent" mechanical property. Quantifying these cement properties instead of using apparent mechanical properties would lead to a more reliable and adaptable prediction of a cement's ability to mechanically prevent gas migration.

2.4 CONCLUSIONS

While SGS was originally adopted to describe the shear stress at interfaces, it is now defined as the slurry resistance to deformation under shear load. Experimental results indicate that gases can only invade the cement slurry from the time when the hydrostatic pressure is lower than the gas pressure to the time when cement develops enough rigidity to withstand the gas pressure (Cheung and Beirute 1985). This critical hydration period is defined as the transition time. As no effective approach to evaluating the potential for gas migration is available, the petroleum industry now tries to minimize, if not prevent, the risk of gas migration by shortening the transition time. API Standard 65-2 (2010a) provides the standards for determining the transition time, employing the concept of SGS for practical application by using commercial SGS measurement devices. Based on limited experimental results (Sabins et al. 1982; Stewart and Schouten 1988), 100 and 500 lbf/100ft^2 are standardized for all slurries and applied conditions (API 2010a). However, a sensitivity study has shown that no relationship was observed between

the transition time and the occurrence of gas migration (Roges et al. 2004; Rocha et al. 2013), though a slurry with a short transition time potentially reduces the time available for gas to infiltrate a cemented annulus. Experimental results (Zhang 2002; Zhu et al. 2012) also contradicted the linear relationship between the SGS and the hydrostatic pressure reduction in the classic theory stress theory. Although fluid loss and chemical shrinkage are recognized to be additional critical factors causing the hydrostatic pressure reduction, gas migration is a multi-phase problem (Beirute and Cheung 1990). Neither SGS nor fluid loss is able to predict the onset of gas-tight conditions in a cement slurry.

The limitations of SGS in evaluating the potential for gas migration drive the demand for improved cement matrix characterization. SGS may be applicable to describe the fluidity of the slurry in the beginning of early hydration. When a gel fluid forms, solids in the slurry primarily govern the mechanical properties. While the gel will deform under a shear mode, gases and other fluids actually need to break the bonding strength between solids and push solids aside in cement matrix, which requires characterizing the cement matrix strength and matrix compressibility. SGS is an "apparent" mechanical property and reflects resistance development within cement slurry. Nevertheless, SGS is not sufficient to characterize the compressibility and permeability of the cement matrix. It is also impossible to distinguish normal bond strength from the shear strength using SGS solely. All of these drawbacks in employing SGS in predicting gas migration indicate the need for replacing SGS as the metric to predict gas-tight conditions. A more accurate approach for replacing SGS is desirable for cement matrix characterization, in which fundamental concepts and variables are used to characterize the solid-fluid coupled matrix.

3.0 A NEWLY-DEVELOPED WELLBORE SIMULATION APPARATUS TO STUDY PERFORMANCE OF OIL WELL CEMENTS UNDER IN-SITU BOREHOLE CONDITIONS

3.1 INTRODUCTION

Annular gas migration has long been recognized as one of the most troublesome problems in the petroleum industry (Bonett and Pafitis 1996). Due to a pressure imbalance at the face of gas-bearing formations, gases and other fluids can invade into the annulus. The severity of the problem ranges from very hazardous, such as a blowout when well control is lost, to the most marginal, such as a sustained casing pressure (SCP) of a few psi at the wellhead. Statistical analysis shows that about 15% of primary cement jobs require remediation and squeezing due to inadequate slurry design or a poorly executed cement job (Newman et al. 2001). U.S. Energy Information Administration (EIA) statistics show that the cost of drilling a natural gas well increases dramatically when remediation efforts are necessary. In 2007, the nominal cost per natural gas well drilled in the U.S. was $3.9 million (EIA 2014). In Pennsylvania, a recent report indicated that $7.6 million is invested, on average, for each Marcellus shale gas well (Hefley et al. 2011). While primary cementing costs are about 5% of the total well cost, an additional 12% of the total well cost is incurred when squeezing is required. However, interzonal gas

communication without surface manifestations is difficult to detect. Thus, the efficiency of squeezing in such circumstances is very poor.

In order to understand the physical process of gas migration at a fundamental level, extensive research has been performed since the 1960s. A range of gas migration laboratory-testing devices have been developed to study the mechanisms of gas migration and determine whether a slurry design is gas-tight. Despite the extensive amount of research dedicated to solving this problem, successful lab experiments that allow a generalized and quantitative prediction of gas migration have not been reported (Nelson 1990). Thus, no laboratory procedure or device is recognized universally for characterizing the ability of a cement slurry to mitigate, if not prevent, gas migration. In addition, an API standard, which is aimed at measuring the ability of a cement slurry to control gas migration, does not exist.

Below, a history of wellbore simulators for assessing the potential for gas migration and a discussion regarding their limitations is provided first. Next, the details of a newly-developed WSC are provided. The WSC is a laboratory-scale device, which can be used to evaluate the potential for gas migration under representative in-situ borehole conditions. Experimental results verify the applicability of the WSC and the benefits of the WSC over other existing apparatuses are then summarized.

3.2 GAS MIGRATION TESTING

Experimental simulators in the literature can be categorized into two main types: large-scale pilot simulators and bench-type devices. Both types of simulation devices, along with their strengths and limitations, are described below.

3.2.1 Large-scale pilot simulators

The purpose of large-scale devices is to simulate in-situ behavior of a cement column under in-situ conditions. Typical large-scale pilot simulators contain cement columns of approximately 10 to 30 ft long, requiring a significant amount of cement and space. These long cement runs can present challenges in controlling the physical properties of cement slurries and conditions under which the tests are performed. As a result of these limitations, large-scale devices capable of simulating cement hydration within a wellbore are rare.

The earliest large-scale simulator found in literature (Figure 3.1a) was first developed by Carter and Slagle in 1972, and later upgraded by Carter et al. (1973). The purpose of this device was to study the effect of important factors on the pressure behavior of a cement column under "more closely simulated well conditions". As can be seen in Figure 3.1a, a 2-7/8 in tubing with an outer diameter of 4.5 in was centralized inside a 7-in casing. A simulated permeable formation (100 md) was attached to the 7-in casing at 5 ft high from the bottom of the annulus. The cemented annulus was 30 ft long and required a slurry volume of approximately 4.7 ft^3. Cement slurries and drilling fluids were pumped into the inner casing string and circulated through the annulus, which replicated the cementing process in the field. This device used two steel casings to provide an annulus between casing string. However, a large amount of cement slurry was required and the casing string could not be reused once the cement hardened in the annulus.

In 1976, Garcia and Clark constructed a gas flow model to study the influence of non-uniform cement setting along the depth of the wellbore by changing the curing temperature at mid-depth of the cement column. This differential curing reflected the representative temperature variation along the depth of the wellbore. Instead of providing an actual annulus as

Carter and Slagle (1972) did, a 2-in pipe was used to simplify the setup. As shown in Figure 3.1b, the model consisted of a 20-ft long vertical pipe, resulting in a slurry volume of approximate 0.45 ft^3. An external heating tape was installed 11 ft from the bottom and a pressure sensor was located at 5 ft from the bottom. A regulated gas supply was provided at the bottom and isolated from the cement slurry by a porous aloxite plate. The gas pressure was regulated to a value equal to the hydrostatic head of the cement column in the pipe. Cement slurry halfway from the bottom was heated using the heat tape to cause the initial set to occur earlier than other portions of the cement along the pipe. Heating the cement at this point accelerated the setting time and isolated the column below this point from the fluid head of slurry above. If a pressure drop occurred at the bottom of the column, gas would flow across the aloxite plate and be measured by a flow meter. This test apparatus reduced the amount of cement slurry required for testing. However, the borehole temperature of other sections was not under control and only qualitative results were obtained.

In order to study the effect of drilling mud above the cement column on pressure evolution, Levine et al. (1979) applied the initial overburden pressure by adding a water column above the cement section. As shown in Figure 3.1c, the simulation apparatus consisted of a 1-in tube centered inside a 4-½-in casing. The cemented annulus was 12 ft long, requiring a slurry volume of approximate 1.1 ft^3. A 35-ft high fluid section was attached on top of the cement to simulate the mud above the cement. The 10-ft cemented annulus was embedded in a heating system, which provided a high-temperature borehole. Pressure and temperature sensors were installed in the cemented annulus to investigate pressure behavior while circulating and curing the cement. A regulated gas supply was installed similar to the design of Garcia and Clark's test apparatus (1976). This apparatus attempted to consider the high hydrostatic pressure above the

tested cement and high borehole temperatures, simulating a cement interval located at larger borehole depths. Only a few variables were considered with this experimental setup.

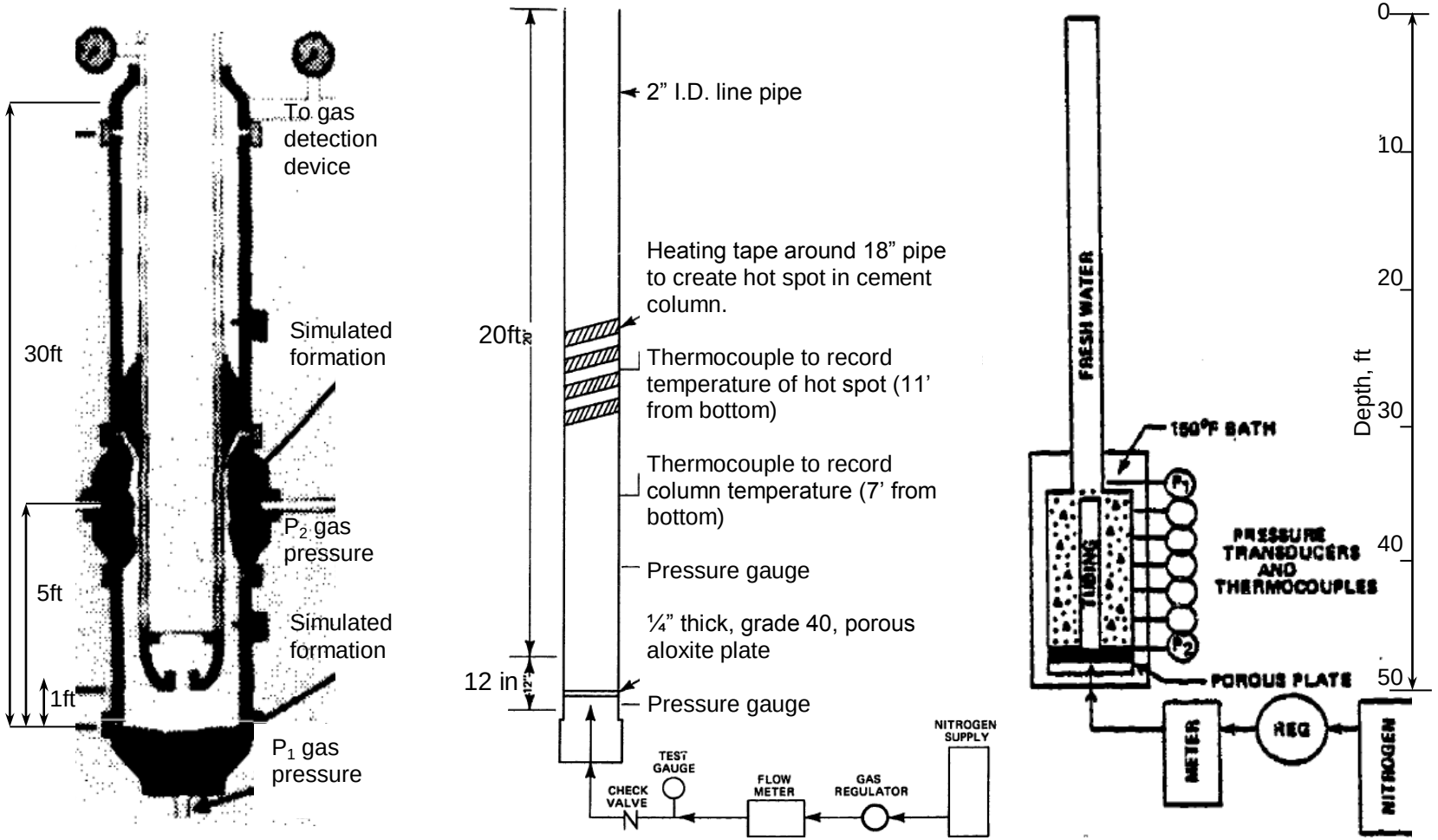

(a) Large-scale simulator by Carter and Slagle (1970)

(b) Gas flow model by Garcia and Clark (1976)

(c) Pressure simulator by Levine et al. (1979)

Figure 3.1. Large-scale devices for pressure-transmission tests.

Later, modifications that allowed for more variables to be studied were applied based on the same design philosophy but with the focus shifted to mechanisms of gas migration. Tinsley et al. (1979) made a great improvement to the basic design of large-scale simulators by adding a piston on the top of the cement column in the annulus. The piston allowed a high mechanical load (500 to 1000 psi) to be applied on the top of the cement, which simulated the hydrostatic pressure generated by cement slurry and drilling mud above in a deeper cement section. For example a 1,000 psi hydrostatic pressure represented a section located at a 1,200 ft depth. As shown in Figure 3.2a, the test cell consisted of a vertical section of 2.07-in diameter pipe with an 18-in long annular core inserted at the center of the pipe. The center core could be of either a permeable or non-permeable material. The non-permeable core consisted of a 2-3/8-in tube in a 4.5-in pipe simulating a zero fluid loss condition. The permeable core consisted of a packed resin/sand mixture enclosed in perforated 7-¾-in pipe to simulate a fluid-accepting formation. Slurry entry and exit lines were installed at the top and bottom of the cell. A gas entry line near the bottom of the cell was installed to simulate a pressurized gas zone with pressurized nitrogen gas used in all tests. The inclusion of the piston ensured the capability of simulating high-pressure conditions. However, flow control of migrated gas was not considered in this setup.

In 1982, Sabins et al. introduced a system for measuring gas volume flow through the cemented column and the fluid loss from slurries to the wellbore simulator. By introducing SGS in the analysis to describe the resistance of hydrating cement, CSGS and OSGS were established experimentally to determine the transition time in which gas invasion can occur. As shown in Figure 3.2b, the lower section of this test cell consisted of a 12.5 ft long, 2-in diameter pipe that included three l.5-in constrictions, which simulated borehole irregularities. The upper portion was filled with water separated from the test slurry by a layer of water-base drilling fluid. Coiled

tubing with a 3/8 in diameter was inserted into the top of the 2-in pipe. The 50 ft long coiled tubing section allowed simulation of a longer section of 2-in pipe, through which a pressure restriction or decrease in pressure transmission could occur because of cement gelation. This tubing extended down below the upper exit valve, which allowed a water cap to be placed at the top of the 2-in pipe after it was filled with the test slurry. Any gas that flowed through the test chamber from the gas-entry line could exit the test cell through the water layer and could enter the gas-trap sight glass. This trap allowed for measurement of the total accumulated gas-flow volume at any time during the test. Fluid loss at this point can also be simulated by removing small volumes of water through the fluid-loss valve. However, due to the complexity of the setup, volume changes of the system were difficult to quantify.

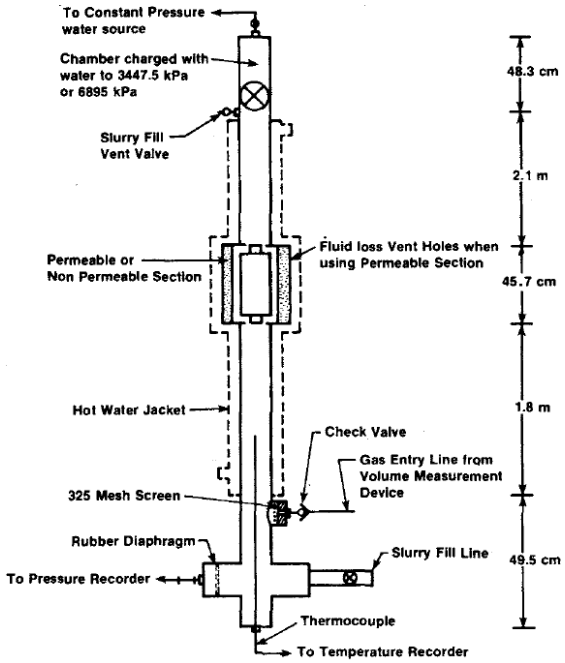

(a) Schematic diagram of test apparatus used to study gas leakage by Tinsley et al. (1980)

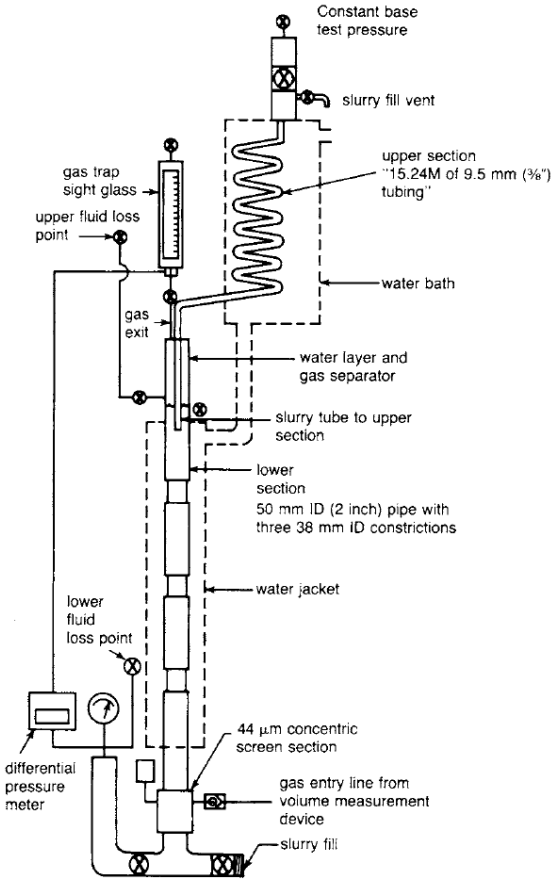

(b) Schematic of test fixture for pressurized gas-percolation and pressure-transmission tests by Sabins et al. (1982)

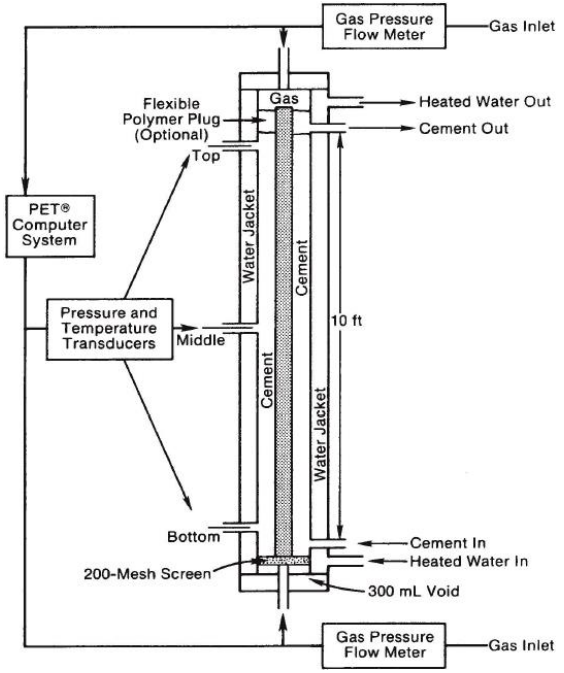

(c) Annular gas flow laboratory testing apparatus by Bannister et al. (1983)

Figure 3.2. Large-scale gas flow simulators.

Bannister et al. (1983) modified Carter and Slagle's design and created a volume-controlled system. As shown in Figure 3.2c, the annular cement test cell consisted of a 2-in test cell surrounded by a heating jacket. A 1-in outside diameter pipe capped at both ends was centralized in the 2-in pipe. The test cell was 10 ft long, forming an annulus of 0.15 ft^3. Three pressure transducers and temperature thermocouples were housed at equal distances from the top to the bottom. Cement slurries were circulated through the bottom of the cell. Heating of the test cell was accomplished by a water heat exchanger (100 to 300 ℉). Gas pressure, up to 260 psi, was applied to the top of the test cell. A porous steel plate was located at the bottom for simulating fluid loss (if desired). Similarly, gas could enter at the bottom of the cell and was relieved through pressure-relief valves also housed in the pressure ports. This test apparatus was originally developed to study filter cakes generated from cement fluid loss and to evaluate the gas conductivity of hydrating cement. However, it provided a rudiment for high-temperature and high-pressure (HTHP) bench-type devices, which are much smaller and easy to operate.

3.2.2 Bench-type devices

Smaller, laboratory-scale devices are more advantageous due to their ease of use and reduced cost. Compared to large-scale devices, the required volume of cement (approximately 25.6 in^3) for bench-type devices is small. The first bench-type device was developed by modifying the API fluid-loss cell (Cheung and Beirute 1982). Figure 3.3 presents the typical laboratory-scale test cell developed by Beirute and Cheung (1990). The device consisted of a 10-in long test cell. A hydraulic piston with a 325-mesh screen was inserted into the cell through the top, simulating a very permeable formation at the top of the cell. A simulated hydrostatic head was applied by pressurizing the piston with mineral oil. The applied overburden pressure was capable of

reaching 1,500 psi, representing a pressure condition approximately 2,000 ft below surface. The test cell was heated to the test temperature by means of a heat tape wrapped around the cell. The hollow piston shaft was connected to a backpressure receiver where water filtration from the top of the cell was collected. Nitrogen gas entry was simulated by connecting a nitrogen gas source to the bottom of the cell. The slurry pore pressure was recorded continuously by using a pressure transducer located in the middle of the cell. By comparing Figure 3.2c and Figure 3.3, it is obvious that the bench-type HTHP device is a scaled design of the large-scale simulator developed by Bannister et al. (1983).

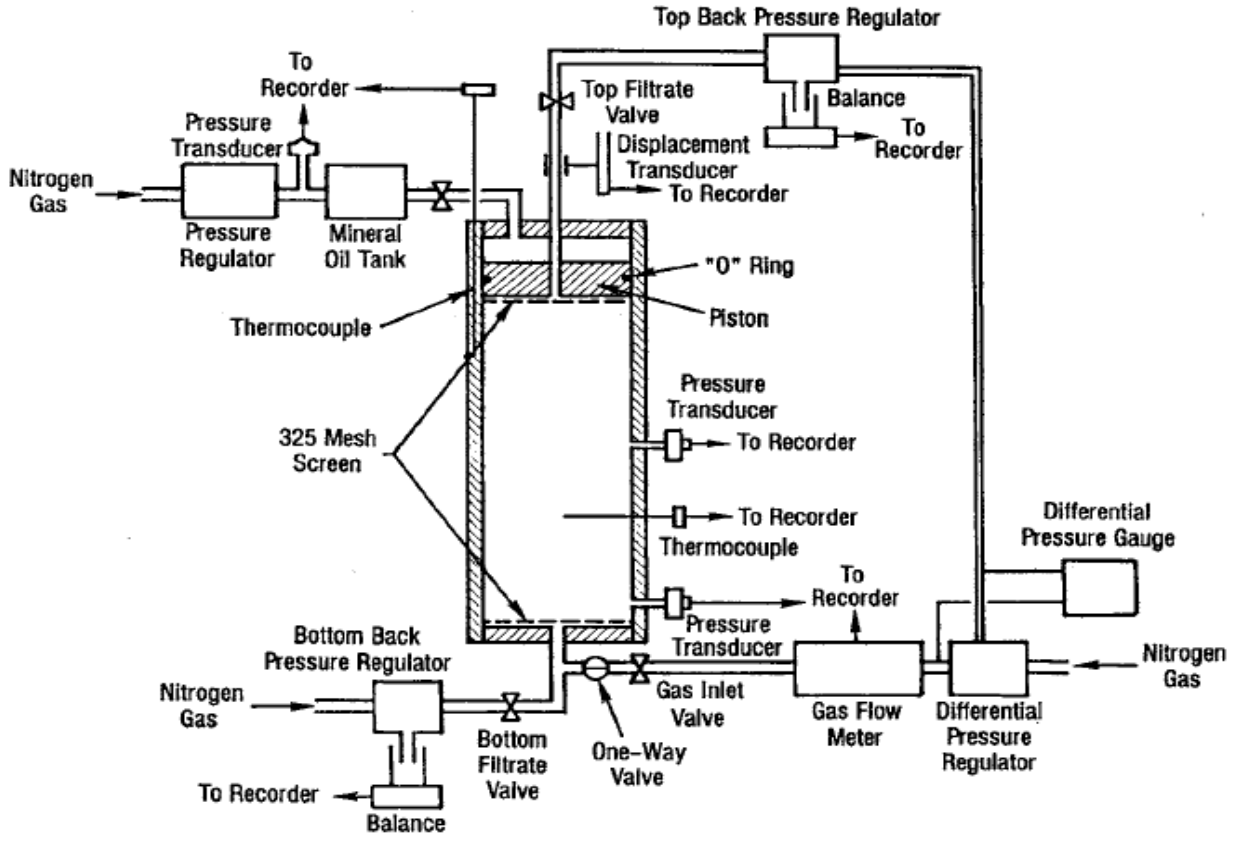

Figure 3.3. Cement hydration analyzer (Beirute and Cheung 1990).

Currently available commercial HTHP devices include the Model 7200 CHA by Chandler Engineering (2014b, 2014c), the Fluid Gas Migration Analyzer #120-57 by OFITE (2014b), the Model 300 Gas Migration Apparatus by CTE (2014b), the Fluid Migration Analyzer by Sanjel Corporation (2014) (from Canada), and the Fluid/Gas Migration Analyzer TG-7150 by Shenyang Taige Oil Equipment (2014) (from China). HTHP devices are typically referred to as CHAs. Although the commercial CHAs seem different from each other, the philosophy and design is basically the same as the modified API fluid-loss device developed by Cheung and Beirute (1982), as shown in Figure 3.3. All available CHAs attempt to replicate the in-situ HTHP curing history by controlling the applied pressure and temperature. The comparison of specifications between different commercial CHAs is shown in Table 3.1. In addition to measuring the cement susceptibility to gas migration, the Model 7200 is advertised to be capable of measuring 1.) shrinkage during curing, 2.) gas permeability of the cement, and 3.) degree of hydration (Chandler Engineering 2014b). However, little information about degree of hydration is available in the instruction manual for the Model 7200 (Chandler Engineering 2014c). Review of the design indicates that the Model 7200 can determine the hydration stage based on temperature increases and decreases but is not capable of analyzing important details of cement hydration.

Table 3.1. Specifications of commercial CHAs.

CHA model	Temperature range	Maximum pressure
Model 7200 (Chandler Engineering)	Ambient to 325 ℉	1,000 psi
#120-57 (OFITE)	Ambient to 400 ℉	2,000 psi
Model 300 (CTE)	Ambient to 212 ℉	3,000 psi

Another notable apparatus, reported by Parcevaux (1984), was developed in an attempt to eliminate the artificial side-effect of fluid loss on slurry pore pressure. As illustrated in Figure 3.4, this equipment was composed of one 2-in diameter by 4 ft long hydrostatic pressure cell (HPC) in which cement pore pressure reduction was recorded versus time. A 2-in diameter by 2 ft long dynamic permeability cell (DPC) capable of measuring the gas conductivity of the cement column is also included. Both cells were placed in a thermostatic oven, and the cement slurry was cured under an initial pressure of 580 psi. The head pressure source was computer-controlled to maintain a differential pressure of zero psi between the top and bottom of the HPC. When the slurry pore pressure indicated by the pressure transducer connected to the bottom of the HPC dropped by 10%, the DPC was placed under a 72.5 psi gas differential pressure and gas outflow rates were monitored. As pressurized gas attempted to invade into the cement matrix, the gas conductivity varied with time. This device led to the idea of separating the effects of different variables on hydrostatic pressure reduction, such as fluid loss. However, no relationship was clearly established between the slurry pore pressure reduction and the differential pressure between the top and bottom of the cement column. Moreover, the operation of two different cells induced significant variability into the experiment.

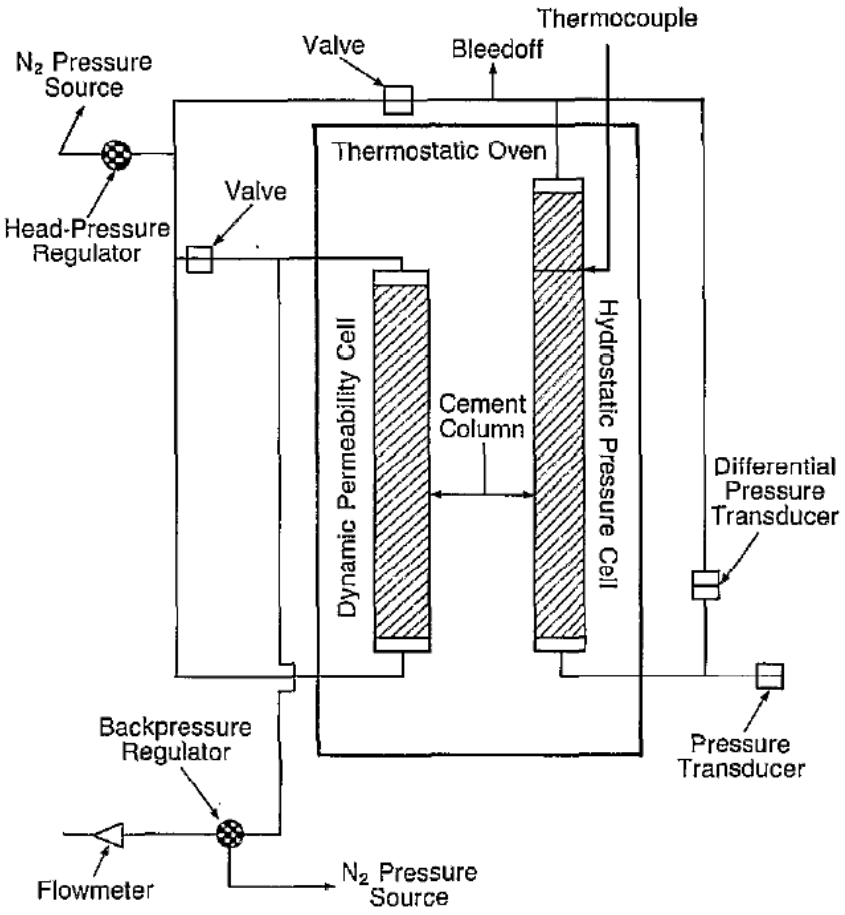

Figure 3.4. Dynamic permeability apparatus (Parcevaux 1984).

3.2.3 Discussions

Currently, CHAs are used to test cement slurries in the lab as an attempt to design appropriate slurries for in-situ borehole conditions. These devices have been adapted for routine use to examine whether slurry designs are gas-tight. However, three factors related to these devices can unduly affect the ability to characterize the potential for gas migration (Nelson 1990). First, reabsorption of free water in inlet or outlet fittings can delay the pore pressure decrease during cement hydration. When applying hydrostatic pressure, water can be filtrated from the slurry and block the fittings. Second, fluid loss at the gas inlet or outlet may result in an impenetrable

filter cake, reducing the probability of gas infiltration. Finally, a constant hydrostatic pressure is typically applied throughout the duration of the test. This does not represent the actual conditions in the wellbore, since in the wellbore the actual hydrostatic pressure is reduced overtime due to the hydration of the cement column above. A short length of the cement column (8 in) is tested in CHAs. Therefore the slurry pore pressure is equal to the applied overburden pressure until the slurry develops sufficient strength to withstand the applied overburden pressure. Therefore, the hydrostatic pressure reduction observed in the simulation device will occur at a later time than when the pressure from the above cement column declines. The high overburden pressure maintained in the simulation device (typically 1,000 psi) can result in an underestimation of the hydrostatic pressure reduction and therefore the potential for gas migration.

Another common problem existing with these simulation devices and techniques described is that a standard procedure has not been developed to satisfactorily test a cement slurry under realistic borehole conditions. All of the scaled-down CHAs attempt to reproduce the physical process of cement hydration and/or gas migration by replicating the pressure and temperature history that will be experienced in the field. After a cement slurry is placed in the test cell, the temperature and pressure are increased as the cement slurry is pumped through the steel casing. The pressure and temperature will reach a maximum as the slurry reaches the bottom of the hole. Later, the temperature and pressure will be lowered to the prescribed values which replicate the condition at the depth of interest.

Nevertheless, factors different from those considered will change the cement hydration significantly, such as w/c ratio and chemical additives. Moreover, other factors such as mud cake, casing eccentricity, inclined annuli and low-pressure, permeable zones cannot be

investigated using the existing CHAs. It is important for wellbore integrity that both their individual and combined effects on the gas migration be studied and quantified.

In summary, the performance of a cement slurry in the borehole is unpredictable, regardless of whether the cement slurry is shown to be gas-tight using the laboratory test devices. Available laboratory equipment and procedures cannot realistically duplicate certain parameters, such as rock formation, borehole geometry and hydrostatic head, which can be critical for designing gas-tight slurries. Moreover, current industry practices mainly rely on empirical principles when designing cement slurries for reducing the risk of gas migration. This process, while it may be helpful, is insufficient to quantify variables affecting cement behavior. Therefore, a means to scale the in-situ wellbore environment to laboratory conditions and a more fundamental manner is needed. This will help to reduce variations between measurements resulting from setup and operational procedures; thereby making experimental standardization of the process possible.

3.3 NEWLY-DEVELOPED WSC APPARATUS

A laboratory-scale WSC has been developed to study the performance of oil well cement (OWC) slurries by simulating the pressure reduction in the cemented annulus and possible gas invasion under in-situ borehole conditions. In addition to the device itself, specific casting and testing protocols have been developed, which detail the procedures required for proper operation of the equipment. Compared to existing CHAs, the WSC is capable of considering a broader range of parameters, such as formation properties, mud cake and eccentricity. Moreover, the mechanism

of hydrostatic pressure reduction can be predicted by introducing fundamental concepts or variables to characterize the cement hydration.

3.3.1 WSC components

3.3.1.1 Testing device

A schematic of the WSC is presented in Figure 3.5 with photos of the device shown in Figure 3.6a and Figure 3.6b. From the inside portion outward, the WSC is comprised of a steel casing, cemented annulus and surrounding rock formation. A piston is used to apply a mechanical load on the slurry to simulate a hydrostatic pressure representative of any depth of interest. Table 3.2 presents the dimensions of the current laboratory setup. The cylindrical pressure chamber is certified up to 1,500 psi operational pressures, which is well above the pressure ranges associated with surface and intermediate casings of a typical borehole. Depending on the simulation requirements, the pressure chamber can be upgraded to a higher working pressure and the geometry of the setup can be modified.

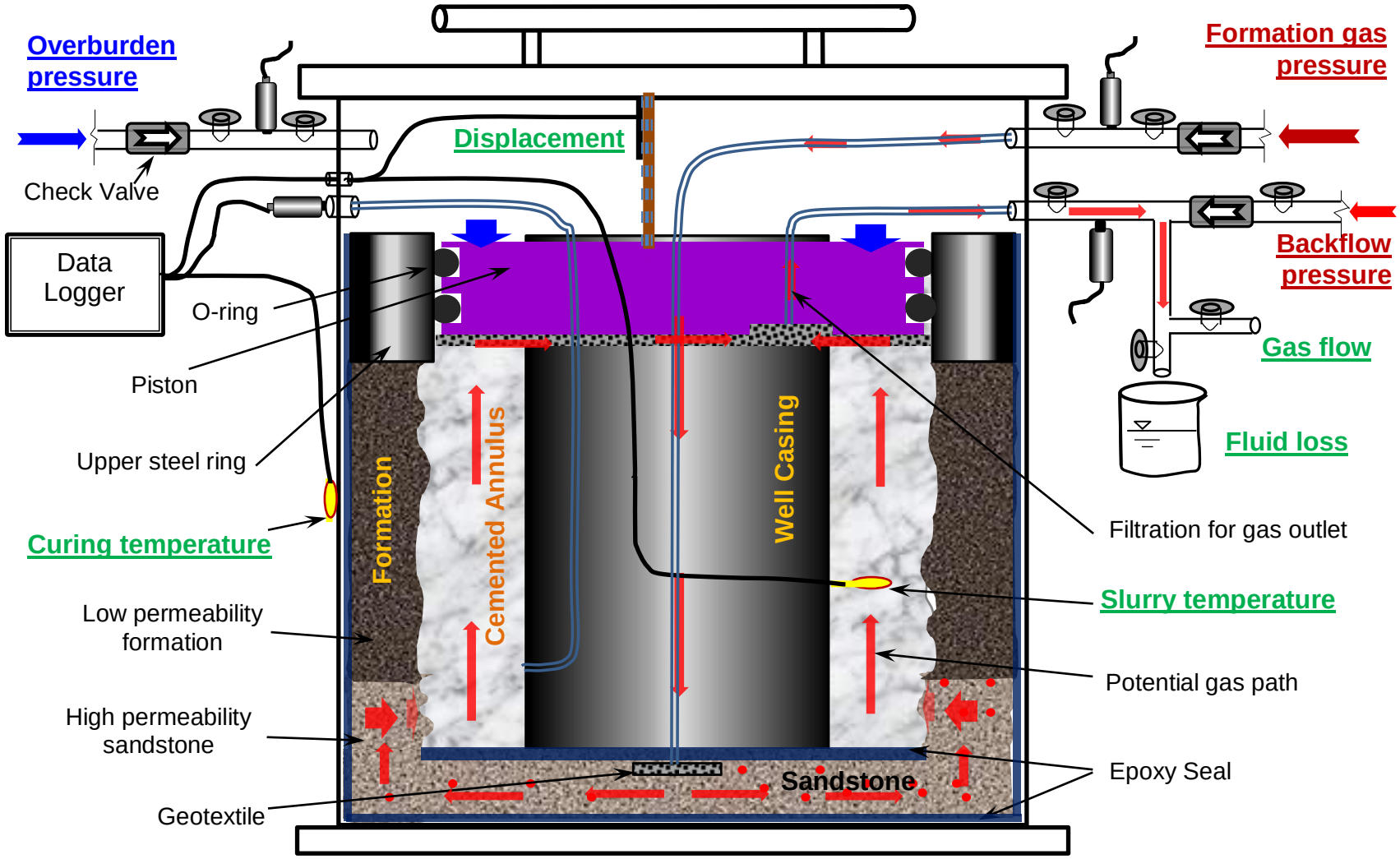

Figure 3.5. Schematic of WSC.

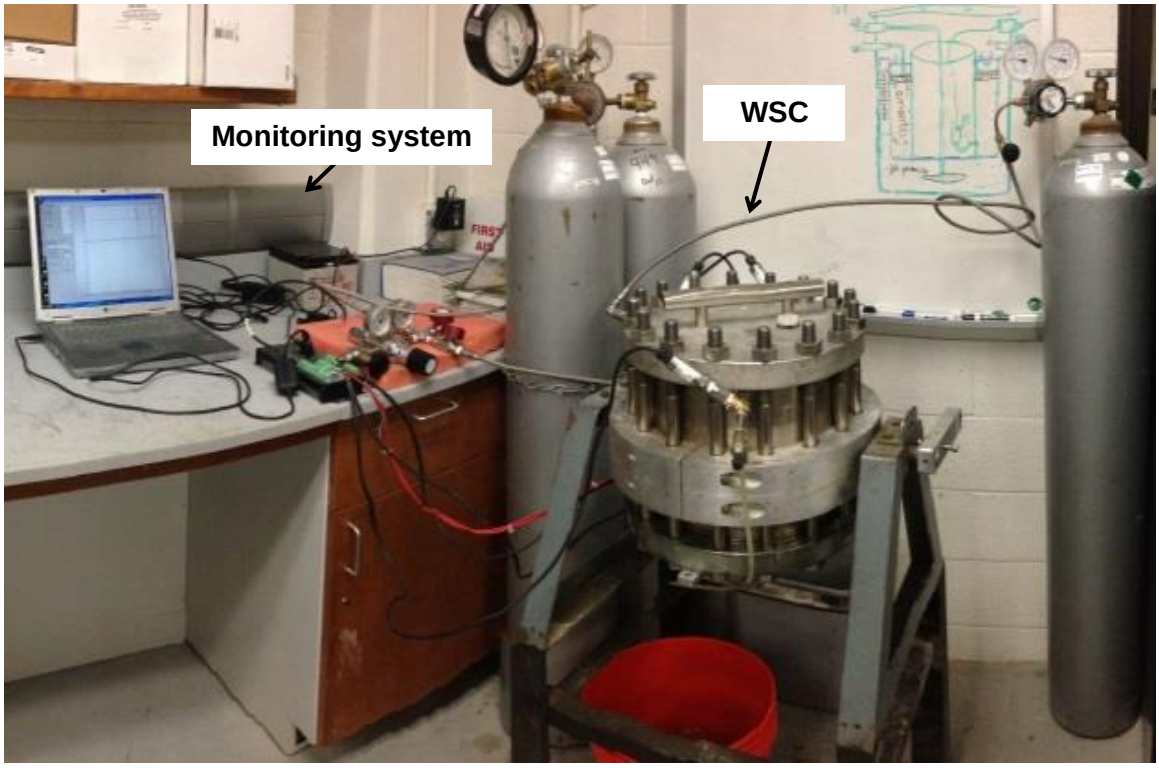

(a) Overview

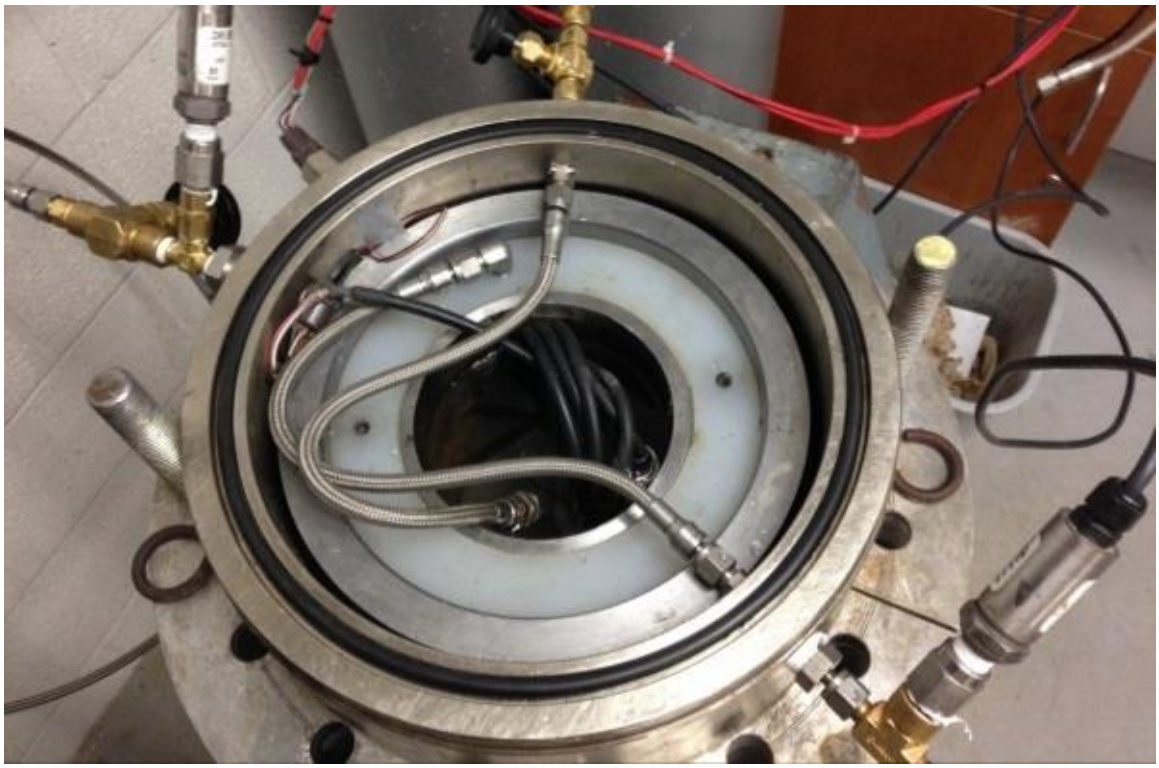

(b) Formation and inner assembly

Figure 3.6. View of WSC.

Table 3.2. Dimensions of WSC apparatus.

Category	Parameter	Value
Pressure chamber	Inner diameter	9.75 in
	Inner height	10.0 in
	Maximum working pressure (Safety factor = 3.0)	1,500 psi
Formation	Outsider diameter	9.4 in
	Borehole diameter	8.0 in
	Total height	5.0 in
	Thickness of low permeability upper formation	3.5 in
	Thickness of gas-dispersion sandstone layer (high permeability)	0.5 in
	Thickness of bottom sandstone layer	1.0 in
	Permeability of sandstone layer	See Table 3.4
	Porosity of sandstone layer	See Table 3.4
Upper ring (housing for the piston)	Total height	3.5 in
	Inner diameter	7.95 in
	Outsider diameter	9.5 in
Inner steel casing	Outside diameter	5.5 in
	Length	7.5 in
	Polished section length	3.5 in
	Non-polished section length	4.0 in
Piston	Thickness	2.0 in
	Outsider diameter	7.995 in
	Inner diameter	5.555 in
	Geotextile thickness at bottom of piston	0.25 in
Cement slurry	Column length	5.5 in
	Total volume	146 in^3

3.3.1.2 Monitoring system

The WSC is equipped with a comprehensive monitoring system that tracks pressures, temperatures, and piston displacement. The backflow system allows the WSC to evaluate the effects of fluid loss on the potential of gas migration for a controlled rate of fluid loss when desired. The extensive pressure control/monitoring system is essential for ensuring field conditions are being replicated in the chamber. The temperature monitoring system incorporated in the WSC allows the hydration stage of the cement slurry to be determined at any point in time

throughout the simulation. This provides researchers with the opportunity to parameterize the slurry designs and wellbore conditions.

After cement slurry is placed in the annulus, the variables underlined in Figure 3.5 can be monitored continuously throughout the experiment, including:

1.) Slurry temperature

A thermocouple is embedded in the slurry at mid-depth of the length of the formation. The slurry temperature is recorded throughout the simulation. Temperature-time history is a key parameter for characterizing the hydration of the cement slurry.

2.) Formation/chamber temperature

A thermocouple is installed on the surface of the chamber. The temperature under which the cement is hydrating is recorded throughout the simulation. This temperature can be controlled by placing the chamber in a temperature controlled water tub or environmental room.

3.) Slurry pore pressure

A hole through the inner steel casing is located at 1.0 in above the bottom of the slurry. A pressure transducer is installed at this location to measure the pore pressure in the slurry column.

4.) Applied overburden pressure

Overburden pressure is simulated using nitrogen gas to apply a pressure on the top of the piston. The space in the chamber is filled with water to reduce the variability in pressure and temperature within the chamber when applying the gas pressure. A pressure transducer and a regulator are installed to control the applied overburden pressure. Currently, a constant overburden pressure is applied to the piston. Although, the pressure

can also be slowly reduced throughout the test to simulate setting of the cement column above the depth at which the evaluation is occurring. The relationship between the effective overburden pressure and the cement hydration stage is currently being developed as part of another companion study.

5.) Formation gas pressure

Gas can be injected into the artificial formation sandstone layer to simulate pressurized gas in a gas-bearing formation (only high permeability formation). A pressure transducer, a pressure regulator and a check valve are installed to control and measure the formation gas pressure.

6.) Backflow pressure

A backflow pressure is applied and controlled with a check valve. The purpose is to provide an outlet for fluid and gas, which simulates fluid loss from slurries into the formation. Also, the pressure difference between formation gas pressure and backflow pressure provides a pressure gradient, thereby forcing gases to flow up through the settable cement matrix to the lower pressure zone.

7.) Backflow free water and gas volume

When gas migration is simulated, two measuring containers are connected to the backflow valve to determine the weight of free water bleeding from the cement matrix, and gas flowing through the cemented annulus. It should be noted that this is a lower bound estimate of the total free water from the cement matrix as the fittings will hold some water. The storage capability of the fitting must be evaluated to obtain quantitative measurements of free water and gas volumes.

8.) Piston displacement

The piston displacement within the annulus is continuously measured. A displacement measuring device was developed that can operate in high-pressure and water-saturated environments. It consists of strain gauges and a deformable spring gauge. By calibrating the deformation and the movement of the spring gauge, piston displacement can be determined.

9.) Permeability of wellbore section

After the cement hardens, the permeability of the borehole section can be determined. This can be done by measuring the gas/water flow through the tested wellbore section. A differential pressure can be applied to the formation gas pressure port and the backflow pressure port. The recorded flow rate indicates the permeability of the entire wellbore section. As the formation permeability is predetermined in the casting process, the flow through the cement matrix and the cement-casing and cement-formation interfaces can be determined by subtracting the measured flow rate from the flow through the formation.

3.3.2 Advantages of WSC

The WSC is capable of experimentally evaluating an in-situ borehole condition representative of a single point along the depth of a surface or intermediate casing. It is also capable of reproducing the flow path and spatial distribution of gas intrusions. Gas intrusion into the annulus may result in channels and/or a localized porous region when the cement gels. Channels may form within the cement matrix or along the casing/annulus interface or annulus/ formation. Each of these can affect the risk of inter-zonal communication. If gas migration occurs, the experimental annulus can be investigated using non-destructive testing techniques, such as a CT

scanner, to determine the nature and path of the gas flow. The key features and advantages of the WSC are as follows.

(1) Real-scale wellbore section

Except for some of the large-scale simulators, as discussed in Section 3.2.1, or field experiments that have been performed, none of the existing simulators have dimensions comparable to those of actual wellbore section. In the WSC, a predetermined wellbore section is simulated with the following components (from the inner portion outward): steel casing, cemented annulus and surrounding rock formation. Depending on the simulation requirements, any sized wellbore section can be simulated. Eccentricity of the casing can be simulated as the position of inner casing string can be relocated accordingly. Additionally, inclined annuli can be simulated by adjusting the position of the WSC from plum.

(2) Formation characteristics

Representative sandstone formation specimens are cast of a cementitious material and coated with epoxy in accordance with a specialized procedure developed to replicate specific in-situ borehole conditions. Two distinct types of formations were cast: 1.) high permeability and 2.) low permeability formation. The formations with a high permeability are used to evaluate gas migration potential, while the low permeability formations are used to evaluate the slurry pore pressure reduction in the annulus as the slurry hydrates. Even though each formation serves a different purpose, the procedures for constructing each are similar. The only difference in the construction of these formations is the mixture design used for the cementitious material used to cast the formation. The dimensions, permeability, surface roughness and other formation properties are controlled by adjusting the mixture design, the casting method, and the preparation process. When a high permeability formation is used, the effect of porosity and pressurized

gases in the formation can be considered. Moreover, mud cake can be prepared on the surface of high permeability surface so its effect on gas migration can be evaluated. None of the existing devices in literature are able to consider the effect of formation conditions when evaluating the gas migration potential of cement slurries.

(3) Variable effective overburden pressures

For all commercial CHAs, the applied overburden pressure is kept constant. Although, the literature (Sabins 1982; Cheung and Beirute 1985; Brufatto et al. 2003) indicates that the hydrostatic pressure drops with the development of cement hydration and fluid loss in the early hydration stage, which exacerbates the potential for gas migration. Researchers attempted to simulate varying effective overburden pressures (Sabins 1982), but the criteria for adjusting effective overburden pressures have not been well established. A significant reason for the development of the WSC is to establish a relationship that better represents the reduction of effective overburden pressure transmitted from the above cement section according to the hydration stage of cement slurry, such as the hydration stage of the cement (Saul 1951; Carino and Lew 2001). When this is achieved, the influence of wellbore temperature, pressure, w/c ratio and chemical additives can be evaluated.

(4) Permeability of hardened cement in wellbore section can be defined

The permeability of the set cement can be measured in the laboratory, but it is difficult to test within a cemented wellbore. In the WSC, the permeability of the wellbore section can be measured without disturbing the cemented annulus. The flow rate through the borehole section is measured by monitoring the differential pressure between the top and bottom of the cemented annulus. The permeability of the cement matrix and the casing-cement and cement-formation can be determined since the formation permeability is already known.

3.3.3 Formation production

A technique has been developed for casting the low and high permeability formations from a cementitious-based mixture, as shown in Figure 3.7. This is advantageous because any prescribed porosity and permeability representative of an actual in-situ formation can be replicated in an inexpensive manner. While the casing can be reused, a new formation must be cast for each simulation, making it imperative that the formation casting process is repeatable. The formation gas can be introduced into the cemented annulus through a discrete location, as would be the case if coming through a fracture in the formation, or in a more dispersed manner representative of gas movement through a high permeability formation. When simulating the latter scenario, the bottom portion of the formation is cast as sandstone with a high permeability and the upper portion of the formation in the chamber is cast to have a low permeability, as shown in Figure 3.5.

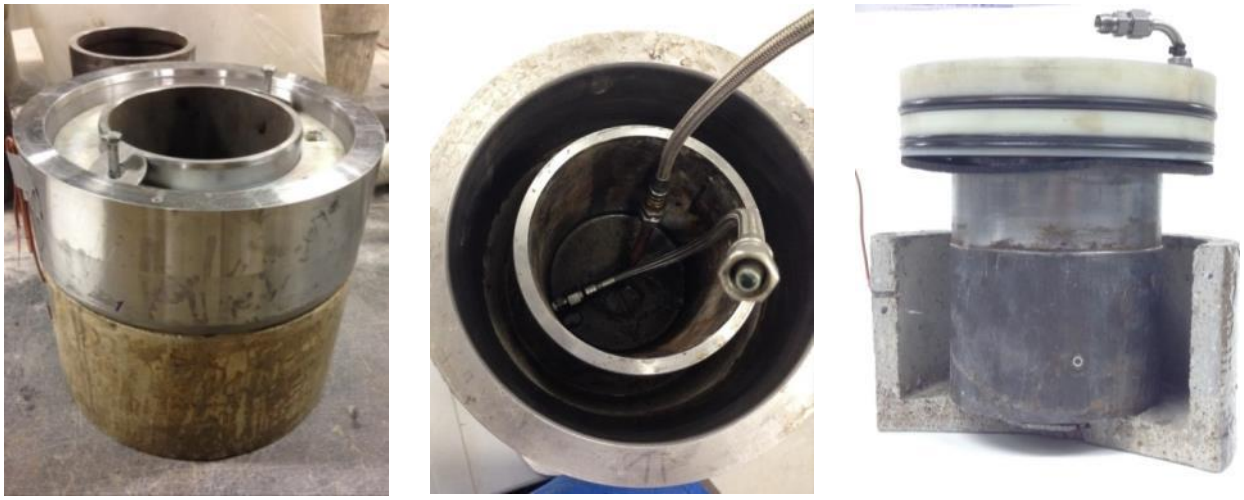

(a) Overview (b) Top view (c) Profile view

Figure 3.7. Formation sample.

3.3.3.1 Determination of formation properties

The mixture designs used to cast the formations are provided in Table 3.3. Mortar mixing for casting the formations is conducted in accordance with ASTM C305 (2006). The concrete mixtures used to cast the various portions of the formation need to be tested to ensure they satisfy the prescribed mechanical properties. Porosity is measured in accordance with ASTM C948 (1981) using 2 in by 2 in by 2 in cubes. Compression strength is measured in accordance with ASTM C109/C109M (2013a) using the same cubes, as shown in Figure 3.8a. Permeability is measured using 4 in by 8 in cylinders. The setup for the permeability testing is shown in Figure 3.8b. Table 3.4 presents the physical properties of mixture designs.

(a) Compressive strength test (b) Permeability test

Figure 3.8. Physical property measurements.

Table 3.3. Mixture designs used for casting the formations.

Formation type	Mixture	Water, lb	Cement, lb	Sand, lb	Water reducer, oz
High permeability	1	24.08	48.16 (Type I)	60.19	0.0
	2	12.06	21.71 (Type III)	113.20	1.569
	3	19.36	42.23 (Type I)	77.43	0.0
Low permeability	4	19.36	42.23 (Type I)	77.43	0.0

Note: 1.) Weights are based on a 1-ft^3 batch size. 2.) Mixture 1 is only used to block the voids at the bottom of the high permeability formations. 3.) For casting a high permeability formation, required amount of Mixtures 1, 2 and 3 are 10.0, 93.1 and 245.5 in^3, respectively. For casting a low permeability formation, required amount of Mixture 4 is 347.0 in^3.

Table 3.4. Physical properties of mixture designs.

Mixture permeability	14-day compressive strength		Porosity		Permeability	
	Average	Std. Dev.	Average	Std. Dev.	Average	Std. Dev.
High (Mixture 2)	1,600 psi	318.6 psi	20.80 %	0.57%	3,740 darcies	1,184 darcies
Low (Mixtures 3 and 4)	2,600 psi	279.1 psi	3.50 %	0.32%	9.27×10^{-4} md	3.71×10^{-4} md

Note: Sample size = 3.

3.3.3.2 Casting protocol for formation

In order to make representative sandstone formations for WSC testing, three separate batches of mixture designs are required for casting on the high permeability formation. The composition of each of the batches can be seen in Table 3.3. A summary of the standard protocol for casting a formation is described as follows. For detail of the protocol, please refer to Appendix A.

1.) Mix Mixture according to ASTM C305 (2006).

2.) Place 7 oz of Mixture 1 into the bottom of the mold. Vibrate using a vibration table to spread the layer out evenly (Figure 3.9b and Figure 3.9c).

3.) Mix Mixture 2. Pour 1.5 lb of Mixture 2 into the mold on top of the first lift and compact the layer by applying a standard weight onto the surface of the lift while vibrating using the vibration table (Figure 3.9e and Figure 3.9f).

4.) Place geotextile and a copper tube at the center of the 1.5-lb layer; The top of the copper tube should be wrapped in with duct tape to prevent concrete from dropping down into the tube; scratch the surface of the layer of the exiting lift for better bond between the layers (Figure 3.9g).

5.) Place 2.5 lb of Mixture 2 on top of existing lift and compact the layer as described in Step 3.

6.) Measure the thickness of the bottom layer and place a circular plastic sheet with a diameter of 7.8 in at the center of the circular mold; scratch the edge of the layer for better bonding between the lifts (Figure 3.9h and Figure 3.9i).

7.) Place an additional 3.5 lb of Mixture 2 and compact the layer as described in Step 3. Slide a steel sleeve over the copper tubing to prevent bonding of the cementitious material to the copper tubing (Figure 3.9j).

8.) Mix Mixture 3. Place Mixture 3 into the mold and then vibrate using the vibration table (Figure 3.9k).

9.) Finish the top surface using a flat plastic ring and gently oscillate it back and forth until the finished surface is at correct depth, smooth and level (Figure 3.9l).

10.) Disassemble the mold after 24 hours and cure formations in an environmental room with a relative humidity of 100% and a temperature of 70 ℉ for 28 days.

For the low permeability formation, the construction process is the same except that only the low permeability mixture (Mixture 4) is used to cast the whole formation sample.

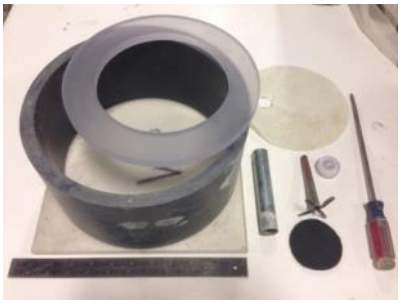

(a) Cylinder model

(b) Mixture 1

(c) Spreading

(d) Mixing in bowl

(e) Weighting proportions

(f) Compacting and vibration

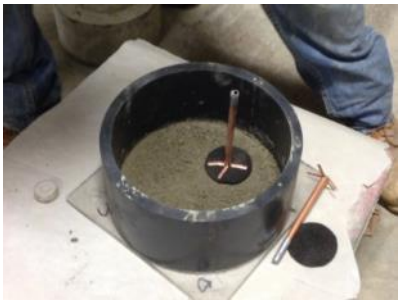

(g) Geotextile and tube installation

(h) Depth check and placement of plastic isolation sheet

(i) Texturing surface

(j) Tube protection

(k) Placement of last lift

(l) Leveling the surface

Figure 3.9. Casting the formation.

3.3.3.3 Protocol for post-cast formation preparation

The formations are removed from the environmental room after 28 days of curing. The steps for the post-cast preparation are shown as shown in Figure 3.10 and described below. For detail of the protocol, please refer to Appendix B.

1.) Coring: To create the natural texture of a borehole surface, the central portion of the formation is cored using an 8-in diameter core drilling bit. This process takes approximately 25 minutes (Figure 3.10b).

2.) Grinding outer surface: To ensure an adequate bond is achieved between the outer formation surface and the epoxy used to coat the surface, the outer surface must be ground using a (hand) grinder. This process takes approximately 20 minutes (Figure 3.10c).

3.) Covering inner surface: To protect the borehole surface from contamination from the epoxy, duct tape is placed over the upper 3 in of the inner surface of the formation (Figure 3.10d).

4.) Drilling thermocouple hole: A ¼-in diameter hole is drilled through the outer surface so that the thermocouple wire can be fed through it. The hole is 3.0 in from the bottom. This process takes approximately 10 minutes. The formation is then air dried for 24 hours before an epoxy is applied to the out surface (Figure 3.10e).

5.) Epoxying outer surface: To isolate the communication between the annulus and overburden pressure applied to the outer portion of the formation, epoxy is applied to the outer surface of the formation. In order to reinforce the formation so that it can resist the high overburden pressures, fiberglass is wrapped around the outer surface of the formation while the epoxy is still wet. After applying the first layer of epoxy and the

fiberglass mesh, the formation is placed under a vacuum chamber so the epoxy can be draw through interconnecting pores. This process takes approximately 40 minutes. The epoxy requires a minimum of 12 hours to harden (Figure 3.10f).

6.) Mounting thermocouple: Clean the hole with a ¼-in diameter drill bit before inserting the thermocouple. After inserting the thermocouple through the hole, fill the gaps around the thermocouple wire with epoxy to seal the hole. The epoxy requires at least 6 hours of hardening before placing upper steel ring (Figure 3.10g).

7.) Attaching upper steel ring: The top surface should be ground to provide a smooth interface for the upper steel ring to rest upon. After epoxy is applied on the interface, the formation is vacuumed to ensure no air bubbles are trapped at the interface. Additional epoxy needs to be applied to the chamfer during epoxy gelation to increase the interfacial bond strength. The epoxy then requires 24 hours of curing to reach appropriate hardness (Figure 3.10h).

8.) Attaching inner casing: The casing is then epoxied at the bottom of the inside of the formation. Center the inner casing and pour the epoxy on the bottom of the formation and stir to ensure the epoxy is evenly distributed. Apply petroleum jelly to the upper portion on the outside of the casing and place the piston in the annulus to guide the inner casing and to keep the inner casing aligned. The epoxy requires 120 hours to achieve sufficient strength (Figure 3.10i).

9.) Saturating formation: The annulus is filled with deionized water for 24 hours to simulate the saturated conditions typically present downhole. Weigh the dry sample before filling it with water. After 24 hours, remove the water and weigh the saturated sample. The

volume of voids in the formation can be estimated by calculating the difference in weight.

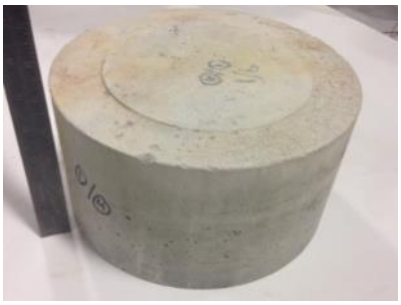

(a) Formation after casting

(b) Core our inside inner portion

(c) Grind the outer surface

(d) Placement of protective tape

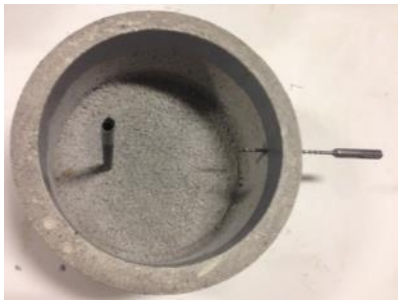

(e) Drill thermocouple hole

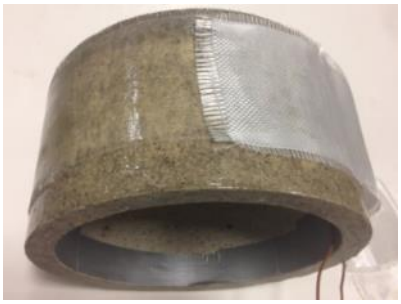

(f) Epoxy outer surface and then apply reinforcing mesh

(g) Install thermocouple

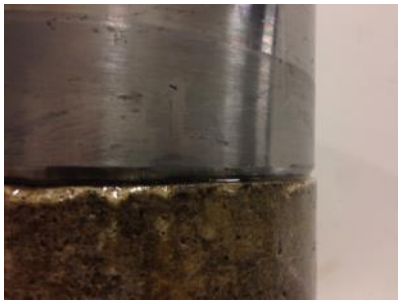

(h) Chamfer to reinforce the interface

(i) Align inner casing

Figure 3.10. Formation sample preparation.

3.3.4 WSC test protocol

Before testing, all materials and slurry devices should be kept in the room where the mixing and conditioning will be conducted for at least 24 hours to ensure the temperature of these items are the same as the room temperature. Also, the WSC and its accessories will be kept where the simulation will be conducted for at least 24 hours. The purpose of this is to obtain accurate temperature measurements and, as a consequence, a consistent curing history.

3.3.4.1 Slurry preparation

The cement slurry to be placed in the annulus is bench-mixed according to API Specification 10A. A 4-liter constant speed blender is used for mixing the slurry, as shown in Figure 3.11a. To simulate the pumping process, a 20-minute conditioning period is necessary after mixing at a stirring speed of 60 rpm using the 1.2-gallon paste mixer shown in Figure 3.11b. The stirring process aids in removing air bubbles from the slurry and thereby guaranteeing a consistent result.

3.3.4.2 WSC assembly process

The WSC setup should be conducted according to the following procedure (see Appendix C for detail):

1.) Start the temperature and pressure monitoring system before mixing the slurry.
2.) Mix 152.6-in^3 slurry in accordance with API Specification 10A using a 4-liter constant speed blender as shown in Figure 3.11a (time = 0). (1 minute)
3.) Pour the slurry in the 1.2-gallon paste mixer and stir continuously at a rate of 60 rpm for 20 minutes. During this slurry conditioning period, place the formation in the chamber and check all of the valves on the chamber are closed. (20 minutes)

4.) After conditioning for 20 minutes, pour the slurry in the annulus and use a depth indicator (Figure 3.11f) to prevent overfills. (5 minutes) (Figure 3.11e)

5.) Lower the piston into the annulus and measure its initial depth from the top of the formation. (5 minutes) (Figure 3.11g, Figure 3.11h and Figure 3.11i)

6.) Connect the fittings and fill the chamber with water containing a red dye. (10 minutes) (Figure 3.11j and Figure 3.11k)

7.) Assemble the chamber. (5 minutes) (Figure 3.11l)

8.) Apply initial overburden pressure at time equals 50 minutes. Adjust the overburden pressure according to the hydration stage (if necessary).

For pressure reduction testing, stop the procedure and disassemble the setup after 24 hours. For gas migration testing with high permeability formations, apply the predetermined formation pressure after Step 8.

a.) Slowly open the backflow filtration valve and control the fluid loss rate accordingly.

b.) To measure the permeability of the wellbore section, apply a low gas pressure at the formation gas port and record the gas flow rate.

c.) After this portion of the test is completed (24 hours), stop the procedure and disassemble the setup.

(a) Mixing the slurry

(b) Conditioning the slurry

(c) Pistion assembly

(d) Setup before cementing

(e) Pouring cement in the annulus

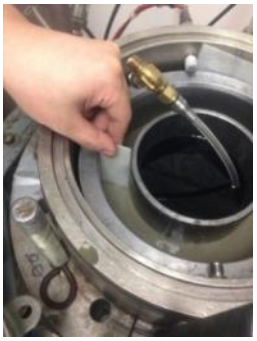

(f) Depth indicator

(g) Piston installation

(h) initial piston compression

(i) Measuring the position depth

(j) Inner connections

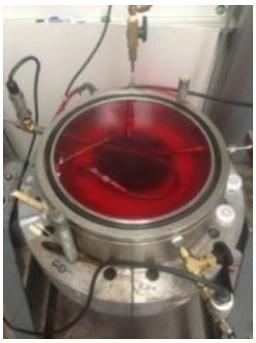

(k) Fill with dye water

(l) Assemble the top plate

Figure 3.11. Initial test setup for the WSC.

3.4 RESULTS FROM CALIBRATION TESTS

3.4.1 Cements

WSC tests were conducted in accordance with the test procedure presented in Section 3.3.4. Class A cement and Type I ordinary Portland cement (OPC) were used. A summary of the composition of these cements is provided in Table 3.5 and the mill sheet for each has been included as Appendix D.

Table 3.5. Cement composition and fineness of cements.

Cement type	C_3S, %	C_2S, %	C_3A, %	C_4AF, %	Gypsum, %	Fineness, m^2/kg
Type I	57.2	11.6	7.21	9.43	5.4	399
Class A	59.52	15.88	3.04	12.17	4.6	362

3.4.2 Reproducibility of the WSC test results

To insure the results of the WSC were accurate and repeatable, several preliminary tests were run. The following section describes some of these preliminary tests performed.

(1) Temperature measurement

Due to the high-pressure and high-moisture condition inside the chamber, a Type T thermocouple could not be placed in the chamber to measure the temperature history of cement within the WSC without compromising the seal. Therefore, a more elaborate method was devised to estimate the temperatures within the chamber. The electronic connector was used to provide the power for the thermocouple placed inside the chamber and to record the signal

(temperature difference between the cement slurry and the chamber). One end of the wire is embedded at mid-depth into the cement slurry through the hole drilled into the formation (Figure 3.7c and Figure 3.10g), and the other end (wire junction) is attached to the inner surface of the chamber. This provides the temperature difference between the cement slurry and the chamber. Attach another thermocouple at the *same* spot as the thermocouple on the inner chamber surface, but this thermocouple is placed on the outer surface of the chamber. As the true temperature of the chamber can be measured directly, the true slurry temperature can be calculated by adding the temperature difference measured from the thermocouple inside the chamber. This temperature methodology can be simplified. For example, a new electronic connector using the T-type thermocouple wire can be machined and the temperature of the cement slurry can be measured directly (Seal is critical though). The easiest way is to replace the T-type thermocouple by a high-tech temperature sensor, which can measure the absolute temperature. The high-tech absolute temperature sensor should be allowed to work in the water under high pressure condition.

The thermocouples cannot be used to directly measure the temperature of the cement in the annulus since the temperature at a reference point is needed. Therefore, a test was conducted to check the accuracy of using this indirect means for measuring temperature. A neat cement slurry was prepared using Type I cement with a w/c ratio of 0.46. The cement slurry was conditioned and tested at 70 ℉. A low permeability formation was used. The WSC was assembled as described in Section 3.3.4.2. No pressure was applied to the system. The room temperature (to be referred to as the "ambient" temperature) as well as the temperature of the chamber above the wellbore section (to be referred to as the "chamber" temperature), were measured. As described previously, the cement temperature (to be referred to as the "measured"

cement temperature) can then be calculated by adding the recorded temperature difference between the cement slurry and the chamber to the chamber temperature. Since no pressure was applied, a temperature sensor was embedded in the slurry to directly record the actual cement temperature (to be referred to as the "true" cement temperature). A summary of these temperatures over a 24-hour period is shown in Figure 3.12.

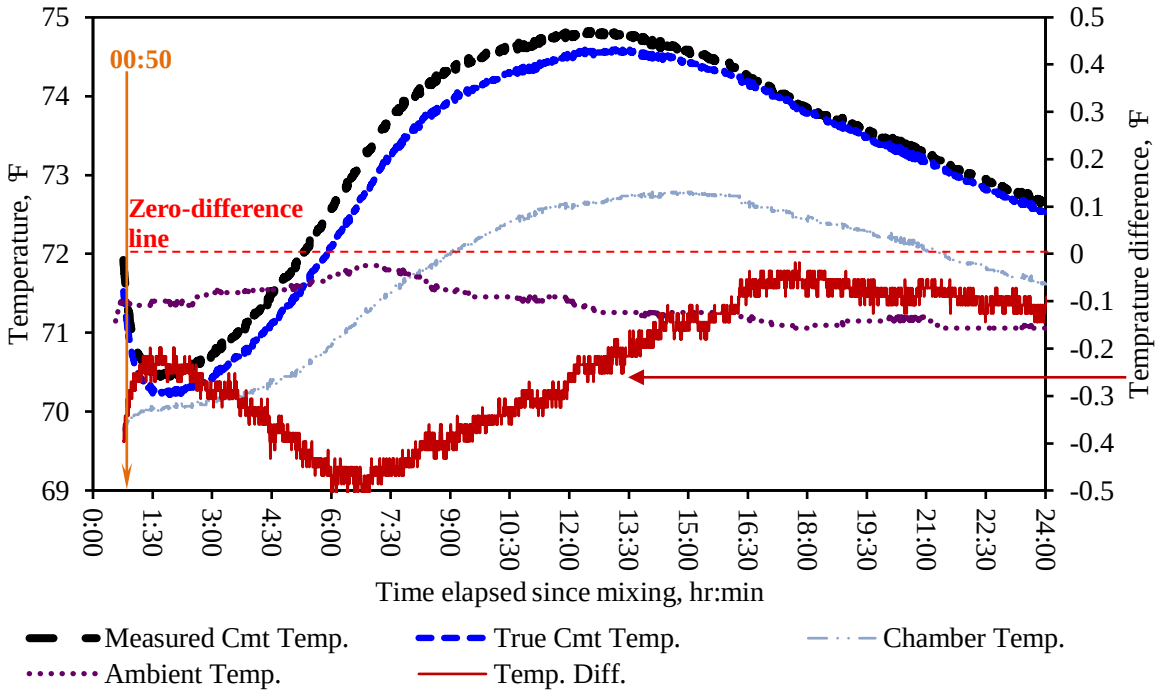

Figure 3.12. Accuracy of temperature measurement.

As can be seen, the "measured" cement temperature was slightly higher than the temperature measured directly in the slurry. The maximum temperature difference between the "true" cement temperature and "measured" cement temperature over a 24-hour hydration period was found to occur after about 7 hours and was 0.5 ℉. A sensitivity analysis (using Pool's study presented in Section 4.2.3) was performed to ensure that this temperature difference would not significantly affect the results. The temperature history obtained from the WSC was used to

perform sensitivity study of temperature on the progress of cement hydration by shifting temperature values, such as ±0.5, ±1.0 and ±2.0 ℉.

Maturity was also used to estimate the accuracy of the temperature measurements. The maturity method (McIntosh 1949; Nurse 1949; Saul 1951) can be used to analyze the measured temperature history of the cement to estimate strength development and other properties during the curing period, when sufficient moisture is available for cement hydration (ASTM 2011c). Therefore, the maturity method can be used to define the times at which equal microstructural development will occur for samples cast with the same mixture design but cured under two different temperature regimes. The maturity index is computed as the product of time and temperature above a datum temperature, as shown in Figure 3.13. The Nurse-Saul maturity method (Saul 1951; Nixon et al. 2008) is commonly used to determine the maturity index, using the relationship defined in Equation (3.1). It assumes that the chemical reaction rate in concrete increases linearly with temperature.

$$MI = \int_0^t (T - T_0)dt \approx \sum_0^t (T_{ave} - T_0)\Delta t \tag{3.1}$$

where, MI = Maturity Index (a.k.a. Temperature-Time Factor) at age *t*;

T = Temperature of the cement at age *t*;

T_0 = Datum temperature;

T_{ave} = Average temperature of the cement during time interval during time interval Δt.

It should be noted that the datum temperature is a function of cement composition and curing conditions (Saul 1951). ASTM C1074 (2011c) recommends that 32 ℉ be used as the

datum temperature for Type I cement used without admixtures when the expected curing temperature is between 32 ℉ and 104 ℉.

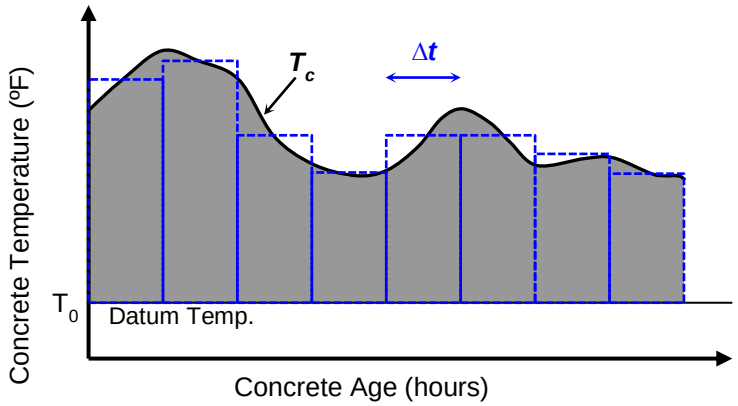

Figure 3.13. Temperature over time and the Nurse-Saul maturity equation.

The sensitivity analysis, along with the maturity concept showed that a temperature difference of 1.0 ℉ for a neat cement slurry cured under the ambient temperature resulted in a 5-minute difference between the cement set times. This difference in set times can be considered insignificant. Therefore, this indirect means for measuring the temperature of the cement slurry in the annulus can be considered a sufficiently accurate estimate of a temperature measured directly inside the cement annulus.

(2) Pressure measurement

Next tests were performed to evaluate the repeatability of the WSC results. An overburden pressure is applied to the top of the cement annulus in the WSC. As the cement slurry transforms from a liquid to a solid, the rigidity of the cement matrix results in a decrease in the slurry pore pressure within the annulus. This pore pressure was measured 1.0 in from the bottom of the cement slurry (see Figure 3.7c) for three separate simulations. First, neat slurries were

prepared using Class A cement with a w/c ratio of 0.46. Cement slurries were mixed and conditioned at 70 ℉. Low permeability formations were used. Once the cement was placed in the annulus and the chamber was assembled, an overburden pressure of 350 psi was applied and maintained throughout the duration of the test. Low permeability formations were used and no fluid loss was simulated. The purpose of this test set is to evaluate the repeatability of the WSC tests.

Figure 3.14 shows the results from the three WSC tests performed under the same operating conditions defined above. This graph includes the ambient temperature, the measured cement temperature and the slurry pore pressure. In this figure, initial and final set are defined using the Vicat test as noted (ASTM C191). As seen in Figure 3.14, the pore pressures measured in the annulus for the three WSC tests are identical during the early hydration stage until final set determined by Vicat test. After that, the pressure drop is slightly different until a minimum value is reached. The pressure for Test 3 starts dropping slightly earlier than that of Test 1. By comparing the temperature history between Tests 1 and 3, the cement temperature for Test 1 is approximate 0.45 ℉ higher, which will increase the rate of cement hydration. For Test 2, the pressure drops more slowly than for that of Test 1 or 2. This may be the result of variation in formation permeability, temperature and/or other factors. The effect of these factors on pressure reduction is further investigated in the next section.

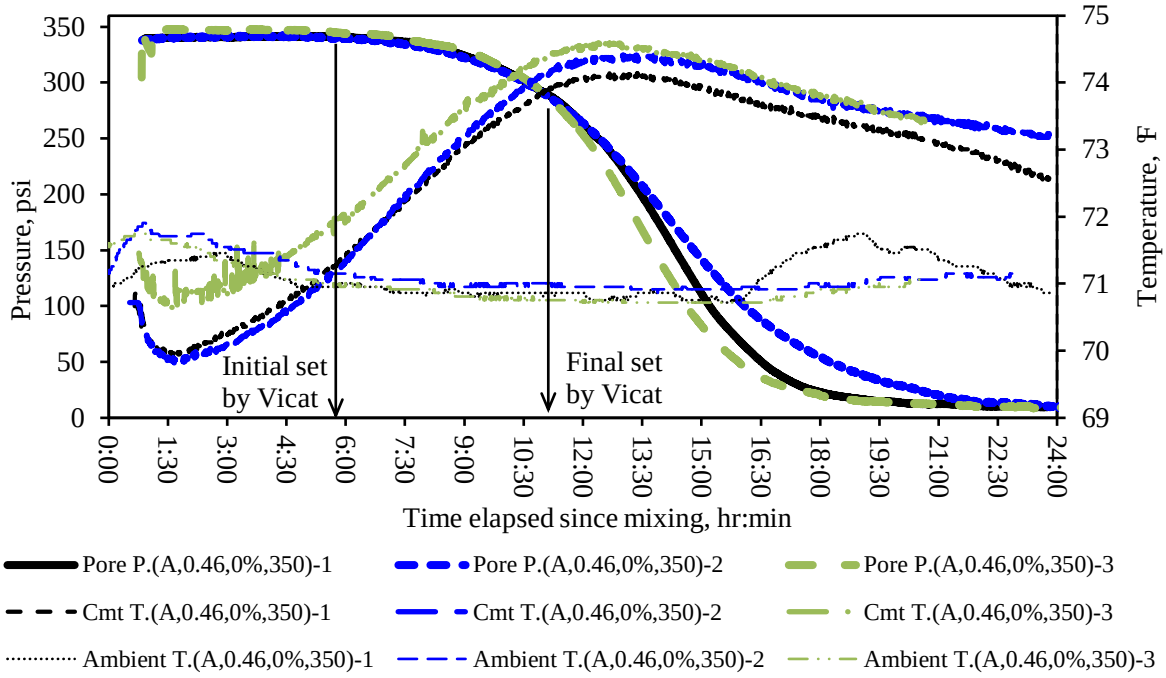

Note: Data legend (cement type, w/c ratio, dosage of $CaCl_2$, pressure level) - test number

Figure 3.14. Reproducibility of WSC testing.

3.4.3 Factors affecting pressure reduction

This study intends to evaluate the capability of the WSC in differentiating the effect of different factors on the hydrostatic pressure reduction within the cemented annulus during the early hydration stage. Factors considered include: formation permeability (zero permeability and a permeable formation), cement types (Type I and Class A cement), curing temperature (70 ℉ and 90 ℉), and a $CaCl_2$-based accelerator (0%, 1% and 2% BWOC). The maturity concept is used to analyze the temperature history of cement. Results verify the capability of the WSC in simulating the behavior of slurry pore pressure under representative borehole conditions. In addition, the advantage of characterizing slurry designs and boundary conditions was illustrated by employing the maturity concept. A summary of these findings are presented below.

(1) Formation permeability

Two WSC tests were performed using two different formations: an impermeable formation and a permeable formation. The formation condition was the only parameter of different for these two tests, while all other variables were held constant. Neat slurries were prepared using Type I cement with a w/c ratio of 0.46 (slurry density of 15.6 ppg). Cement slurries were conditioned and tested at 70 ℉ and placed in the WSC. An overburden pressure of 90 psi was applied representing a depth of 110 ft. For this simulation, pressurized formation gas was not applied and all the pressure ports were closed.

The results can be seen in Figure 3.15. The overburden pressure (OBP) measured above the cement annulus as well as the pore pressure (Pore P.) measured within the cement annulus are plotted over time in Figure 3.15. As can be seen, the slurry pore pressure starts to drop at the same time in both tests. However, the reduction rates of slurry pore pressure are significantly different. The test conducted with an impermeable formation has a steeper reduction rate. This comparison demonstrates the advantage of the developed WSC apparatus, which is capable of simulating the effect of rock formation conditions on the performance of cement slurry.

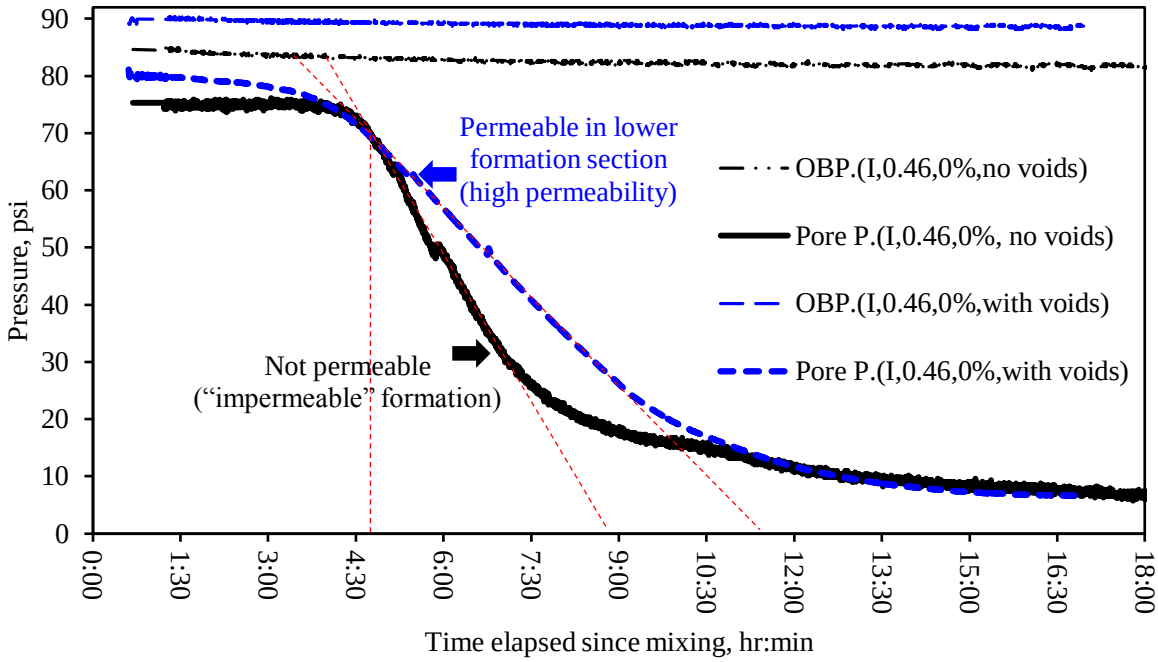

Note: Data legend (cement type, w/c ratio, dosage of $CaCl_2$, formation permeability).

Figure 3.15. Sensitivity of formation permeability on pressure reduction.

(2) Cement type

Figure 3.16 shows the effect of cement type on the hydrostatic pressure reduction in the cemented annulus. Other than cement type, all other parameters were held constant. Two slurries were prepared using Type I and Class A cements. Cement composition and fineness information can be found in Table 3.5 with additional information provided in Appendix D. Cement slurries were blended with a w/c ratio of 0.46 and tested at 70 ℉. After placing the cement in the annulus and closing the chamber, an overburden pressure of 350 psi was applied representing a depth of 430 ft. Low permeability formations were used in both tests so no fluid loss occurred from the annulus into the formation.

As seen in Figure 3.16, the slurry pore pressure for Type I cement starts to drop earlier than that of Class A. For the Type I cement, the slurry pore pressure starts to drop before the

initial set as determined by the Vicat test (ASTM 2013b). Compared with Class A cement, Type I cement presents a poor gas-flow-control property as the slurry pore pressure for Type I cement starts to drop before the cement develops sufficient strength to withstand pressurized gas.

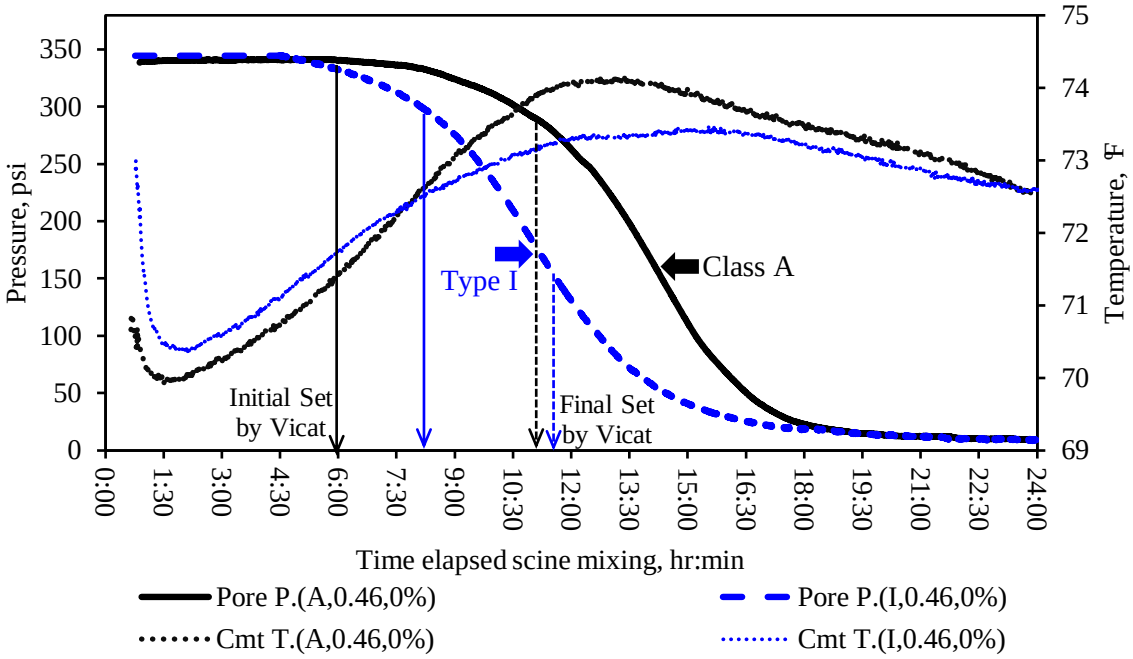

Note: Data legend (cement type, w/c ratio, dosage of $CaCl_2$).

Figure 3.16. Sensitivity of cement composition on pressure reduction.

(3) Curing temperature

To differentiate the effect of the wellbore temperature on the hydrostatic pressure reduction within the annulus, two WSC simulations were conducted using different curing temperatures: 70 ℉ and 90 ℉. Other than curing temperature, all other variables were held constant. Neat slurries were prepared using Class A cement with a w/c ratio of 0.46. Cement slurries were mixed and conditioned at 70 ℉. Once the cement was placed in the annulus and the chamber was assembled, an overburden pressure of 350 psi was applied, representing a depth of 430 ft. Low

permeability formations were used in both tests so fluid loss from the annulus into the formation did not occur.

Figure 3.17 shows that temperature affects the rate of cement hydration. The higher the temperature, the faster hydration occurs, as was anticipated. An interesting observation can be made when normalizing the data in Figure 3.17a using the maturity concept. Figure 3.17b shows the pressure history with respect to maturity index. As no datum temperature was established for Class A cement, a datum temperature of 50 ℉ is determined by matching the maturity index of the two tests. When comparing the pressures for the cements setting at 70 ℉ with that of 90 ℉, they are nearly identical if plotted against maturity instead of time.

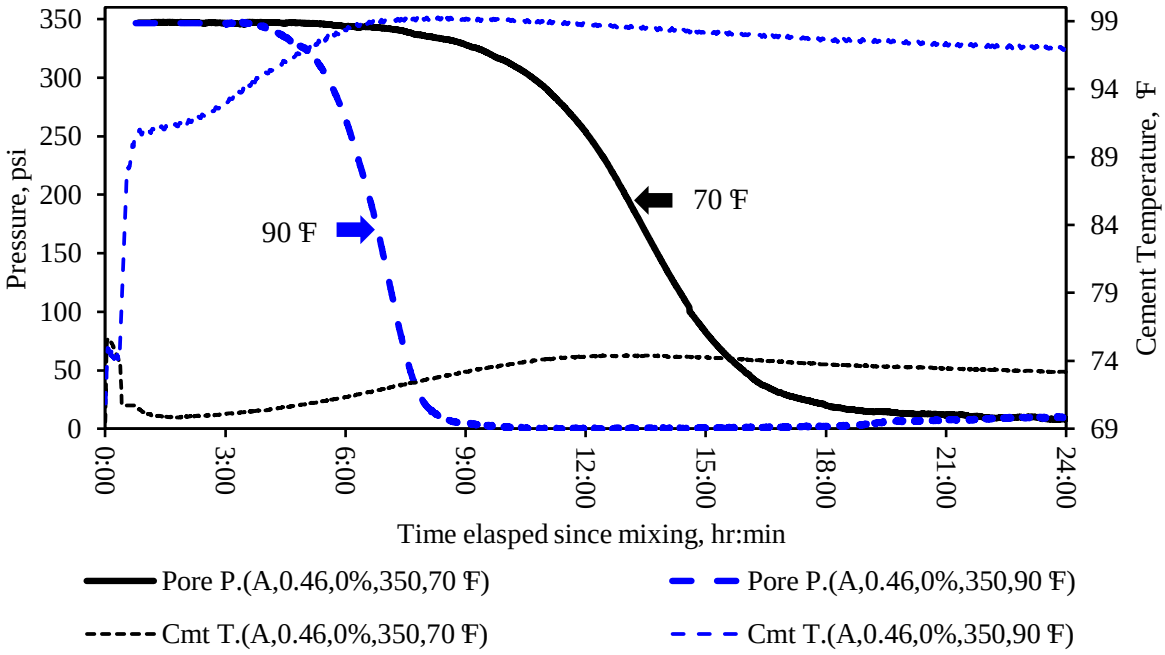

(a) Pressure reduction with time

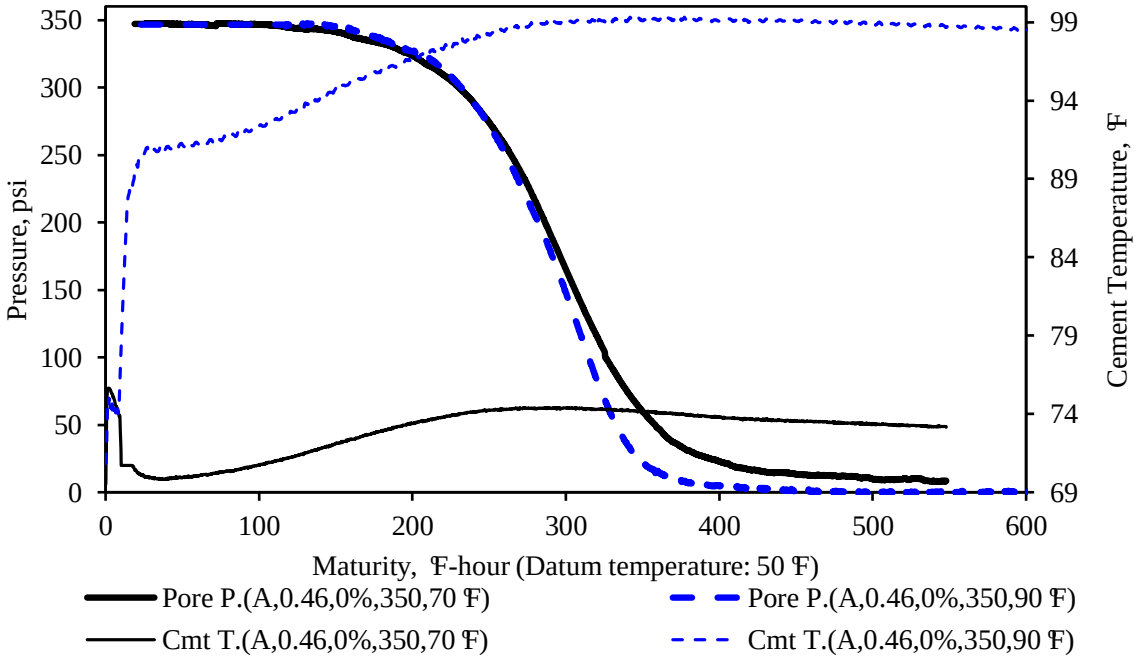

(b) Pressure reduction as the cement hydrates

Note: Data legend (cement type, w/c ratio, dosage of $CaCl_2$, pressure level, curing temperature).

Figure 3.17. Sensitivity of curing temperature on pressure reduction.

(4) Calcium chloride accelerator

WSC simulations were performed using cement slurries have three different dosages of $CaCl_2$: 0%, 1% and 2%. While the dosage level of $CaCl_2$ was changed, all other variables were held constant. Neat slurries were prepared using Class A cement with a w/c ratio of 0.46. Cement slurries were mixed and conditioned at 70 ℉ and then placed into the annulus. After the chamber was assembled, an overburden pressure of 350 psi was applied representing a depth of 430 ft. Low permeability formations were used in the tests and no fluid loss from the annulus was simulated.

It is well known that $CaCl_2$ accelerates the cement hydration, as shown in Figure 3.18a. The greater the dosage of $CaCl_2$, the faster hydration occurs. Figure 3.18b shows the pressure history with respect to maturity index. A datum temperature of 70 ℉, which is the ambient temperature, is determined by matching the maturity index for the cases of 1% and 2% $CaCl_2$. As seen in Figure 3.18b, the pressure curve for 0% $CaCl_2$ is different from that for 1% and 2%, which can be attributed to the effect of $CaCl_2$ on cement hydration. When comparing the pressure curves for 1% and 2% $CaCl_2$, they are nearly identical, although the time histories differ by 1.5 hours for the linear portion of the reduction rate. The maturity index captures the hydrostatic pressure reduction trend, indicating the advantage of characterizing bulk properties of cement slurry. However, the maturity concept requires determining the datum temperature, which is a function of cement compositions. Therefore, a fundamental concept, such as degree of hydration, should be used to describe cement hydration, and therefore the development of slurry properties.

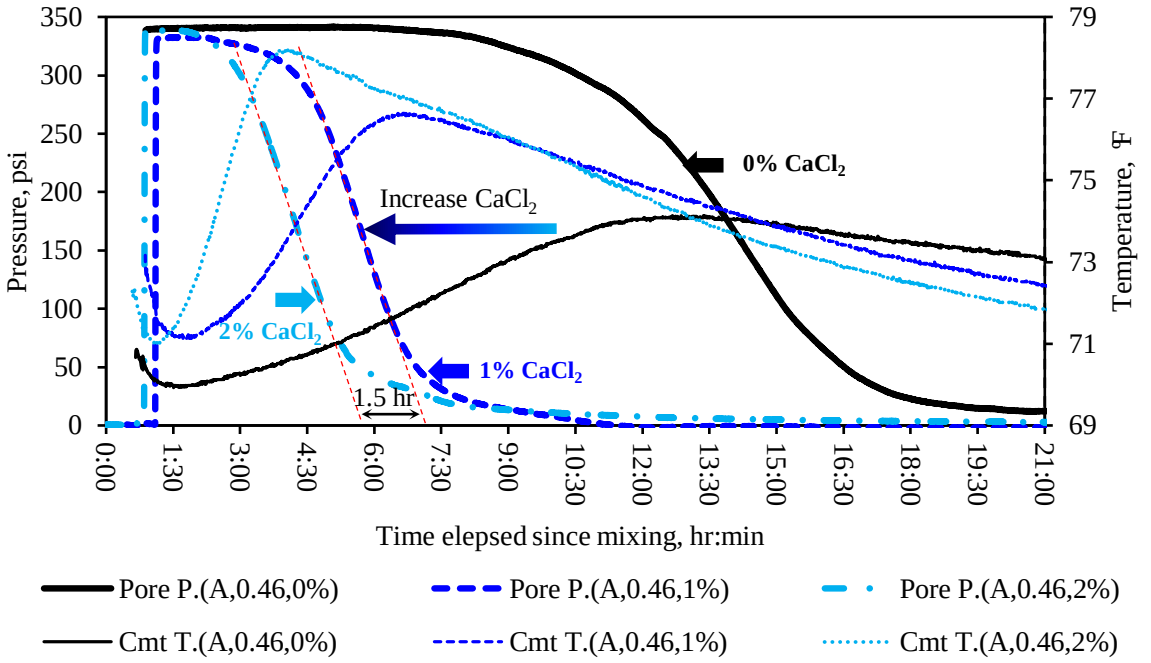

(a) Time history

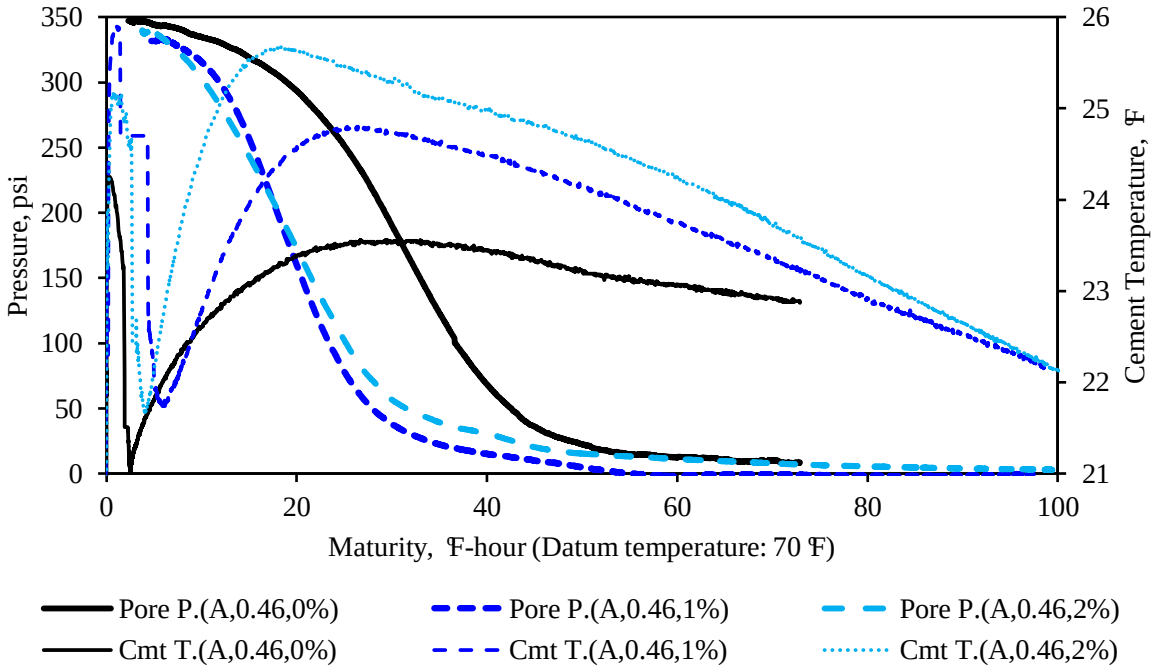

(b) Maturity of cement hydration

Note: Data legend (cement type, w/c ratio, dosage of $CaCl_2$)

Figure 3.18. Sensitivity of calcium chloride on pressure reduction.

3.5 CONCLUSIONS

This chapter discussed the development and testing of the enhanced laboratory-scale WSC in detail, which has been developed to study hydrostatic pressure reduction within the cemented annulus and possible gas invasion under representative borehole conditions. In addition to the device itself, specific casting and testing protocols have been developed, which detail the procedures required for proper operation of the apparatus. The WSC is an improvement over existing CHAs by providing an environment more similar to in-situ wellbore conditions. The effects of rock formation conditions, real-scale wellbore section, and varying effective overburden pressure can also be simulated in the WSC. Mud cakes, casing string eccentricity and inclined annuli can also be simulated in the WSC. Rather than testing the cement slurry in an unrealistic worst-case scenario, the WSC attempts to control and monitor the curing conditions when cement slurries gel under representative field conditions. This tool makes it possible to evaluate different factors and quantify their effects on the slurry pore pressure reduction. Potential gas channeling and migration patterns can also be investigated. Moreover, the permeability of the tested wellbore section can be measured under representative in-situ condition. The design of the WSC can be adjusted according to the simulation requirements, including formation properties, wellbore geometries and pressure magnitudes.

WSC results from calibration tests verify the capability of the developed WSC in simulating cement hydration under in-situ wellbore conditions. The WSC is capable of differentiating the effect of formation permeability, cement types, curing temperature and a $CaCl_2$-based accelerator on the slurry pore pressure reduction within the cemented annulus during the early gelation of cement hydration. Formation properties affect the rate of the slurry pore pressure reduction, which highlights the advantage of the WSC over other CHAs in being

able to consider rock formation conditions. The maturity concept was introduced to normalize the hydrostatic pressure reduction of cement slurries cured under different temperatures and blended with different dosages of $CaCl_2$-based accelerator. Result analysis illustrates the need for characterizing wellbore conditions and slurry designs using fundamental concepts. If instead fundamental concepts were used, different tests could be more readily compared regardless of curing temperature, applied pressure, and chemical additives used.

4.0 CHARACTERIZATION OF FACTORS AFFECTING SLURRY PERFORMANCE DURING EARLY HYDRATION UNDER IN-SITU BOREHOLE CONDITIONS

4.1 INTRODUCTION

Gas migration into hydrating slurries, which requires costly remedial well treatments, is a major reason for well completion failures (Bonett and Pafitis 1996). The first documented research attempting to explain the gas communication by means other than leakage at interfaces was performed by Carter and Slagle in 1970. It was found that gases and other fluids can invade the cemented annulus as a result of hydrostatic pressure reduction during the early hydration stage. Since then, an extensive amount of research has been conducted to study annulus cement behavior and the mechanisms of gas migration during early hydration (Carter et al. 1973; Garcia and Clark 1976; Levine et al. 1979; Tinsley et al. 1980; Sabins et al. 1982; Banniser et al. 1983; Parcevaux 1984; Cheung and Beirute 1985; Drecq and Parcevaux 1988; Beirute and Cheung 1990; Roges 2004). Available theories regarding gas migration during this early hydration stage attribute the occurrence of gas migration to an ineffective initial hydrostatic head, an unstable cement slurry design, fluid loss after cement placement, and bonding at interfaces as cement hydrates. Gases do not invade the cement slurry as long as the slurry pore pressure remains above the formation gas pressure (Cheung and Beirute 1985). It was found that hydrostatic

pressure in the cement column declines shortly after cement placement (Kellingray 2007; Brufatto et al. 2003). Once the hydrostatic pressure decreases to a point below that of the formation gas pressure, gas migration may occur, if the cement matrix has not developed sufficient strength to withstand gas invasion.

Cement hydration involves changes in both the chemical and physical properties of the cement slurry. Due to the difficulties in modeling time-dependent properties of hydrating cement slurry, the petroleum industry utilizes empirical approaches when designing cement slurries able to reduce the risk of gas migration. Unfortunately, no successful scaled-laboratory experiment is universally recognized for characterizing the ability of a cement slurry to mitigate gas migration (Nelson 1990). Moreover, a single slurry design that is capable of preventing gas migration in all wellbore conditions does not appear to exist. Therefore, a standardized approach for predicting cement behavior and preventing gas migration is needed.

In this chapter, results from WSC testing are discussed. The purpose of this testing is to study hydrostatic pressure reduction in the cemented annulus (hydrostatic pressure testing) and possible gas invasion under representative borehole conditions (gas migration testing). The effects of different factors on hydrostatic pressure reduction are investigated, including: formation permeability, initial overburden pressure at the depth of interest, wellbore temperature, w/c ratio, cement composition, and the use of a $CaCl_2$-based accelerator. As will be seen in this chapter, experimental results prove the feasibility of using fundamental concepts, such as degree of hydration and capillary porosity, to quantify the hydrostatic pressure reduction in the cemented annulus.

4.2 CEMENT HYDRATION

4.2.1 OWC testing

The design of slurries with a short transition time has been the focus of industry (Mueller 2002). It is widely accepted by the petroleum industry that a short transition time can reduce the risk of gas migration. API Standard 65-2 (2010a) provides a standardized procedure for determining transition time. The transition time is the time between the first measurable SGS (typically taken as 100 lbf/100ft^2) and 500 lbf/100ft^2. In the classic shear stress theory, hydrostatic pressure reduction expressed as a function of SGS (Sutton et al. 1984a, 1984b). Sabins, et al. (1982) published the first paper in which the relationship between SGS and gas migration occurrence was evaluated. Since then, numerous slurry designs have been reported to shorten the transition time measured by the SGS tests.

Although a slurry with a short transition time potentially reduces the time available for gas to invade the annular cement, a sensitivity study has shown that no relationship was observed between a short transition time and the occurrence of gas migration (Roges et al. 2004; Rocha et al. 2013). As shown in Table 4.1, nineteen slurry designs were tested to evaluate the relationship between transition time and gas migration occurrence. Results indicate that a short transition time does not necessarily reduce the occurrence of gas migration. Neither SGS nor ultra-low fluid loss is singularly critical for preventing gas migration through a hydrating cement system (Roges et al. 2004). Gas migration was found to be a multi-phase problem requiring a broader testing approach (Beirute and Cheung 1990).

The following conditions are required for the occurrence of gas invasion into a setting slurry (Bonett and Pafitis 1996): 1.) a driving force (differential pressure) to initiate the gas flow,

and 2.) space within the cemented annulus for the gas to occupy. The internal volume of cement slurry will decrease due to chemical shrinkage and fluid loss (Sykes and Logan 1987; Jones and Carpenter 1991; Zhou and Wojtanowicz 2000). Currently, the ideal design parameters widely accepted for preventing gas migration include (API 2010a; Mueller 2002): 1.) shortening the transition time (time interval from 100 to 500 lbf/100 ft^2 SGS) to 30 minutes or less, and 2.) reducing the fluid loss to 3.38 oz/30 minutes or less.

Table 4.1. Transition time and gas migration occurrence (adapted from Rocha et al. 2013).

Slurry	Time@100 lbf/100ft^2, min	Time@500 lbf/100ft^2, min	Transition time, min	Gas tight
1	401	436	35	**No**
2	220	262	42	Yes
3	389	443	54	**No**
4	380	435	55	**No**
5	414	472	58	**No**
6	405	465	60	Yes
7	482	544	62	Yes
8	398	466	68	**No**
9	288	359	71	**No**
10	241	319	78	Yes
11	217	296	79	**No**
12	203	286	83	**No**
13	375	464	89	Yes
14	252	347	95	**No**
15	316	452	136	Yes
16	278	477	199	Yes
17	91	319	228	Yes
18	288	524	236	Yes
19	137	399	262	Yes

Note: SGS was determined using an ultrasonic SGS analyzer. Gas-tight tests were performed using the commercial CHA. Variables considered in the slurry designs (API Class G) are water content (40, 42, 44 %BWOC), latex-based additive (0.0, 4.7, 8.14 %BWOC), fluid-loss control agent (0.0, 0.36, 0.72 %BWOC), and dispersant (0.09, 0.28, 0.46 %BWOC).

4.2.2 Cement hydration characterization

Dehydration, gelation, settling, packing and setting all occur while the slurry hydrates (Carter and Slagle 1972). Cement hydration is a time-dependent process, which is very difficult to quantify. Moreover, the curing history during cement hydration may significantly change the physical properties of the cement matrix. In commercial CHAs (Chandler Engineering 2014c; OFITE 2014b; CTE 2014b; Sanjel 2014; Shenyang Taige 2014), the slurry is designed to experience a dynamic history of temperature and pressure for a time frame consistent with that which is expected during the cement placement. The thought is that SGS can be determined, once the cement slurry has been subjected to representative conditions experienced during typical pumping operation. While the conditioning process tries to minimize variations caused by the placement of the cement, no conditioning procedure is standardized. Moreover, the temperature and pressure conditions are not identical for the entire depth of cement column. As the hydration along the wellbore is affected by temperature and pressure, SGS for the entire depth of cement column is not identical at any one point in time. Therefore, the prediction equations (Equations (2.2) and (2.5)) derived from the classic shear stress theory (Equation (2.1)) capture the causes of the decay of hydrostatic pressure in the cemented annulus but are not actually representative of in-situ conditions.

In order to capture the development of cement properties, fundamental concepts should be employed to describe the chemical evolution of cement hydration and the micromorphology of the cement matrix. Cement hydration is a chemical reaction in which the major constituents of cement clinker form chemical bonds with water molecules and become hydrates or hydration products. Slurry compositions vary in the type and quantity of constituents present. As mentioned above, curing conditions can affect strength development, and therefore hydration

products. Nevertheless, the overall fraction of Portland cement that has fully reacted with water can always be employed to describe the hydration development for a given slurry design. As cement hydration is an exothermic reaction, the amount of heat generated corresponds to the hydration stage of cement reaction.

4.2.3 Degree of hydration

The progress of cement hydration can be quantified by degree of hydration. Degree of hydration is defined as the fraction of Portland cement that has fully reacted with water, which ranges from 0 to 1, with a value of 1 indicating complete hydration. Degree of hydration is taken as the ratio of heat evolved at time, *t*, to the total amount of heat available, as shown in Equation (4.1) (Copeland et al. 1960; Kada-Benameur et al. 2000).

$$\alpha = H(t)/H_{ult} \tag{4.1}$$

where, α = degree of hydration at time *t*; *H(t)* = heat evolved from time 0 to time *t* (J/gram); and

H_{ult} = total heat available for reaction (J/gram), which can be calculated as follows:

$$H_{ult} = H_{cem} \cdot p_{cem} + 461 \cdot p_{slag} + 1800 \cdot p_{FA-CaO} \cdot p_{FA} \tag{4.2}$$

where, p_{slag} = slag mass to total cementitious content ratio;

p_{FA} = fly ash mass to total cementitious content ratio;

p_{FA-CaO} = fly ash CaO mass to total fly ash content ratio;

p_{cem} = cement mass to total cementitious content ratio;

H_{cem} = heat of hydration of the cement (J/gram), which can be calculated as shown in Equation (4.3) (Schindler and Folliard 2005).

$$H_{cem} = 500 \cdot p_{C_3S} + 260 \cdot p_{C_2S} + 866 \cdot p_{C_3A} + 420 \cdot p_{C_4AF} + 624 \cdot p_{SO_3} + 1186 \cdot p_{FreeCa} + 850 \cdot p_{MgO} \quad (4.3)$$

where, H_{cem} = total heat of hydration of portland cement (J/gram) at α = 1.0;

p_i = mass of i-th component to total cement content ratio.

The concept of "equivalent age" is necessary to normalize the development of hydration at various curing temperatures. Equation (4.4), proposed by Freiesleben-Hansen and Pedersen (1977), is the most common expression used to compute equivalent age, and is used in this study to model the effects of time and temperature on hydration:

$$t_e(T_r) = \int_o^t e^{-\frac{E_a}{R}\left(\frac{1}{T_c}-\frac{1}{T_r}\right)} \cdot dt = \sum_0^t e^{-\frac{E_a}{R}\left(\frac{1}{T_c}-\frac{1}{T_r}\right)} \cdot \Delta t \quad (4.4)$$

where, $t_e(T_r)$ = equivalent age at reference temperature (T_r);

T_c = temperature of the concrete (℉K);

E_a = activation energy (J/mol);

t = time interval;

R = natural gas constant (8.314 J/mol/ ℉K).

The shape of the hydration curve for the mixtures can be best described by three-parameter model defined in Equation (4.5) (Pane and Hansen 2002; Schindler and Folliard 2005).

$$\alpha(t_e) = \alpha_{ult} \cdot e^{-(\tau/t_e)^{\beta}} \quad (4.5)$$

where, $\alpha(t_e)$ = degree of hydration at equivalent age t_e;

τ = hydration time parameter (hours);

β = hydration shape parameter;

α_{ult} = ultimate degree of hydration.

The parameters of the model, α_{ult}, τ, and β, related to the shape of the hydration curve, are used to capture the effects of different mixture constituents on the amount of acceleration, retardation, rate of hydration, and degree of hydration of a mixture. In this model, α_{ult} corresponds to the total amount of heat that evolves for a mixture, τ corresponds to the timing of the accelerating portion of the hydration curve, and β provides an indication of the rate of hydration.

Poole (2007) performed a study to develop a hydration model for ASTM cements with common additives for construction applications. The parameters for developing the hydration model in Poole's study (2007) are presented in Table 4.2. In order to evaluate the feasibility of developed models for this study, a statistical comparison of cements used in the development of these models was made with the cements used in this study. The results are summarized in Table 4.3 with the nine cements used in the model development on the left side and the Class A and Type I cement used in this study on the right side of the table. As can been seen in Table 4.3, the base cement phase compositions are within acceptable ranges with respect to those used in Poole's study (2007).

Table 4.2. Parameters considered in hydration model development (Poole 2007).

Parameter	Range
Curing temperature, ℉	41, 59, 73.4, 100.4, and 140
w/c ratio	0.32, 0.4, 0.44, 0.5, 0.55, 0.68
Cement type	9 cements including Types I, 1/II, III, and V
Fly ash (FA), wt% replacement	15 – 55
Blast furnace slag (GGBFS), %	30 – 70
Silica fume (SF), wt% in mixture	5 – 10
ASTM Type C calcium-nitrate based accelerator (ACCL), %BWOC	0.74 – 2.23
Air-entraining admixture (AEA), %BWOC	0.04 – 0.09
ASTM Type A&D water reducer/retarder (WRRET), %BWOC	0.18 – 0.53
ASTM Type A water reducer (LRWR), %BWOC	0.22 – 029
Mid-range water reducer (MRWR), %BWOC	0.34 – 0.74
ASTM Type F naphthalene or melamine-based high-range water reducer (NHRWR)	0.78 – 1.25
Polycarboxylate-based HRWR (PCHRWR)	0.27 – 0.68

Table 4.3. Cement comparison.

Cement mill test results (ASTM C114)		9 cements (Types I, I/II, III and V)			Class A	Type I
		Range	Average	Std. Dev.		
Silicon Dioxide (SiO_2), %		19.18-21.63	20.36	0.84	21.2	**19.1**
Aluminum Oxide (Al_2O_3), %		3.88-5.43	4.84	0.55	**3.7**	4.7
Ferric Oxide (Fe_2O_3), %		2.01-5.29	3.12	1.03	4.0	3.1
Calcium Oxide (CaO), %		61.45-64.51	63.59	0.98	63.6	62.0
Magnesium Oxide (MgO), %		0.77-2.64	1.27	0.56	**2.7**	**4.3**
Sulphur Trioxide (SO_3), %		2.38-4.4	3.24	0.69	2.7	3.2
Alkalies (Na_2O equivalent), %		0.42-0.85	0.56	0.15	0.37	0.82
Loss of Ignition (LOI)		1.2-4.1	2.20	0.85	**1.03**	2.1
Insoluble Residue, %		0.18-1.43	0.56	0.52	**0.08**	0.31
Free CaO, %		0.91-4.0	2.29	1.06	**0.42**	1.84
Base cement phase composition (Bogue calculations)	C_3S, %	49.85-66.54	57.95	5.50	60.0	57.2
	C_2S, %	7.38-24.41	14.64	5.56	15.9	11.6
	C_3A, %	1.76-10.99	7.55	3.08	3.0	7.0
	C_4AF, %	6.12-16.10	9.50	3.13	12.06	9.4
Blaine (ASTM C204), m_2/kg		350-552	423.7	72.1	362	399
Total heat available for reaction H_{cem}, J/g		458-530	488.7	23.5	461.1	494.6

Note: Solid underline denotes the value is outside one standard deviation from the average while a dash underline denotes the value is outside two standard deviations of the average. Bold denotes values that are outside the range of values used for model.

E_a was determined from a multivariate regression model by Poole (2007), as shown in Equation (4.6).

$$E_a = 41{,}230 + 1{,}416{,}000 \cdot \left[\left(p_{C_3A} + p_{C_4AF}\right) \cdot p_{cem} \cdot p_{SO_3} \cdot p_{cem}\right] - 347{,}000 \cdot Na_2O_{eq} - 19.8 \cdot Blaine + 29{,}600 \cdot p_{FA} \cdot p_{CaO-FA} + 16{,}200 \cdot p_{GGBFS} - 51{,}600 \cdot p_{SF} - 3{,}090{,}000 \cdot WRRET - 345{,}000 \cdot ACCL \quad (4.6)$$

where, p_{cem} = % cement in mixture;

p_{FA} = % fly ash in mixture;

p_{CaO-FA} = % CaO in fly ash;

p_{GGBFS} = % GGBFS in mixture;

p_{SF} = % silica fume in mixture;

Blaine = Blaine fineness of cement;

Na_2O_{eq} = % Na_2O_{eq} in cement (= 0.658 × %K_2O + %Na_2O);

WRRET = ASTM Type A&D water reducer/retarder, % solids per gram of cementitious material;

ACCL = ASTM Type C calcium-nitrate based accelerator, % solids per gram of cementitious material.

The parameters of the model, α_{ult}, τ, and β, were determined from a multivariate regression model by Poole (2007), as shown in Equations (4.7), (4.8) and (4.9).

$$\alpha_{ult} = \frac{1.031 \cdot w/c}{0.194 + w/c} + \exp\begin{pmatrix} -0.885 - 13.7 \cdot p_{C_4AF} \cdot p_{cem} \\ -283 \cdot p_{Na_2Oeq} \cdot p_{cem} - 9.90 \cdot p_{FA} \cdot p_{CaO-FA} \\ -339 \cdot WRRET - 95.4PCHRWR \end{pmatrix} \quad (4.7)$$

$$\tau = \exp\begin{pmatrix} 2.68 - 0.386 \cdot p_{C_3S \cdot p_{cem}} + 105 \cdot p_{Na_2O} \cdot p_{cem} + 1.75 \cdot p_{GGBF} \\ -5.33 \cdot p_{FA} \cdot p_{CaO-FA} - 12.6 \cdot ACCL + 97.3 \cdot WRRET \end{pmatrix} \quad (4.8)$$

$$\beta = \exp\begin{pmatrix} -0.494 - 3.80 \cdot p_{C_3A} \cdot p_{cem} - 0.594 \cdot p_{GGBF} + 96.8 \cdot WRRET \\ +39.4 \cdot LRWR + 23.2 \cdot MRWR + 38.3 \cdot PCHRWR + 9.07 \cdot NHRWR \end{pmatrix} \quad (4.9)$$

where, *LRWR* = ASTM Type A water reducer;

MRWR = mid-range water reducer;

NHRWR = ASTM Type F naphthalene or melamine-based high-range water reducer.

As no water reducer/retarder, fly ash, silica fume, or slag was used in this research, Equations (4.2), (4.6) to (4.9) can be simplified as:

$$H_{ult} = H_{cem} = 500 \cdot p_{C_3S} + 260 \cdot p_{C_2S} + 866 \cdot p_{C_3A} + 420 \cdot p_{C_4AF} + 624 \cdot p_{SO_3} + 1186 \cdot p_{FreeCa} + 850 \cdot p_{MgO} \quad (4.10)$$

$$E_a = 41{,}230 + 1{,}416{,}000 \cdot \left[\left(p_{C_3A} + p_{C_4AF}\right) \cdot p_{cem} \cdot SO_3 \cdot p_{cem}\right] - 347{,}000 \cdot Na_2O_{eq} - 19.8 \cdot Blaine - 345{,}000 \cdot ACCL \quad (4.11)$$

$$\alpha_{ult} = \frac{1.031 \cdot w/c}{0.194 + w/c} + \exp\left(-0.885 - 13.7 \cdot p_{C_4AF} \cdot p_{cem} - 283 \cdot p_{Na_2Oeq} \cdot p_{cem}\right) \quad (4.12)$$

$$\tau = \exp\left(2.68 - 0.386 \cdot p_{C_3S} \cdot p_{cem} + 105 \cdot p_{Na_2O} \cdot p_{cem} - 12.6 \cdot ACCL\right) \quad (4.13)$$

$$\beta = \exp\left(-0.494 - 3.80 \cdot p_{C_3A} \cdot p_{cem}\right) \quad (4.14)$$

4.3 METHODOLOGY

4.3.1 Factors considered

The WSC is used to characterize hydrostatic pressure reduction in the annular cement and the effect of parameters on the potential for gas migration. These parameters include: 1.) formation

permeability, 2.) initial overburden pressure at depth of interest, 3.) wellbore temperature, 4.) w/c ratio, 5.) cement composition, and 6.) $CaCl_2$-based accelerator.

4.3.1.1 Formation permeability

A great advantage of the WSC is that a real-scale section of a wellbore containing a steel casing, a cemented annulus and a rock formation can be simulated. A technique has been developed for replicating formations with any prescribed mechanical properties representative of an actual in-situ formation. In Chapter 3, mixture designs for low permeability and high permeability formations were established. 1.) Low permeability formations represent the nearly "impermeable" rock formations. The texture of the formation wall provides a representative borehole condition for an "impermeable" section. Low permeability formations are only prepared for evaluating the hydrostatic pressure reduction during early hydration and are incapable of simulating gas or fluid invasion. 2.) High permeability formations consist of a 0.5-in section for gas to invade into the cemented annulus if gas migration is to occur. The high permeability layer represents localized gas-bearing sandstone. The permeability, porosity and other properties may be achieved by adjusting the mixture design used in casting the formation. High permeability formations are used for gas migration tests to investigate the effect of the high permeability section in terms of formation voids and mud cake. Table 3.4 presents the physical properties of low and high permeability formations used in the WSC tests.

4.3.1.2 Pressure level

Surface casing strings (in the Marcellus play) typically range from 350 to 800 ft deep, and in some cases, up to 3,000 ft (Williams, et al. 2012). Most state regulations require cementing to surface for surface casing (Richardson, et al. 2013). Therefore, the hydrostatic pressure

generated by the cement column can be calculated and typically ranges from 270 to 650 psi, but up to 2,450 psi for a 3,000 ft cement column. An initial overburden pressure of 350 psi was selected for the WSC testing, corresponding to a depth of approximate 430 ft. To evaluate the effect of initial overburden pressure, a different pressure level of 225 psi was selected (approximate 280 ft deep).

4.3.1.3 Wellbore temperature

For a surface casing string, the highest geothermal temperature is approximate 120 ℉. It is known that the hydration products from cement hydration will be the same if the curing temperature is less than 140 ℉ (60 ℃). Therefore, standard room temperature (70 ℉) was selected as the test temperature for simplicity and ease of evaluation. To evaluate the effect of curing temperature, another temperature level was selected to be 90 ℉. To minimize the variability caused by preconditioning and conditioning, all materials and devices were temperature-equipollent for 24 hours at standard room temperature.

4.3.1.4 Slurry density

Standard slurry density in API Specification 10A is selected for the WSC testing at a w/c ratio of 0.46. This standard w/c ratio corresponds with a slurry density of 15.6 ppg. The slurry design may be adjusted due to the density requirement. Fluid loss or fluid infiltration can also result in a change in w/c ratio. Therefore, w/c ratios of 0.4 and 0.46 are selected to evaluate the effect of w/c ratio.

4.3.1.5 Cement type

API Class A cement is typically used when cementing the surface casing strings. Occasionally, ASTM Type I cement is used. Therefore, both Class A and Type I cements are selected for comparing the behavior of different cement composition in this study. Table 3.5 shows the cements used for this research.

4.3.1.6 Calcium chloride

Although calcium chloride anhydrate ($CaCl_2$) is typically used in the petroleum industry practices, calcium chloride dihydrate ($CaCl_2 \cdot H_2O$) was selected for use in this study due to its high purity. Calcium chloride dihydrate was dissolved in the mix water. The solution was allowed to equilibrate to standard room temperature (70 ℉) for 24 hours before using it to mix the slurry. Calcium chloride dihydrate should not be added directly to the cement as a dry blended admixture because the chemically-bound water molecules within the admixture may cause premature cement hydration. The primary reasons for dissolving the admixture in the mix water are: 1.) to avoid the temperature variation caused by calcium chloride dissolution, 2.) to reduce the composition variation of prepared cement slurries, and 3.) to obtain a more accurate estimate of degree of hydration from calorimetric measurements. Three levels of $CaCl_2$ are considered: 0.0, 1.0 and 2.0 %BWOC.

4.3.2 Experimental design

As discussed in Chapter 2 and Section 4.2.2, curing history affects the properties of hydrating cement. To be consistent, cement slurries are bench-mixed according to API Specification 10A (2002). A 245-in^3 constant speed blender is used for preparing slurries, as shown in Figure

3.11a. To ensure that the same energy is introduced to cement slurries, slurry volumes are kept constant are 152.6 in^3 (versus required cement volume of 146.5 in^3) when w/c ratio is adjusted. The slurry formulas are presented in Table 4.4. To simulate filed pumping history, a 20-minute conditioning under the ambient condition is applied to cement slurries at a stirring speed of 60 rpm using the blender shown in Figure 3.11b. Table 4.5 shows the slurry designs and boundary conditions considered in the WSC tests. The WSC testing was conducted according to the operation procedure described in Section 3.3.4.

Table 4.4. Mixing quantities of cement and water for slurry.

Slurry design	w/c ratio	
	0.4	0.46
Cement, lb (specific gravity: 3.15)	7.717	7.092
Water, lb	3.087	3.261

Table 4.5. Summary of WSC testing performed.

WSC Test	Cement type*	w/c ratio**	$CaCl_2$, %BWOC	Overburden pressure level, psi	Temperature, ℉	Formation permeability	Test type***
1	Class A	0.4	0.0	350	70	Low	Pressure
2	Class A	0.46	0.0	350	70	Low	Pressure
3	Class A	0.46	0.0	350	90	Low	Pressure
4	Class A	0.46	1.0	350	70	Low	Pressure
5	Class A	0.46	2.0	350	70	Low	Pressure
6	Class A	0.46	2.0	225	70	Low	Pressure
7	Class A	0.46	0.0	475	70	High	Migration
8	Type I	0.46	0.0	350	70	Low	Pressure
9	Type I	0.46	0.0	100	70	Low	Pressure
10	Type I	0.46	0.0	100	70	High	Pressure
11	Type I	0.46	0.0	500	70	Low	Shrinkage
12	Type I	0.46	0.0	1	70	High	Bubbling

Note: * Composition and fineness of cements are listed in Table 3.5.

** Table 4.4 shows the slurry designs.

*** "Pressure" = hydrostatic pressure reduction test; "Migration" = gas/fluid migration test; "Shrinkage" = volume reduction of cement matrix; "Bubbling" = gas bubbling through slurry.

4.4 RESULTS AND ANALYSES

4.4.1 Cement matrix shrinkage and gas channeling

4.4.1.1 Volume reduction

The first WSC test was conducted on a neat slurry prepared using Type I cement with a w/c ratio of 0.46 (Test 11 in Table 4.5). Cement slurries were conditioned and tested at 70 ℉. An overburden pressure of 500 psi was directly applied to the 6-in cement section. This simulated a pressure representative of the cement wellbore section at 620 ft deep. The purpose of this test is to evaluate the cement behavior under a high fluid pressure applied *directly* on the top of cement column.

As can be seen in Figure 4.1, the top surface of the cement slurry dropped by 3/16 in after the cement hardened. This volume reduction of 3.1% is attributed to the chemical shrinkage and consolidation of the cement matrix. No fluid loss into the formation occurred during the test since the formation was saturated before testing. At final set, as determined using the Vicat test (ASTM C191), chemical shrinkage resulted in a 0.4% volume reduction. Under the high overburden pressure, the cement matrix was seen to experience compaction during early hydration. As shown in Figure 4.1a and Figure 4.1b, the residue on the formation wall indicates that the cement had developed sufficient strength to maintain a deformed shape when the top surface of the cement was near the original elevation of the slurry. As the cement hydrated, the water in the cement domain was first consumed through the hydration reaction. Under the high pressure applied on the top of the cement slurry, cement gel was pushed down to displace the available space produced by the chemical shrinkage, leaving a failure surface along the cement-

formation interface. Segregation may also occur and lower the top surface, but the compaction of the cement matrix is the primary reason for the volume reduction.

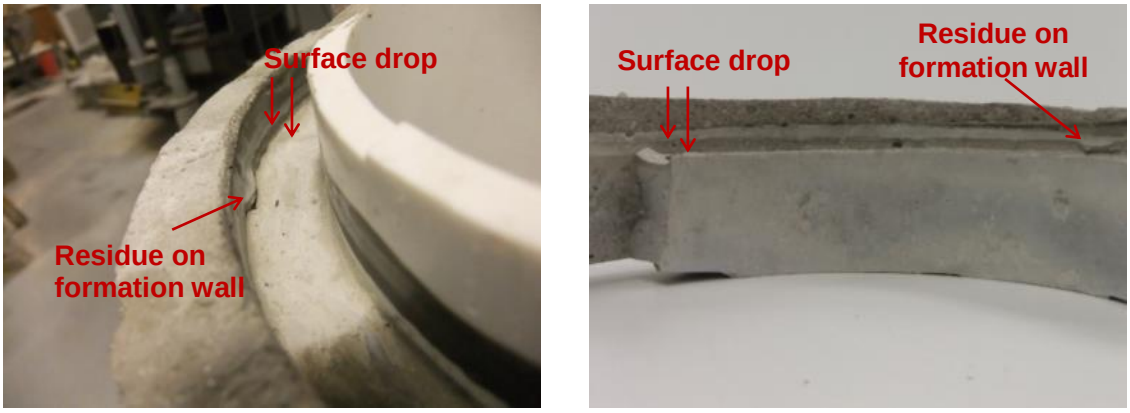

(a) Top of the chamber (b) Top slice of formation sample

Figure 4.1. Shrinkage of the cement column.

After the WSC testing was completed, the wellbore sample was removed from the chamber. The wellbore sample included the exterior formation, the cemented annulus and the inner casing. Saw cuts were made perpendicular to the wellbore, providing 7 sectional pieces that were approximately 1-in thick. These cross-sectional slices were all air dried for 72 hours. Figure 4.2a shows the effect of drying shrinkage on a slice of the wellbore sample. As the sample dries, the cement sheath shrinks, resulting in radial cracks that are perpendicular to the casing. As can be seen in Figure 4.2b, the cracking initiates from the inner radius.

(a) Radius cracking due to dry shrinkage

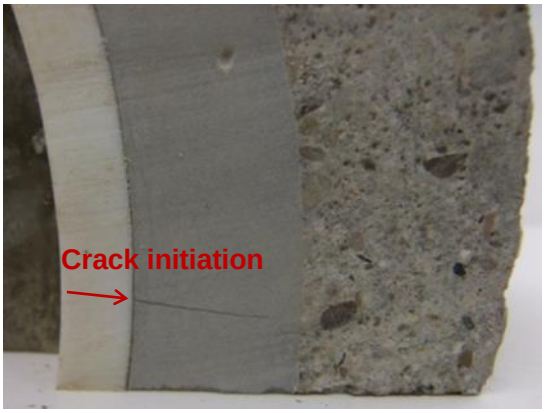

(b) Cracking from inner

Figure 4.2. Radial cracking in the cemented annulus.

4.4.1.2 Gas bubbling

In order to study the occurrence of gas migration due to insufficient hydrostatic pressure before the cement sets, a WSC test was conducted by bubbling gas through the annular cement. A neat slurry was prepared using Type I cement with a w/c ratio of 0.46 (Test 12 in Table 4.5). Cement slurries were conditioned and tested at 70 ℉. No overburden pressure was applied during the test. A high permeability formation was used and the formation gas was injected through the bottom of this sandstone layer. After the cement was placed in the annulus, pressurized formation gas was applied through the bottom of the high permeability sandstone layer. As the purpose of this test was to investigate defects in the annulus as a result of gas bubbling, a small formation gas flow rate was used until the cement hardened.

Once the formation gas pressure was applied, gas bubbles migrated immediately from different locations within the annulus, ultimately forming six bubble channels on the cement surface. Figure 4.3 shows the gas bubbling on the cement surface. As the cement hydrated, the bubbling rate decreased in some of the channels. As the cement continued to set, several channels were observed to “disappear”, leaving only three channels that could be detected. After

the cement had hardened, the wellbore section was sawed into slices to investigate the gas channels. As can be seen in Figure 4.3e, Figure 4.3f, and Figure 4.3g, some of the gas channels are sub vertical and at times merge together as they migrate upward.

(a) Gas bubbling in cement

(b) Close look of gas bubbling

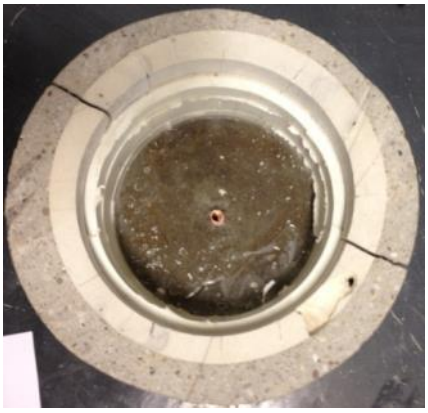

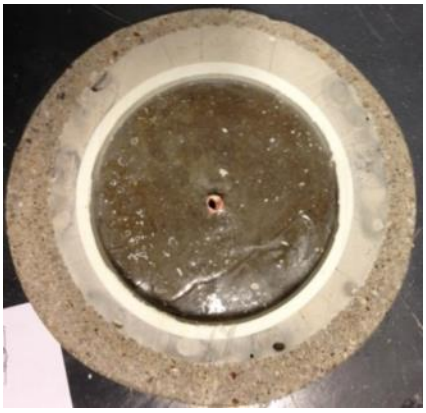

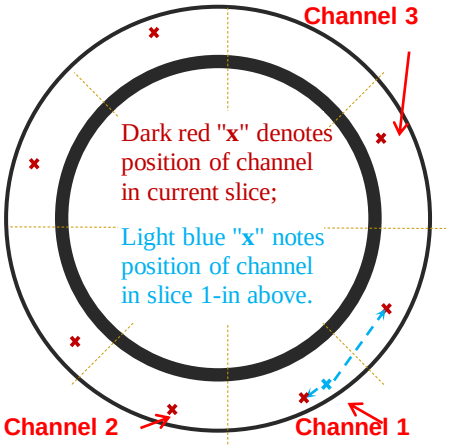

(c) Channel position 1-in below the top

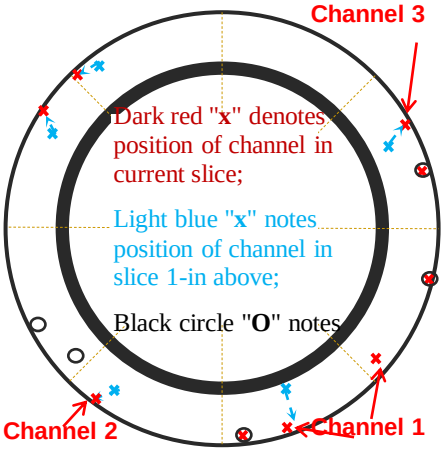

(d) Channel position at bottom layer

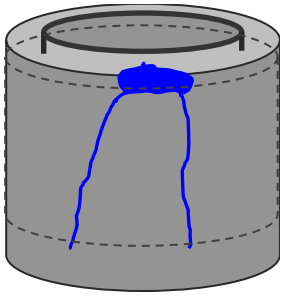

(e) Shape of Channel 1

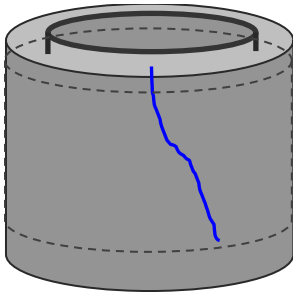

(f) Shape of Channel 2

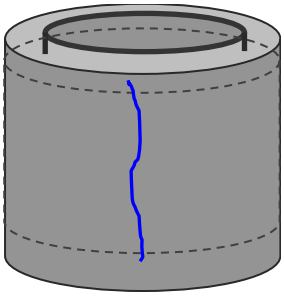

(g) Shape of Channel 3

Figure 4.3. Sections through WSC showing channels created by gas bubbling.

4.4.1.3 Gas infiltration due to pore pressure reduction

The intent of the next simulation performed is to replicate pressurized fluid migration due to hydrostatic pressure reduction below the formation gas pressure. A fluid migration test was performed in the WSC using nitrogen-saturated water introduced to the cement through the formation. A neat slurry was prepared using Class A cement with a w/c ratio of 0.46 (Test 7 in Table 4.5). The cement slurry was conditioned and tested at 70 ℉. After the cement was placed in the annulus, pressurized gas was injected into the water-saturated high permeability sandstone layer at the bottom of the formation. The overburden pressure was maintained at 475 psi. The pressure of the nitrogen-saturated water was maintained at 470 psi throughout the duration of the test. For migration to occur, the pressurized fluid must invade into the cemented annulus from the gas-bearing zone located at the bottom of the formation.

Measurements indicate that the slurry pore pressure starts to drop after the cement reaches initial set, as determined by the Vicat test. Due to the compensation of the pressure as a result of the gas invasion, the slurry pore pressure dropped only to 445 psi after 18 hours. A forensic analysis revealed that the nitrogen-saturated water penetrated into the cemented annulus. Figure 4.4 shows the patterns of migration channels created by the nitrogen-saturated water. The infiltration of the nitrogen-saturated water increases the localized w/c ratio and results in a porous area with a 0.25-in diameter. The color of the cement in this porous area is lighter than the cement unaffected by fluid migration. The cross-section of the gas channel created by the nitrogen-saturated water is more circular in shape than that of the water invasion. As shown in Figure 4.4b, a 0.04-in diameter gas channel formed. The fluid that invaded the cemented annulus has no means to escape since the simulation was run with the backflow port closed. The nitrogen-pressurized water invaded the cement column from the bottom, channeled upward, and

stopped in upper portion as the cement hardened, resulting in a tortuous path as shown in Figure 4.4c. Similar to what was found in Section 4.4.1.2, channels formed within the cement matrix domain, and not along the formation-cement or cement-casing interfaces. Gases and other fluids always take the path of least resistance within the compressible cement matrix domain (as discussed in Section 2.3.1). By pushing the solids aside, gases infiltrate the cement matrix, resulting in a defected cemented annulus.

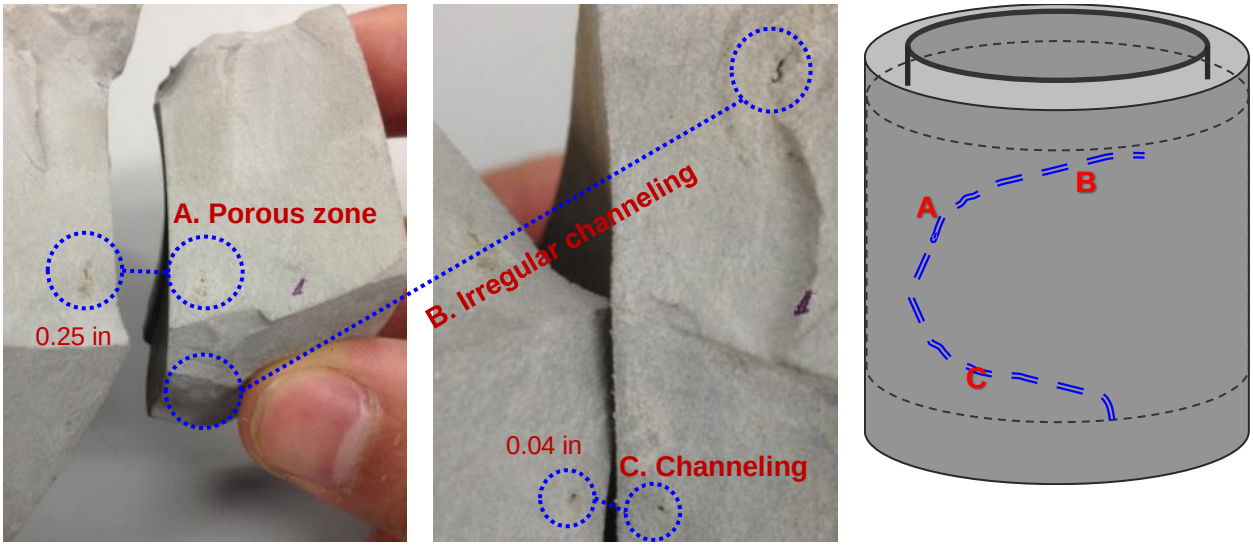

(a) Matrix degrading (b) Gas channeling (c) Shape of channel

Figure 4.4. Nitrogen-saturated water channel formed in cement matrix.

4.4.2 Factors affecting hydrostatic pressure reduction

The factors affecting the hydrostatic pressure reduction within the cemented annulus were investigated. In order to accurately quantify the w/c ratio of the mixture, a no fluid loss condition with a low permeability formation was simulated, thus maintaining the initial w/c ratio. A range of cement design characteristics, as well as a range of downhole conditions, were evaluated. These factors include: formation permeability (zero permeability and a permeable

formation), initial overburden pressures of 225 psi and 350 psi representing a wellbore section at approximately 277 ft and 430 ft deep, respectively, and downhole temperatures of 70 ℉ and 90 ℉. The cement design factors considered are w/c ratio (0.4 and 0.46), cement composition (Type I cement and Class A cement), and a $CaCl_2$-based accelerator (0%, 1% and 2% BWOC). Tests are numbered and the corresponding testing conditions can be found in Table 4.5.

4.4.2.1 Formation permeability

The purpose of Tests 9 and 10 (Table 4.5) is to evaluate the effect of formation voids on the hydrostatic pressure reduction within the annulus. Figure 4.5 shows the WSC results with the pressure measured in the cement annulus (Pore P.) and the overburden pressure measured in the upper portion of the chamber (OBP) plotted over the time period for which the test was run. The legend label in Figure 4.5 is defined as follows (cement type, w/c ratio, dosage of $CaCl_2$, formation type). For these two tests, the formation permeability was the only parameter of interest. All other variables were held constant. Neat slurries were prepared using Type I cement with a w/c ratio of 0.46. Cement slurries were conditioned and tested at 70 ℉. An overburden pressure of 90 psi was applied, simulating a depth of 110 ft. In Test 9, an impermeable formation was used, while Test 10 used a high permeability formation. No formation gas was applied and all the pressure ports were closed for the duration of the test.

As seen in Figure 4.5, the slurry pore pressure starts to drop at the same time in both tests. However, the slurry pore pressure reduction rates are not the same. The test with the impermeable formation has a greater pressure reduction rate (Test 9) and therefore a shorter period of time the cement would be vulnerable to gas migration. This comparison demonstrates one of the advantages of the WSC, as it is capable of simulating and evaluating the effect of rock formation characteristics on the performance of cement slurry.

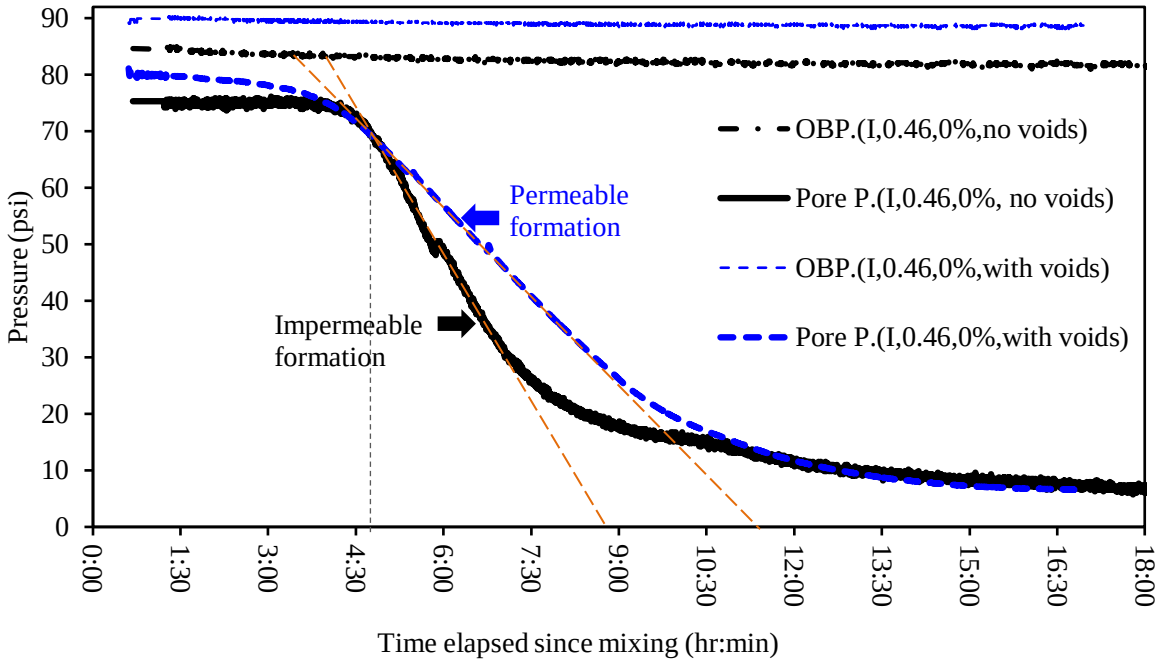

Note: Data legend (cement type, w/c ratio, dosage of $CaCl_2$, formation property).

Figure 4.5. Effect of formation permeability on pressure reduction.

4.4.2.2 Depth in the wellbore

The purpose of the next set of tests is to evaluate the effect of the depth in the wellbore on the hydrostatic pressure reduction within the annulus. Figure 4.6 shows the WSC results with the pressure measured in the cement annulus (Pore P.), the slurry temperature in the annulus (Cmt T.), and the ambient room temperature (Ambient T.) plotted over the time period for which the test was run. The legend label in Figure 4.6 is defined as follows (cement type, w/c ratio, dosage of $CaCl_2$, pressure level). All other variables were held constant. Neat slurries were prepared using Class A cement with a w/c ratio of 0.46. Cement slurries were conditioned and tested at 70 ℉. A low permeability formation was used for both tests. In Test 6, an overburden pressure of 350 psi was applied, representing a depth of 430 ft, while an overburden pressure of 225 psi was applied for Test 7, representing a depth of 280 ft. The purpose of these tests is to evaluate

the effect of the depth in the wellbore on the hydrostatic pressure reduction within the annulus. Figure 4.6 shows results from Tests 6 and 7 in Table 4.5.

Figure 4.6a shows the pressure history of the two WSC tests. To better illustrate the findings, the difference between the initial overburden pressure and the pressure measured at each individual point in time is plotted, as shown in Figure 4.6b. The temperature history is similar for the two tests; therefore, the degree of hydration will be approximately equal at any given time within the test period. Interestingly, the hydrostatic pressure reductions are nearly identical until the pore pressures approaches zero psi. The critical hydration period occurs before final set, as determined by the Vicat test (ASTM C191), and therefore falls within the earlier portion of the pressure history data. This indicates that the magnitude of the overburden pressure does not affect the pressure reduction rate in the cemented annulus. Instead, the ability of the cement slurry to transmit the hydrostatic pressure is a function of the stage of the hydration of the cement slurry.

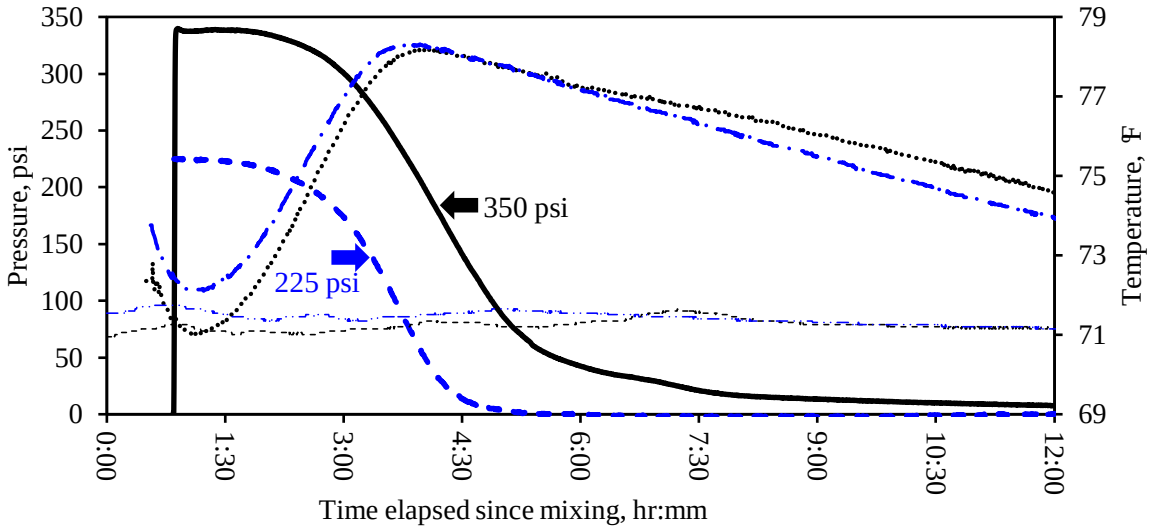

(a) Time history

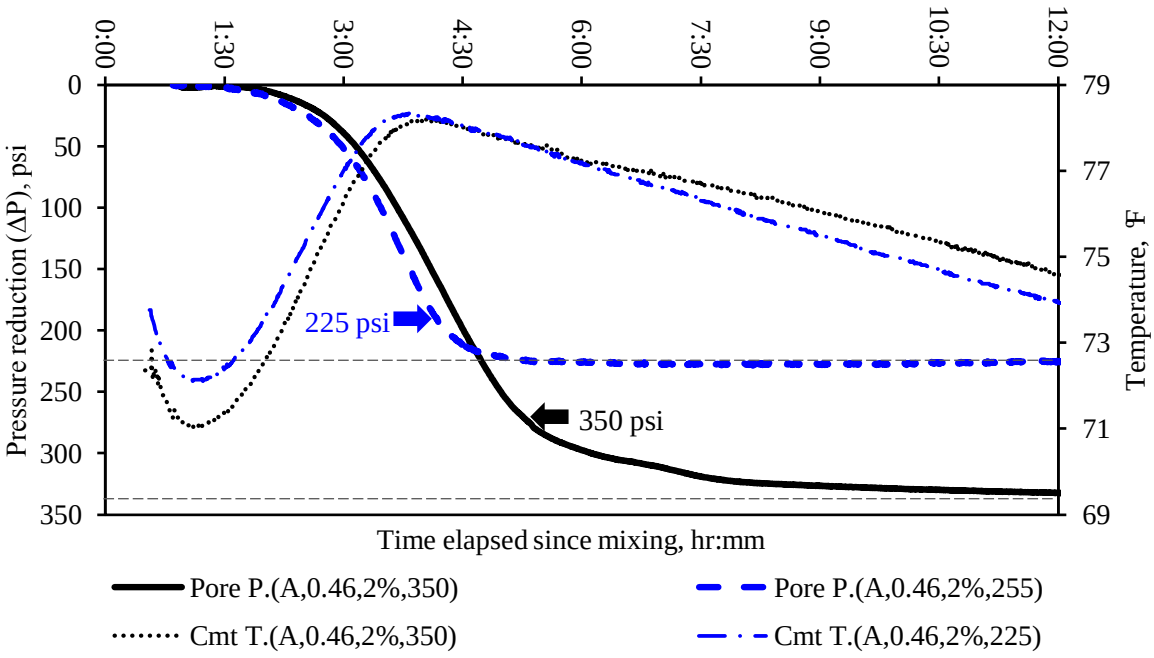

(b) Pressure reduction

Note: Data legend (cement type, w/c ratio, dosage of $CaCl_2$, pressure level).

Figure 4.6. Effect of initial overburden pressure on pressure reduction.

4.4.2.3 Wellbore temperature

Along the depth of the wellbore, the temperature profile is assumed to be a function of depth. As the wellbore depth increases, the temperature also increases. Moreover, a localized abnormal temperature profile may exist within the wellbore, especially when gas-bearing sandstones are encountered. Therefore, the simplified relationship derived based on classic shear stress, as shown in Equation (2.3b), cannot predict the hydrostatic pressure accurately due to the assumption that the rate of cement hydration is the same for the entire cement column. A method to quantify the hydration stage should be developed to better predict the ability of a cement section to transmit hydrostatic pressure along the depth of wellbore.

Wellbore temperatures can affect the rate of hydrostatic pressure reduction during cement hydration. To test this affect, the temperature under which the simulation was performed was varied. Figure 4.7 shows the results from Tests 2 and 3 in Table 4.5 with the pressure measured in the cement annulus (Pore P.) and the slurry temperature in the annulus (Cmt T.) plotted over the time period for which the test was run. The legend label in Figure 4.7 is defined as follows (cement type, w/c ratio, dosage of $CaCl_2$, pressure level, curing temperature). The curing temperature was the only parameter of interest of these two tests, while all other variables were held constant. Neat slurries were prepared using Class A cement with a w/c ratio of 0.46. Cement slurries were mixed and conditioned at 70 ℉. An overburden pressure of 350 psi was applied throughout the duration of the test representing a depth of 430 ft. A low permeability formation was used for both tests and simulating a no fluid loss condition. In Tests 2 and 3, the WSC temperature was set to 70 ℉ and 90 ℉, respectively. As temperature increases, the hydration rate also increases (Figure 4.7a). For the case of 90 ℉, the slurry pore pressure drops to 175 psi after 6.75 hours, while it takes 13.25 hours at 70 ℉ for the same pressure reduction.

During the linear portion of the pressure reduction, the pressure reduction rate is 151.0 psi/hr and 62.3 psi/hr for 90 ℉ and 70 ℉ simulations, respectively.

An encouraging observation can be made when the pressure is plotted against degree of hydration, as shown in Figure 4.7b. As discussed in Chapter 2 and Section 4.2.3, degree of hydration is a fundamental property that can be used to characterize the evolution of the microstructure of the cement. As seen in Figure 4.7b, the slurry pore pressure with respect to degree of hydration is nearly identical for both sets of test results. For the same slurry design, the effects of borehole conditions, such as temperature, can be distinguished by employing degree of hydration to describe the cement hydration better than SGS.

The results also verify that shortening the critical hydration period cannot change the occurrence of gas migration. Compared to the simulation ran at 70 ℉, the transition time for the 90 ℉ simulation is reduced because the increased curing temperature results in a greater hydration rate. If gas migration is to occur for the simulation at 70 ℉, gases will invade into the identical microstructure of the 90 ℉ simulation at the same hydration stage. The time to reach the same degree of hydration has been reduced due to a higher curing temperature. A shorter time period when the cement is vulnerable for gas migration could potential reduce the risk for gas migration. Nevertheless, shortening the transition time cannot change the occurrence of gas migration, although it may potentially reduce the time available for gas to invade the cemented annulus.

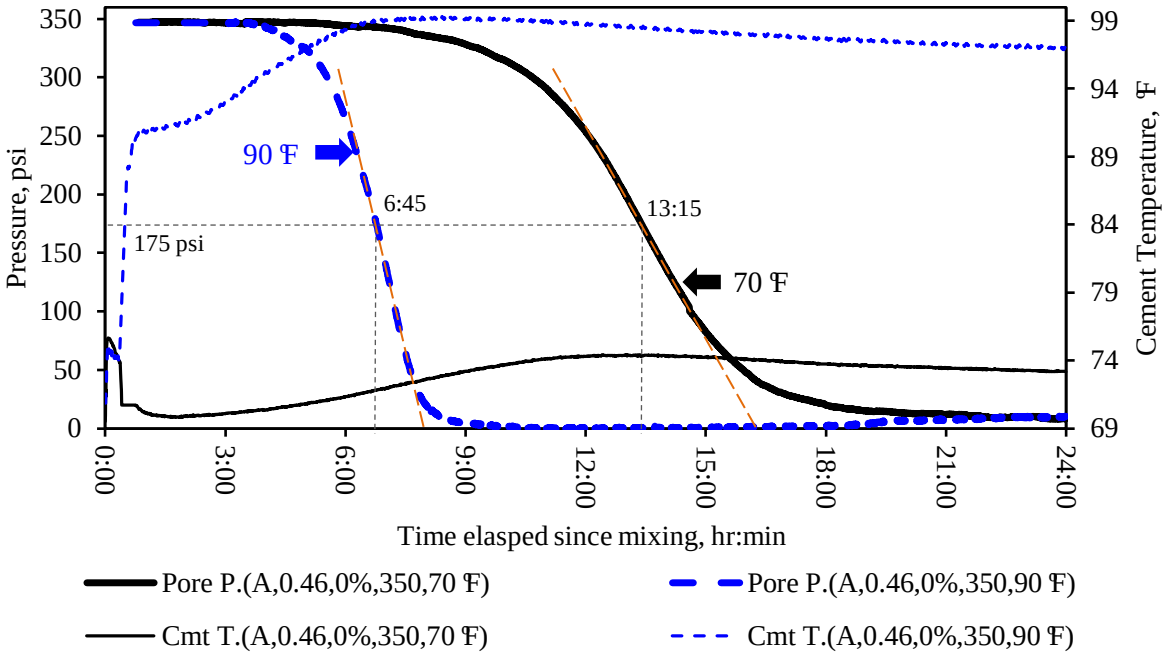

(a) Time history

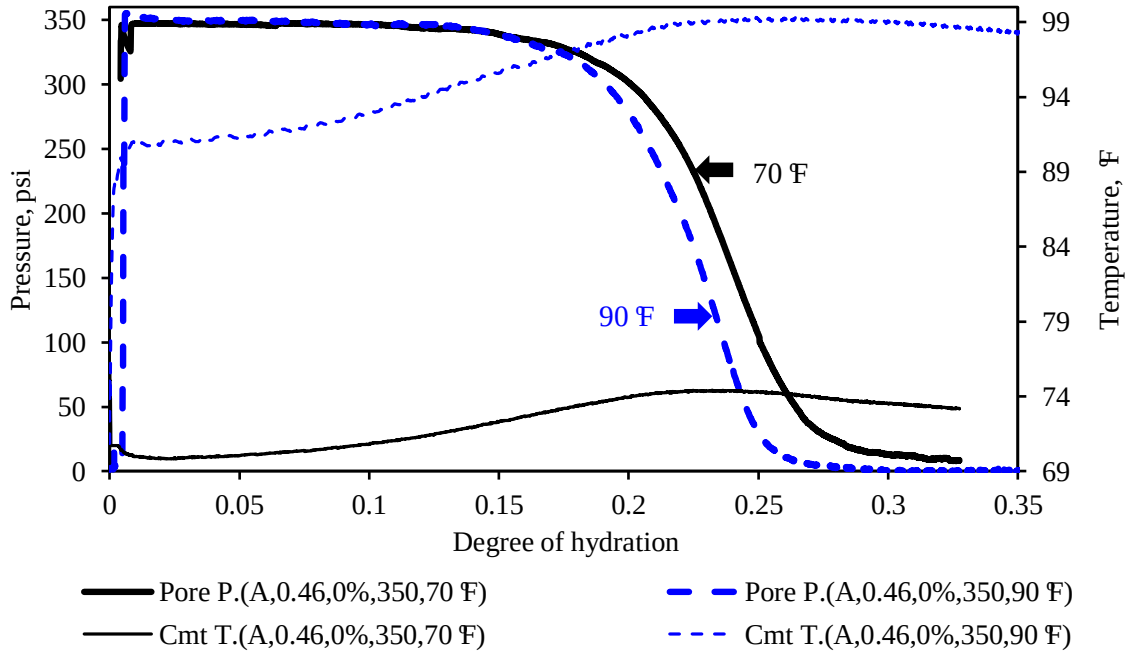

(b) Degree of hydration

Note: Data legend (cement type, w/c ratio, dosage of $CaCl_2$, pressure level, curing temperature).

Figure 4.7. Effect of wellbore temperature on pressure reduction.

4.4.2.4 W/c ratio

W/c ratio affects the time of initiation of hydrostatic pressure reduction within the cemented annulus. Class A cement was blended at two different w/c ratios (0.4 and 0.46 for tests 1 and 2, respectively) to evaluate the effects of w/c ratio on pressure reduction. Cement slurries were prepared and tested at 70 ℉. An overburden pressure of 350 psi was applied throughout the duration of the simulation representing a depth of 430 ft. Low permeability formations were used in each test to simulate a no fluid loss condition.

Figure 4.8 shows the WSC results with the pressure measured in the cement annulus (Pore P.) and the slurry temperature in the annulus (Cmt T.) plotted over the time period for which the test was run. The legend label in Figure 4.8 is defined as follows (cement type, w/c ratio, dosage of $CaCl_2$, pressure level). In Figure 4.8, the initiation of pressure drop occurs earlier as the w/c ratio decreases. The w/c ratio affects the microstructural development of the cement matrix. When the w/c ratio is high, the cement particles are suspended in the water and have little contact with other particles. As the distance between particles increases, the interactions between particles are lower and a high fluidity is observed. More hydration products must form in order to fill the space between particles. Therefore, a high w/c ratio design needs to achieve a higher degree of hydration to develop the same cement matrix strength as compared to that of a lower w/c ratio design. The theory explaining these statements has been presented when considering the degree of hydration in Section 2.3.3.2.

Figure 4.8b shows the slurry pore pressure with respect to degree of hydration. The pressure reduction initiated at a lower degree of hydration for the slurry with a lower w/c ratio. However, the shapes of the pressure curves are identical other than a shift in the degree of hydration of 0.052. When the slurry pore pressure is 320 psi (nonlinear portion), the degrees of

hydration for 0.4 and 0.46 w/c ratios are 0.134 and 0.185, respectively. When the slurry pore pressure is 175 psi (linear portion) the degrees of hydration for 0.4 and 0.46 w/c ratios are 0.185 and 0.237, respectively. This shift in degree of hydration can be explained by the fraction of solids generated from hydration products to fill extra space for the slurry with a 0.46 w/c ratio. Therefore, the volumetric fraction of solids and the matrix percolation should be predicted together with degree of hydration.

To determine the porosity of the cement matrix for different w/c ratios, the concept of capillary porosity is used. Capillary porosity is defined as a ratio of the capillary pore volume to the original volume of the cement slurry (Sidney et al. 2003):

$$P_c(\alpha) = \frac{V_c}{V_p} = \frac{w/c - 0.36 \cdot \alpha}{w/c + 0.32} \tag{4.15}$$

where, $P_c(\alpha)$ = capillary porosity at degree of hydration of α;

V_c= capillary pore volume;

V_p = original volume of cement slurry.

By using Equation (4.15), the capillary porosities at 175 psi for 0.4 and 0.46 w/c ratios can be calculated as 46.3% and 48.0%, respectively. Therefore, when the hydrostatic pressure is reduced to the same level (from 350 to 175 psi), the solid fraction in the cement matrix is nearly identical though the w/c ratios are different.

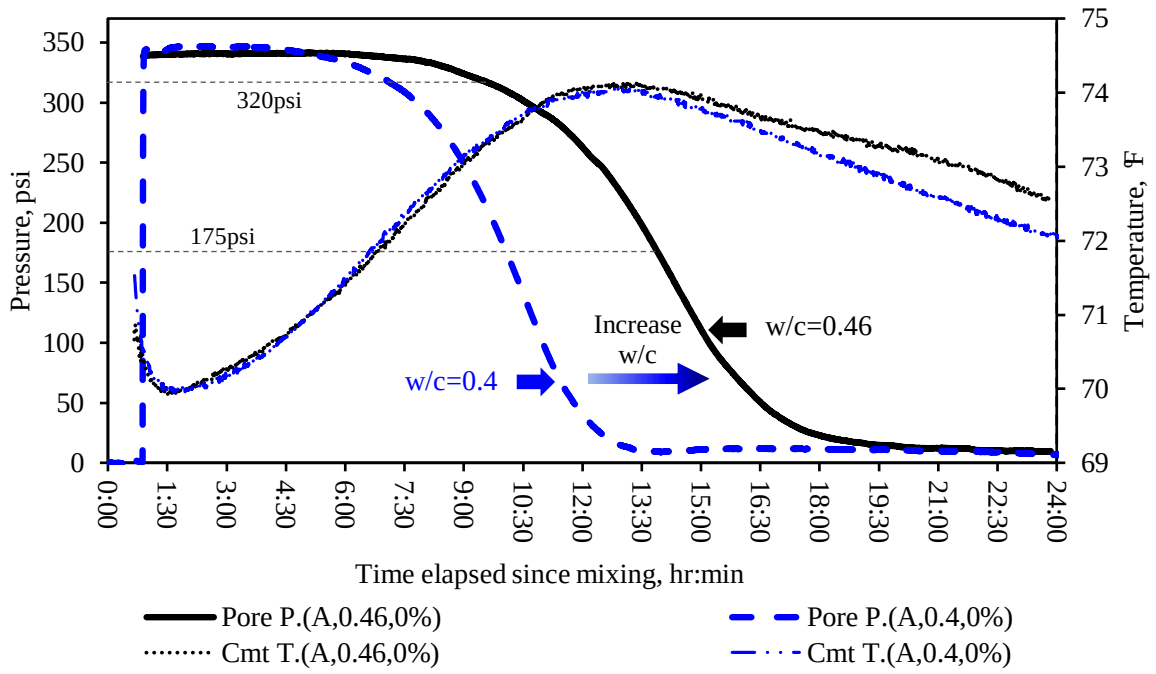

(a) Time history

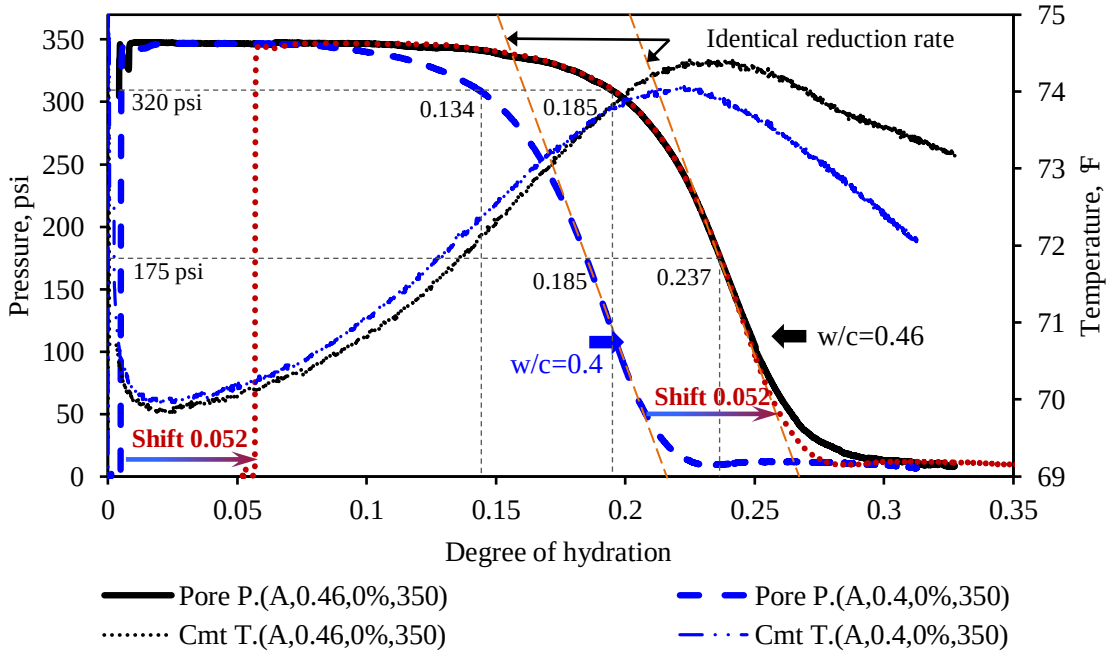

(b) Degree of hydration

Note: Data legend (cement types, w/c ratio, dosage of $CaCl_2$, pressure level).

Figure 4.8. Effect of w/c ratio on pressure reduction.

4.4.2.5 Cement composition

Cement compositions can have a significant effect on the microstructural development and therefore, the mechanical properties of the cement matrix. Tests were performed to evaluate the effect of cement composition on the hydrostatic pressure reduction within the annulus. Figure 4.9 shows the WSC results from Tests 2 and 8 in Table 4.5 with the pressure measured in the cement annulus (Pore P.) and the slurry temperature in the annulus (Cmt T.) plotted over the time period for which the test was run. The legend label in Figure 4.9 is defined as follows (cement type, w/c ratio, dosage of $CaCl_2$, pressure level). Two slurries were prepared using Type I and Class A cement. A summary of the cement composition and fineness for these cement types can be found in Table 3.5. Cement slurries with a w/c ratio of 0.46 were prepared and tested at 70 ℉. An overburden pressure of 350 psi was applied throughout the duration of the simulation, representing a depth of 430 ft. A low permeability formation was used for each test so that a no fluid loss condition could be simulated.

Compared to Class A cement, Type I cement presents a poor gas-flow-control property as the slurry pore pressure starts to drop before the cement develops sufficient strength to withstand pressurized gas. As seen in Figure 4.9a, the slurry pore pressure for Type I cement starts to drop earlier than that for Class A. Assuming that normal formation pressure exists, formation gas pressure is estimated to be 185 psi at 430 ft deep. For the Type I cement, the slurry pore pressure starts to drop before the initial set (8:15) and reaches 185 psi at 10:56, 23 minutes before the final set (11:19). Initial and final set was established using the Vicat test (ASTM C191). As the strength of cement matrix is still low, pressurized gas, if present, may invade into the cement matrix.

The performance difference in pressure reduction between Class A and Type I cement discussed above may be the result of the specific type of hydration product that generated by the difference in percentage of aluminates (C_3A and C_4AF) and/or silicates (C_3S and C_2S), when comparing the cement compositions shown in Table 3.5. Ettringite, produced from the hydration of tricalcium aluminate (C_3A) and/or tetracalicium alumino-ferrite (C_4AF), consists of well crystalized needles, which will move crystals and grains out of its way (Mindess et al. 2003). As the resistance of the cement slurry to deform increases with the growth of hydration product, the slurry cannot move downward as freely to compensate for the volume reduction caused by chemical shrinkage and/or fluid loss. Figure 4.9b shows the slurry pore pressure with respect to degree of hydration. Type I cement loses its ability to transmit the hydrostatic pressure at a lower degree of hydration than that of Class A cement. As shown in Figure 4.9b, the degree of hydration for Type I cement (α=0.157) is approximately 51.0 % greater than that of Class A (α=0.237), when the hydrostatic pressure declines to a level of 175 psi. Class A cement has a higher rate of pressure reduction with increasing degree of hydration than that of Type I cement. As shown in Figure 4.9b, the rates of decrease in pressure with respect to change in degree of hydration are 52.9 psi/0.01 and 47.6 psi/0.01 for Class A cement and Type I cement, respectively.

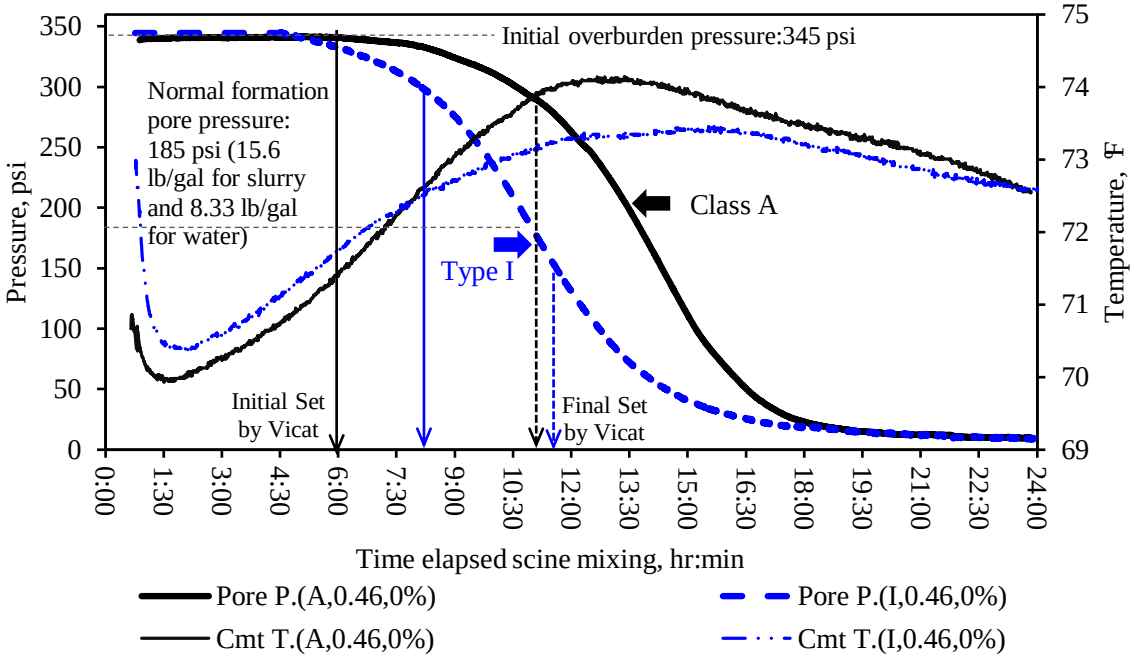

(a) Time history

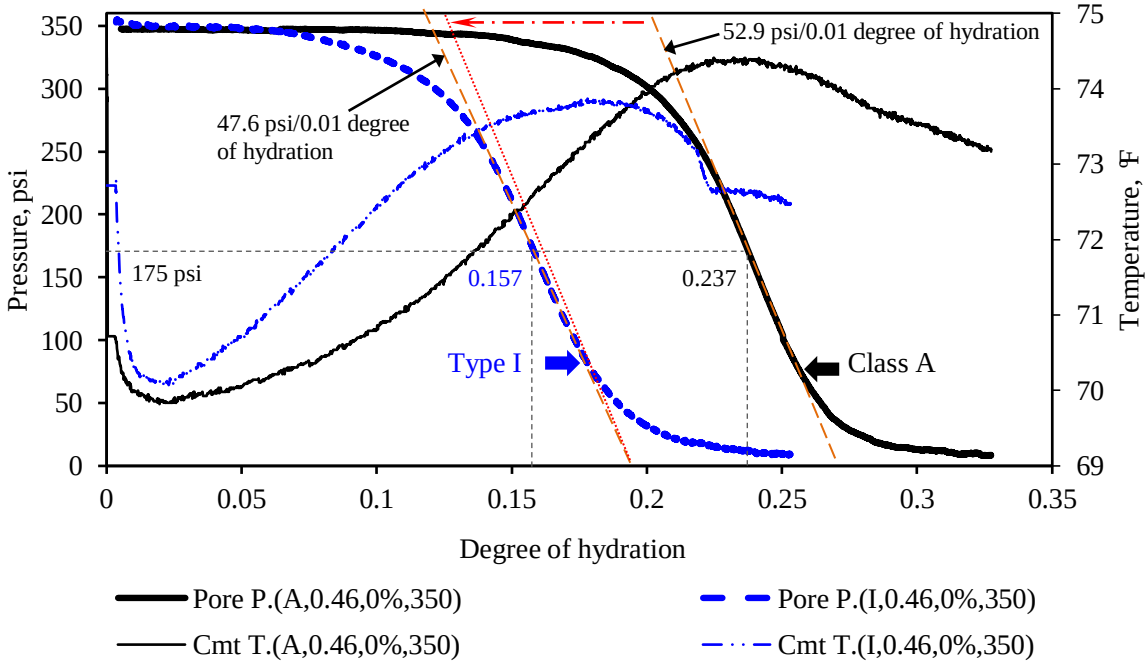

(b) Degree of hydration

Note: Data legend (cement type, w/c ratio, dosage of $CaCl_2$, pressure level).

Figure 4.9. Effect of cement composition on pressure reduction.

4.4.2.6 Calcium chloride

A series of tests were performed to evaluate the effect of $CaCl_2$-based accelerator on the hydrostatic pressure reduction within the annulus. The calcium chloride ($CaCl_2$) additive is the most widely used and accepted accelerator for all classes of OWC. It is widely used in shallow, low-temperature formations to shorten the set time of the cement. Three simulations were performed using Class A cement at a w/c ratio of 0.46 with three different dosages of $CaCl_2$: 0%, 1% and 2% BOWC (Tests 2, 3 and 4, respectively, in Table 4.5). The additive dosage level was the only parameter of interest of these three tests, while all other variables were held constant. Cement slurries were prepared and the simulations were performed at 70 ℉. An overburden pressure of 350 psi was applied throughout the duration of the simulations, representing a depth of 430 ft down the borehole. Low permeability formations were used to simulate a no fluid condition.

Figure 4.10 shows the WSC results with the pressure measured in the cement annulus (Pore P.) and the slurry temperature in the annulus (Cmt T.) plotted over the time period for which the test was run. The legend label in Figure 4.10 is defined as follows (cement type, w/c ratio, dosage of $CaCl_2$, pressure level). As can be seen in Figure 4.10a, the higher the dosage of $CaCl_2$, the earlier the slurry pore pressure drops. For example, the slurry pore pressure for 0% $CaCl_2$ drops from 350 psi to 175 psi after 13.84 hours. In comparison, the same pressure drop will occur after 5.94 and 4.25 hours for a dosage level of 1% and 2% $CaCl_2$, respectively.

The presence of the $CaCl_2$-based accelerator is not accounted for in Equations (4.10) to (4.14); therefore, the degree of hydration was determined by Equation (4.1) using isothermal calorimetry. The pressure data is standardized using degree of hydration, as shown in Figure 4.10b. As can be seen, the pressure curve for 0% $CaCl_2$ is different from those of 1% and 2%.

These differences are a result of the effects of $CaCl_2$ on the hydration of different constituents in the cement. Calcium chloride increases the hydration rate of dicalcium silicate (C_2S) and tetracalicium alumino-ferrite (C_4AF) and deceases that of tricalcium aluminate (C3A), but has little effect on tricalcium silicate (C_3S) during the first 24 hours (Rapp 1935).

When comparing the pressure curves for 1% and 2% $CaCl_2$, they are nearly identical, although the time history differs by 1.69 hours when the slurry pore pressure reaches 175 psi, as shown in Figure 4.10a. For slurries with the same w/c ratio, the effects of chemical additives, such as $CaCl_2$-based accelerator, can be better distinguished by employing degree of hydration to describe the cement hydration, and therefore the slurry pore pressure reduction. Chemical additives will change the history of cement hydration with respect to time, however, the history may be identical when plotted against degree of hydration.

These tests also support the conclusion that shortening the critical hydration period cannot change the occurrence of gas migration, as the microstructural development may occur in the same manner, although the rate of hydration will be different. As shown in Figure 4.10b, the same slurry pore pressure drop corresponds to the same interval of degree of hydration. For example, assume that the formation gas pressure is 175 psi. The critical hydration period is reduced from 5.94 hours to 4.25 hours by adding another 1% $CaCl_2$ to the slurry with 1% $CaCl_2$-based accelerator, as shown in Figure 4.10a. However, when plotting pressure versus degree of hydration as shown in Figure 4.10b, the pressure reduction curves are nearly identical. The degree of hydration increases from 0 to 0.11 as the slurry pore pressure drops from 350 psi to 175 psi.

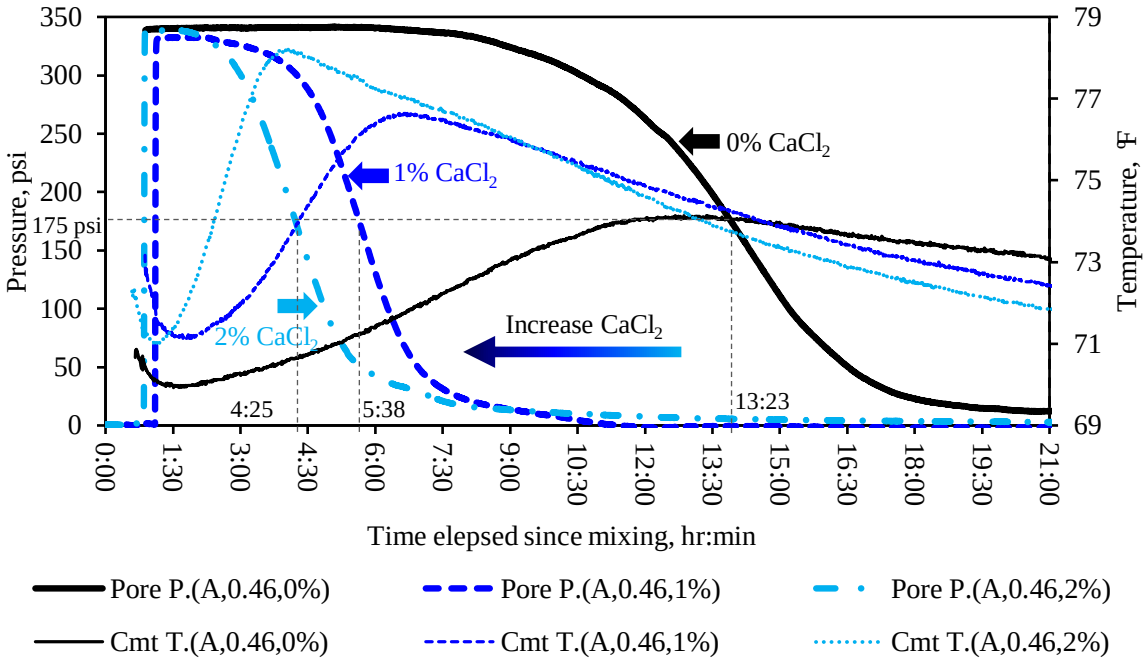

(a) Time history

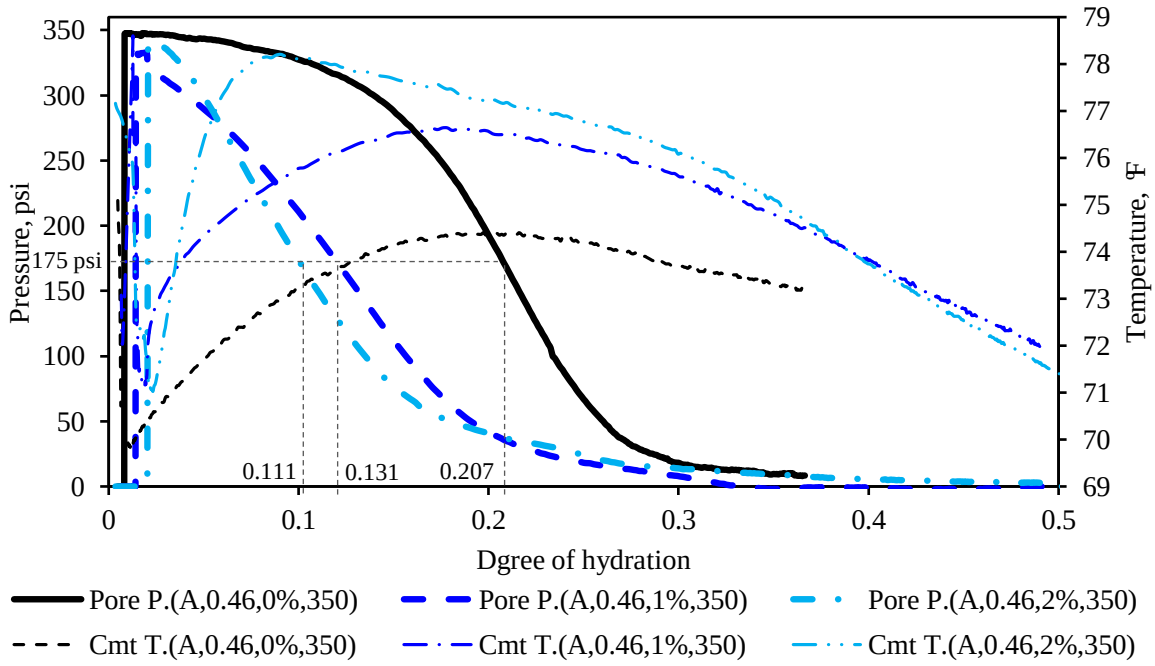

(b) Degree of hydration

Note: Data legend (cement type, w/c ratio, dosage of $CaCl_2$, pressure level).

Figure 4.10. Effect of calcium chloride on pressure reduction.

If hydration products are the same, the degree of hydration can be used to characterize the performance of cement slurries under different curing temperatures and blended with different dosages of accelerators. As discussed in Section 2.3.3.1, microstructure characterization can be performed to broaden the application of the proposed analysis approach. For example, a curing temperature greater than 140 to 149 ℉ may result in different hydration products. If degree of hydration and microstructure characterization are performed, different tests may be more readily compared regardless of curing temperature, applied pressure, or chemical additives.

4.5 CONCLUSIONS

The potential for gas migration in the annular cement was investigated. Experimental results show pressurized fluids can result in a region of porous cement along with the gas channeling that develops during the early gelation stage of cement hydration. Gases and other fluids will find the weakest path to invade into the cement matrix. Water and gas both affect the integrity of the cement sheath, but the channel patterns from invasion of a gas and gas-pressurized fluid are not the same.

The effects of different factors on slurry pore pressure were also studied. These factors include: formation permeability, initial overburden pressure, wellbore temperature, w/c ratio, cement composition, and a $CaCl_2$-based accelerator. The permeability of the formation affects the rate of hydrostatic pressure reduction, which illustrates the advantage of the WSC in simulating rock formations as well as the increased risk in gas migration for formations with a higher permeability. It was also found that the magnitude of the overburden pressure does not affect the pressure reduction rate in the cemented annulus. Instead, the ability of the cement

slurry to transmit the hydrostatic pressure is a function of the hydration stage of the cement slurry. As expected, wellbore temperature, w/c ratio, cement composition, and $CaCl_2$-based accelerator affect the temporal properties of the cement, and therefore the slurry pore pressure reduction during early hydration stage.

Degree of hydration is introduced to characterize the process of cement hydration. By analyzing the temperature history of hydrating cement, the evolution of cement hydration was characterized using the concept of degree of hydration for slurry designs cured at different hydration rates. Although blended with additives of different dosages and cured under different temperature, the cement hydration of the same slurry designs (identical type of cement and w/c ratio) can be standardized using degree of hydration. As explained in Sections 4.4.2.3 and 4.4.2.6, WSC test results also verifies that shortening the critical hydration period cannot change the occurrence of gas migration, although it will potentially reduce the time available for gas to invade and migrate up the cemented annulus.

Comparisons between the performance of the slurries with different w/c ratios shows that the characterization of the volumetric fraction of solids and matrix percolation should be introduced to broaden the applicability of this analysis approach to different slurry designs. Capillary porosity was used to analyze the volumetric fraction of voids in cement slurries with respect to degree of hydration. The results showed that the degree of hydration is nearly identical at the same pressure reduction, although the w/c ratio is different for the same cement slurry.

Slurries blended with 0%, 1% and 2% BWOC $CaCl_2$-based accelerator were also investigated. Comparisons indicate that the hydration of different cement compositions will be affected by this accelerator. The dosage of $CaCl_2$ changes the hydration rate for different

constituents in the cement, but may not change the hydration products. This provides the opportunity to parameterize the slurry designs, such as w/c ratio, dosage of accelerator, and other important factors associated with wellbore conditions, such as temperature.

It should be noted that the findings reported in this study are only valid for the cement and $CaCl_2$-based accelerator used under the operations and conditions herein. Other combinations of cements, supplementary cementitious materials (SCM) and admixtures can exhibit different characteristics. For example, the purified calcium chloride dihydrate ($CaCl_2 \cdot H_2O$) is used for slurry designs in this research. The temperature-equipollent calcium chloride solution is used to reduce the variation caused by the exothermal heat generated from calcium chloride dissolution. In cement jobs, the flake of calcium chloride with a purity varying from 60 % to 100 % is typically used. Other chloride compositions include potassium chloride (KCl, 1 % to 5 %) and sodium chloride (NaCl, 1 % to 2 %). Moreover, a $CaCl_2$-based accelerator will either be blended with the cement powder or will be added to the cement slurry while mixing. However, the trends and findings should be the same as the findings presented in this study, as summarized in Section 5.1.

5.0 CONCLUSIONS AND RECOMMENDATIONS

5.1 SUMMARY

A comprehensive literature review of research activities associated with SGS for characterizing slurry properties with respect to preventing gas migration was summarized. These evaluations show that SGS fails to adequately describe the observed hydrostatic pressure reduction that occurs in the cement annulus as the cement hydrates. Experimental results contradict the linear relationship between the SGS and the hydrostatic pressure reduction assumed in classic shear stress theory employed in the gas and oil industry (Zhang 2002; Zhu et al. 2012). Correctly predicting the hydrostatic pressure reduction is important for achieving zonal isolation because experimental results illustrate that gases can only invade the cement slurry from the time when the hydrostatic pressure is lower than the formation gas pressure, to the time when cement develops sufficient strength to withstand the gas pressure (Cheung and Beirute 1985). This critical hydration period is defined as the transition time (Mueller 2002). Based on limited experimental results (Sabins et al. 1982; Stewart and Schouten 1988), the transition time has been standardized for all cement slurries and field conditions as the period of time between when the cement slurry has reached a SGS of 100 lbf/100ft^2 until it reaches 500 lbf/100ft^2 (API 2010a, 2010b). However, a sensitivity study has shown that no relationship was observed between a short transition time and the occurrence of gas migration (Roges et al. 2004; Rocha et al. 2013).

Although fluid loss and chemical shrinkage are recognized to be additional critical factors causing the hydrostatic pressure reduction, gas migration is a multi-phase problem (Beirute and Cheung 1990). Neither SGS nor fluid loss is able to predict the onset of gas-tight conditions in a cement slurry.

A discussion has been provided regarding the limitations of SGS for characterizing slurry properties with respect to preventing gas migration. SGS may be suitable for describing the fluidity of the slurry in the early gelation stage of cement hydration. When a gel fluid forms, solids in the slurry primarily govern the mechanical properties. While the cement gel will deform under a shear mode, gases and other fluids actually need to break the bonding strength between solids and push solids aside in the cement matrix domain. This requires that the normal bond strength be overcome and the cement matrix be compressed. SGS reflects resistance development within cement slurry as hydration occurs. However, SGS is not sufficient to characterize the compressibility and permeability of the cement matrix. It is also impossible to distinguish normal bond strength from the shear strength between solids using solely SGS. All of these drawbacks in employing SGS in predicting gas migration indicate the need for replacing SGS as the metric to predict gas-tight conditions.

A laboratory-scale WSC was developed to study the performance of cement slurries. The WSC is used to perform two separate types of tests. The purpose of the first type, *hydrostatic pressure testing*, is to simulate the pressure reduction in the cemented annulus during cement hydration. The second, *gas migration testing*, is used to investigate the potential for gas invasion under in-situ borehole conditions. In addition to the device itself, specific protocols for casting the artificial formations and WSC testing have been developed, which detail the procedures required for proper operation of the WSC. The WSC provides improvements over the existing

CHAs by simulating representative in-situ wellbore conditions, accounting for in-situ rock formation properties, providing real-scale wellbore conditions, and accommodating a variable overburden pressure.

Cement slurries were tested using the newly-developed WSC. Next, the phenomena of gas migration in the cemented annulus were investigated. Finally, the effects of a range of factors that influence the drop in slurry pore pressure were also investigated. These factors include: formation permeability, initial overburden pressure, curing temperature, w/c ratio of the cement slurry, cement composition and a $CaCl_2$-based accelerator.

Degree of hydration is introduced to characterize the process of cement hydration and its effects on gas migration. By analyzing the temperature history of the hydrating cement, the evolution of heat through the exothermic hydration process is characterized for slurry designs with different hydration rates due to different curing temperatures. Though cured under different temperature conditions, the cement hydration of same slurry designs (same type of cement and w/c ratio) can be standardized using the concept of equivalent age – degree of hydration. Capillary porosity is used to analyze the volumetric fraction of the voids in cement slurries with respect to degree of hydration. The employment of these fundamental concepts provides the opportunity to characterize the feature of the slurry design and other important factors associated with the in-situ wellbore conditions on the potential for gas migration. The results experimentally reveal the advantages of the newly-developed WSC.

5.2 CONCLUSIONS

Results from the two types of testing performed using the WSC (hydrostatic pressure testing and gas migration testing) are provided below:

(1) The cement matrix will be consolidated under the overburden pressure during early hydration. This is caused by chemical shrinkage and fluid loss from the cement matrix into the formation under the overburden pressure. The resulting volume reduction in the cement matrix provides space for pressurized gas to enter into the cemented annulus. This increases the compressibility of the cement matrix and therefore increases the ease at which the gas can form a channel. The hydrostatic pressure within the cement matrix declines due to the volume reduction. This decline in pressure increases the potential for gas to invade into the cemented annulus. One means to prevent gas migration is to maintain the slurry pore pressure during the early hydration stage. Expanding agents and foam cement have been employed in cement jobs to prevent gas migration. By increasing the amount of expansive hydration products in the matrix or expansion of entrained nitrogen bubbles, the hydrostatic pressure in the cemented annulus can be maintained as hydration occurs.

(2) Gases and other fluids will find the path of the least resistance when invading the cement matrix during early hydration when the slurry pore pressure is lower than gas pressure. The pressurized formation gases and fluids have to break through the cement matrix by pushing bonded solids apart to generate a path. As the cement matrix is still deformable at the early gelation stage of cement hydration, the resistance within the cement matrix is more susceptible than that at the interfaces.

While gases can push solids to both sides in the cement matrix, gases have to make a larger deformation and compression on only one side of the cement matrix when channeling at the interfaces. To study the mechanisms of the interaction between gas bubbles and solid matrix, a means to characterize cement matrix strength at a microstructural level should be developed first, as discussed in Chapter 2.

(3) Pressurized fluid invasion was simulated during cement gelation. Experimental results show that the localized regions of porous cement caused by these pressurized fluids is as important as, if not more important than, gas channeling in the cement matrix during cement gelation. While gas migration creates open channels in the cemented annulus, pressurized fluids, such as water, will increase the porosity of the cement matrix. This not only reduces the strength of the cement sheath, but also increases the permeability. This emphasizes the importance of considering the shallow water flow into the cemented annulus when performing cement jobs on offshore wells.

(4) Gas bubbles entering the cemented annulus migrate in the annulus before the cement sets. Migrating gas bubbles may conglomerate together while travelling upward in the wellbore. Therefore the size of gas bubbles increases while traveling upward. This reduces hydrostatic pressure in the cemented annulus and increases the potential for blowouts. As gas bubbles merge together and continue to migrate upwards, they escape into the atmosphere when they reach the surface. Therefore, slurry density should be designed appropriately to prevent the migration of bubbles before the cement sets.

(5) Formation properties affect the rate of the pressure reduction in the cement slurry, which illustrates the advantage of the WSC in simulating rock formations. None of the existing CHAs account for the properties of the formation. Increasing the permeability of the formation results in a lower pressure reduction rate. However, the slurry pore pressure starts to drop at the same time and approaches to the same residue pressure.

(6) The magnitude of the overburden pressure does not affect the pressure reduction rate in the cemented annulus. Instead, the ability of the cement slurry to transmit the hydrostatic pressure is a function of the stage of the hydration of the cement slurry. This indicates that the ability of cement slurry to transmit pressure can be characterized by the microstructure of the cement matrix, which again emphasizes the need for a better means to quantify the microstructural development of the cement, as discussed in Chapter 2. In this study, only relatively low pressures representing conditions higher up in the borehole were considered; therefore, the effect on the cement hydration is negligible. When investigating the slurry behavior in HTHP condition in the deeper wellbore, the accelerating effect of higher pressures on the cement hydration should be considered.

(7) Degree of hydration is introduced to characterize the process of cement hydration. An analysis of the hydrostatic pressure reduction with respect to degree of hydration provides a means for characterizing the effects of curing temperature and a $CaCl_2$-based accelerator. Although blended with additives at different dosage rates and cured under different temperatures, the microstructural development, and hence criteria for gas migration potential can be standardized using the concept of degree

of hydration for a specific slurry design. The curves of hydrostatic pressure reduction are identical with respect to degree of hydration though the rates of cement hydration are different. This verifies that shortening the critical hydration period cannot change the occurrence of gas migration, as the microstructural development may be identical for the same slurry although the hydration occurs at different rates.

(8) The cement composition affects the slurry pore pressure reduction. Compared to Class A cement, Type I cement presents a lower gas-flow-control property. Occasionally, for reasons such as economic and/or availability, Type I cement, instead of Class A cement, is used when performing cement jobs on surface casing strings. This may pose a more severe risk for gas migration. The WSC results show that Class A cement presents a better ability to transmit hydrostatic pressure than Type I cement during the early hydration stage. Therefore, Class A and not Type I cement would be preferred for cement jobs, when gas migration potential exists.

(9) Capillary porosity was proved capable of describing microstructural development for slurries with different w/c ratios at any given degree of hydration. The lower the w/c ratio, the earlier the initiation of pressure drop occurs. A high w/c ratio design needs to achieve a higher degree of hydration to develop the same ratio of space to hydration product as compared to that of a low w/c ratio design. Capillary porosity was used to analyze the volumetric fraction of voids in cement slurries with respect to degree of hydration. The results show that the capillary porosity is nearly identical at the same pressure reduction, although the w/c ratio is different for the same cement slurry.

(10) Comparisons were made between the performance of different cements in the WSC and different w/c ratios. Results reveal that the characterization of the volumetric fraction of solids and percolation properties of the matrix should be used to broaden the applicability of this analysis approach to different slurry designs. Characterizing the microstructure of the cement matrix provides the opportunity to study the mechanism of pressurized gas invading the cement matrix, which can be further used to optimize slurry designs and other important factors associated with wellbore conditions for preventing gas migration.

(11) WSC results, as presented above, verify the applicability of the WSC and its improvements over other existing apparatuses. This tool can be used to extend the understanding of the cement behavior and in-situ wellbore conditions on the potential for gas migration.

5.3 RECOMMENDATIONS FOR FUTURE RESEARCH

The following suggestions are provided regarding further enhancements that can be made to the WSC and additional work to be performed to better understand factors contributing to gas migration potential.

Additional optimization of the WSC can be performed to reduce the difficulties in operating the system. For example, the gas supplies can be upgraded to a computer-based control system, which will be automatic and more accurate. The T-type temperature sensor can be replaced by an absolute temperature transducer, which will reduce the complexity of the temperature measuring system.

As discussed in Section 4.4.2.5, compared to Class A cement, Type I cement presents a lower gas-flow-control property. This conclusion is drawn from hydrostatic pressure testing. To further validate this conclusion, gas migration testing should be performed in the WSC. This can be done by controlling the time the formation gas pressure is introduced to the cemented annulus. The gas migration testing should be performed using a high permeability formation. To perform the test, start out by closing the formation gas pressure port. Until the pore pressure reaches 175 psi (assuming that an overburden pressure of 350 psi is being applied), open the formation gas pressure port and apply a 175-psi gas pressure. After the cement has set, perform a forensic investigation on the cemented annulus to determine if gas migration occurred. This test should be performed for a slurry containing a Type I cement and the exact same slurry design but using a Class A cement. 1.) If gas migration occurs for both cases (the slurry with the Type I cement and the slurry with the Class A cement), additional trial tests should be performed by reducing the formation gas pressure applied. 2.) If no gas migration occurs, the applied formation gas pressure should be increased. If the cement matrix of the Type I cement slurry is less resistant to gas migration than that of Class A cement, channeling will be observed in the cement annulus for the Type I cement slurry and not the Class A cement slurry, even though the hydrostatic pressure in the cemented annulus is identical (such as 175 psi).

Other factors should be studied using the WSC to broaden the understanding of in-situ conditions on gas migration. For instance, the effect of contaminated slurry, annulus dimension and eccentricity on hydrostatic pressure reduction can be investigated. For gas migration testing, formation permeability, fluid loss, mud cake, inclined annuli and formation gas pressure can be evaluated by applying first a single and then a multi-factorial analysis. a range of conditions for each parameter should be investigated. For example, the angles of inclined annuli can be set to

be 0, 30, 60 and 90 degrees. The result can then be used to populate a performance database that can further be used to develop and/or calibrate a numerical model, as discussed below.

A standardized procedure for slurry preparation along with a means to convert the non-standard conditions, such as mixing temperature, should be developed. As discussed in Chapter 2, the conditioning history of cement slurry will affect the strength characteristics of hydrating cement. In order to minimize the variation of slurry properties, the same mixing procedure, conditioning and ambient conditions are followed to prepare cement slurries in this study. The minimal variation in results proves the advantage of a standardized procedure for slurry preparation, and therefore provides the opportunity to develop an experimental standard for measuring cement properties.

A constitutive model describing the interaction between solids in the cement matrix should be developed to establish the relationship between the cement hydration stage and the bulk properties of cement slurry. As discussed in Sections 2.3.3 and 4.4.2, hydration products can be estimated based on the cement compositions, w/c ratio and additives/additive dosage rates. Although degree of hydration is capable of describing the behavior of cement, such as hydrostatic pressure reduction in the cemented annulus for one type of cement, capillary porosity should be incorporated to differentiate the effect of different w/c ratios. As different additives, such as latex, are added to the slurries, more fundamental variables can be introduced to develop a fundamental approach for predicting cement behavior in regards to preventing gas migration. If the interaction between cement particles in the cement matrix can be established, a model capable of describing the bulk properties of the cement slurry with respect to the hydration stage can be developed. Therefore, a critical hydration time can be determined and additionally, the

interaction between pressurized gases/fluid and the cement matrix can be investigated using a computational approach.

The optimum goal of this research is to develop an evaluation tool to predict the behavior of cement slurry in the wellbore. This pioneering work serves as the foundation for developing this evaluation tool. Laboratory testing is needed to provide reliable inputs for developing the constitutive model capable of characterizing the interaction between solids in the cement matrix. A database populated with the WSC test results can be used to validate/calibrate the numerical model. The numerical model can then be used to predict the hydrostatic pressure in the cemented annulus. By introducing pressurized gas bubbles into the numerical model, the occurrence of gas migration and/or channeling can be predicted. Once the in-situ conditions for a specific wellbore are established and applied to the model, this tool can help with evaluating cementing jobs. The model can be used to perform sensitivity analyses so that the array of parameters needed to prevent, or reduce gas migration can be identified and critical parameters affecting gas invasion can be determined. The results from the computational model can be used to populate the database for an extended the range of parameters in a more timely and economically efficient manner than relying solely on the WSC. Guidelines for optimizing slurry and annular designs to reduce gas migration can be established and customized for each individual wellbore based on the specific on-site conditions.

APPENDIX A

STANDARD PROTOCOL FOR FORMATION CAST

A.1 HIGH PERMEABILITY FORMATION

In order to make a representative sandstone formation for WSC testing, three separate mixture designs are needed for casting three different zones of *one high permeability* formation, as shown in Figure A.1. The compositions of each mixture are provided in Table A.1. The properties of material are summarized in Table A.2.

Figure A.1. Casting zones shown for a cross-section of a high permeability formation.

Table A.1. Mixture designs used for casting high permeability formations.

Mixture	Water, lb	Cement, lb	Sand, lb	Water reducer (Superplasticizer), oz
1	24.08	48.16 (Type I)	60.19	0.0
2	12.06	21.71 (Type III)	113.20	1.569
3	19.36	42.23 (Type I)	77.43	0.0

Note: 1.) Weights are based on a 1-ft^3 batch size. 2.) Mixture 2 is for a high permeability layer (Zone 2) that is used for gas dispersion during WSC testing. 3.) Type III cement is only used for Mixture 2 so that high early strength can be achieved. 4.) The water reducer used in this study is CATEXOL 1000N from Axim Concrete Technologies, Inc.

Table A.2. Properties of the materials used for casting formation.

Material	Specific gravity	Absorption capacity, %	Moisture content, %	Fineness modulus	Recommended dosage, oz /100 lb of cementitious materials
Sand	2.61	1.24 %	4.43 %	2.86	
Cement	3.15				
Water	1.0				
Super plasticizer					1.0 - 4.0

As the volume of one formation is 347.0 in^3, required volumes of each mixture for one high permeability formation are 10.0, 93.1 and 245.5 in^3. Weight quantities of each mixture for one high permeability formation are shown in Table A.3.

Table A.3. Material quantities for casting a high permeability formation.

Mixture	Water, lb	Cement, lb	Sand, lb	Water reducer, oz	Volume, in^3
1	0.14	0.28 (Type I)	0.35	0.0	10.0
2	0.65	1.17 (Type III)	6.10	0.0845	93.1
3	2.75	6.00 (Type I)	11.00	0.0	245.5

Note: 1.) Mixture 2 is for Zone 2 of the high permeability layer that is used for gas dispersion during WSC testing. 2.) Type III cement is only used for Mixture 2 so that high early strength can be achieved.

A.1.1 Casting procedure for high permeability formations

Steps for casting a high permeability formation are presented below.

Step 1: Mold preparation

a. Scrape and wash debris off molds with a screwdriver and/or steel-wire brush and dry them.
b. Assemble molds by attaching the square base to the cylindrical PVC pipe. After assembly, place a strip of duct tape over the small gap of cylinder to prevent leakage of the cement.
c. Apply form oil/grease to all surfaces.
d. Collect and set near vibration table (Figure A.2d) all necessary materials for casting, including (see Figure A.2a for Items i to ix, and Figure A.2b for Items xi):
    i. Casting mold
    ii. Plastic surface ring with a 6-in inner diameter and a 9.5-in outer diameter
    iii. 3-in diameter piece of geotextile
    iv. 3/8-in diameter copper tubing 8.0 in long
    v. Protective steel sleeve 4.5 in long with a ½-in inner diameter and a ¾-in outer diameter
    vi. 8-in diameter plastic sheet with 0.5-in pre-cut hole to allow for copper tubing
    vii. Bullseye leveler
    viii. Screw driver
    ix. Ruler
    x. Plastic sheet cover

xi. 27.0-lb standard compaction dead weight and modified compaction dead weight with hole to accommodate copper tubing

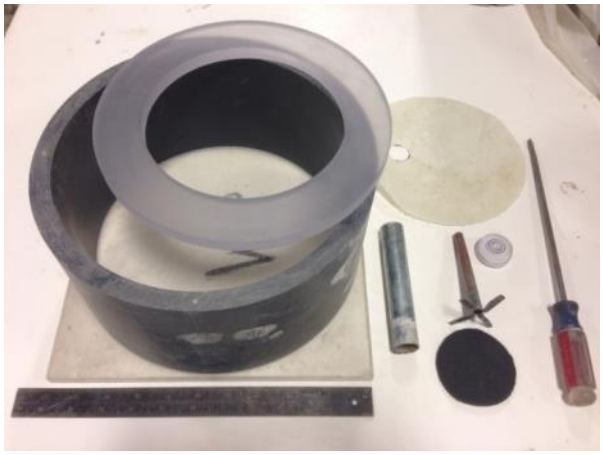

(a) Cylinder mold, surface ring, plastic sheet and other tools needed

(b) Compaction dead weights

(c) Mortar mixer

(d) Vibration table

Figure A.2. Mold and other accessories for formation casting.

Step 2: Material measurements

a. Before weighing out the batch materials, as seen in Table A.3, determine the moisture content of the sand. A Speedy Tester (ASTM D4944) and/or

Microwave Test (ASTM D4638) were used for this study. The aggregate (sand) moisture content will affect the batch quantities for the sand and water. Use the material weight sheet to adjust material quantities based on the moisture content of the sand.

b. Weigh each material after accounting for the moisture content of the sand and place each in a separate container. Be sure to cover the water and sand to avoid moisture loss.

Step 3: Batching Mixture 1

After all materials are properly weighed and measured, mix mixtures in ascending order according to the general procedure presented below.

a. Begin by mixing Mixture 1. Add water and cement to the mixing bowl and mix for 1 minute at low speed (Level 1 on the mortar mixer, agitator 107 rpm). If a water reducer is used, this should be added to the water before adding the water to the mixing bowl.
b. Add the sand to the mixing bowl within 15 seconds after 1 minute of mixing;
c. Continue mixing at low speed for 45 additional seconds until 2 minutes of mixing is achieved;
d. Increase mixing speed to high speed (Level 2 on the mortar mixer, agitator 198 rpm) and continue mixing for another 2 minutes until the 4-minute mark is reached;
e. Turn off the mixer and use a spoon/scraper to scrape the sides of the mixing bowl to fully incorporate all of the materials and let stand until the 6-minute mark;

f. Restart the mixer on high speed (Level 2) for the final 3 minutes of mixing until the 9-minute mark is reached.

Step 4: Placing Mixture 1

After Mixture 1 has been made, weigh out approximately 0.44 lb (200 grams) of the mix into the bottom of the mold. This should be just enough to fully cover the bottom of the mold. Place the mold onto the vibration table to assist in spreading layer out evenly (Zone 1 as shown in Figure A.1).

a. Note: Set vibration table to 3/8 turn intensity.

(a) Mixture 1 in the mixing bowl

(b) Weighing Mixture 1

(c) Placing Mixture 1

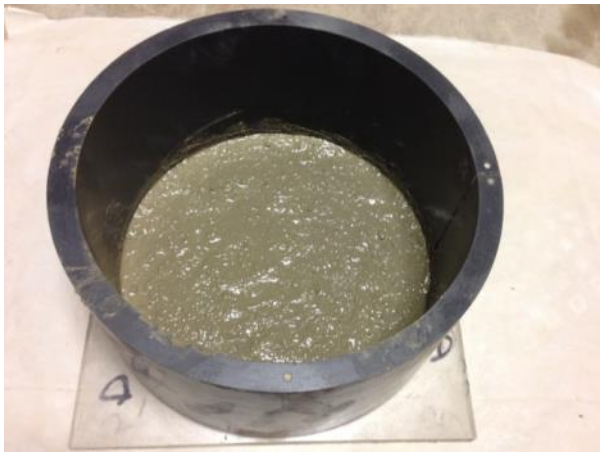

(d) Mixture 1 evenly covering the bottom

Figure A.3. Casting of Mixture 1 (Zone 1 as shown in Figure A.1).

Step 5: Repeat Step 3 for mixing Mixture 2 (high permeability batch).

a. Note: As stated above, be sure to add water reducer to the water and add the water to the bowl at the beginning of the mixing procedure for Mixture 2 only.

Step 6: After Mixture 2 has been made, take three separate samples from the mix having weights of 1.5, 2.5, 3.5 lb to be used for constructing different layers of the formation within high permeability portion of the formation.

a. Note: Weigh out quantities individually. Do not weigh out next quantity until preceding quantity has been placed and compacted in mold (as will be described in Step 7 below). It is important to cover the mixing bowl while placing each of the separate layers of the formation to avoid moisture loss.

Step 7: Placement/compaction of Mixture 2

a. Ensure that the surface of the vibration table is level and then place the formation mold onto the table.
b. Place the first layer using 1.5 lb of Mixture 2 evenly (level) directly on top of Zone 1 (Mixture 1 layer) in the mold.
c. Cover first layer just placed with the 8-in diameter plastic sheet before placing the consolidation dead weight on the top of the layer.
    i. Note: Place the bullseye leveler on the consolidation weight to ensure even compaction. The plastic sheet prevents the weight from the surface of the lift and prevents loss of material due to the mortar clinging to the bottom of the weight when lifting weight after vibration.
d. Turn on the vibration table and compact first layer of Zone 2 for 1 minute. Remove consolidation weight and plastic sheet after compaction is complete.
e. Place the 3-in diameter geotextile and gas-dispersing copper tubing on top of the first high permeability layer. Be sure to line up copper tubing placement with pre-fabricated hole in the consolidation weight.
f. With the copper tubing and geotextile in place, place the second layer using 2.5 lb of Mixture 2 around the copper tubing and geotextile and evenly spread mix throughout the mold. Place the 8-in diameter plastic sheet over the copper tubing

and center the sheet in the bottom of the mold. Use the modified consolidation dead weight that has the circular hole for accommodating the copper tubing, to compact the second layer for 1 minute.

i. Note 1: Be sure to adjust the weight with the assistance of the bullseye leveler to ensure uniform compaction. Additionally, the distance from the top of the second compacted layer to the top of the mold should be measured to ensure this distance is 4.0 in. Make a note of measurement if it is significantly more or less than 4.0 in so this can be accounted for when performing the coring after curing. This measurement is obtained based on the desire to have the bottom layer be 1.0 in thick.

ii. Note 2: After the 4 in measurement is confirmed, be sure to texture the outer area of the second layer with a small screw driver where the plastic sheet is not covering. This step will help increase the strength of the bond between the second and third layer of the high permeability mixture (Zone 2) to prevent a cold joint from forming. Without the texturing, a shear failure can occur while coring the formation (as will be described later).

iii. Note 3: Do **NOT** remove the plastic sheet after the compaction has been completed.

g. Place the third (and final) high permeability using 3.5 lb of Mixture 2 evenly (level) on top of second layer of (and plastic sheet) in the mold. Compact layer with the modified weight in the same manner as was performed in Step 7f above. The thickness of this final high permeability layer should be 0.5 in. After this layer is compacted, use a small screw driver to remove enough material around

the copper tubing to allow for the protective steel sleeve to be placed around copper tubing down to the plastic sheet in between the second and third layer of Mixture 2. Replace material removed back around the steel sleeve and compact with your hand to keep protective tubing in place.

(a) Mixing Mixture 2

(b) Weighing materials

(c) Checking levelness of surface while compacting

(d) Placement of geotextile and tubing

(e) Depth check and plastic isolation sheet

(f) Texturing to enhance the bond between the lifts

(g) Placing the third layer of Mixture 2

(h) Placement of protective steel sleeve

(i) Backfilling material around the steel sleeve

Figure A.4. Mixing and placing Mixture 2 (high permeability mixture).

Step 8: Once Mixture 2 has been placed, repeat the mixing procedure described in Step 3 for Mixture 3.

Step 9: After mixing, place Mixture 3 into the mold. Fill the mold until the mortar is level with the top surface of the mold. Be careful not to disturb the copper tubing and steel sleeve when placing Mixture 3.

Step 10: Turn on the vibration table for 3 minutes to allow for air bubbles to escape from the surface and the layer to be completely consolidated.

a. Note: It may be necessary to add more material from Mixture 3 if the layer falls below the surface of the mold once the mortar has been consolidated is complete.

Step 11: Once entrapped air has been removed and the final layer is level with the top of the mold, remove the mold from the vibration table and place it on a level surface. Then, place the plastic surface ring on top of the final layer and rotate it until most of the air bubbles are removed from beneath the ring.

a. Note: A bullseye leveler should be used to level the bottom of the plastic ring (cement top-outer surface) to the same level as the top of the mold. The final height from the bottom of the formation (the top of mold base) to the top-outer, leveled surface should be approximately 5 in when completed.

Step 12: Finally, keep the plastic surface ring on the formation and place a plastic sheet over the mold and allow formation to cure for 24 hours.

a. Note: Additional water should be added to the formation via the copper and steel sleeve after initial set and before the specimen is demolded to assist with the curing process.

(a) Mixture 3 in the mixing bowl

(b) Placing Mixture 3 (Zone 3)

(c) Finishing the surface

(d) Leveling surface with plastic ring

Figure A.5. Mixing and placement of Mixture 3.

Step 13: Clean tools.

Step 14: After 24 hours, carefully remove the plastic surface ring from the top of the formation specimen and demold the specimen. Place the formation into a moist-curing room for 3 weeks before WSC sample preparation, as discussed in Appendix B.

a. Note: After specimens are demolded, clean molds for next casting.

A.2 LOW PERMEABILITY FORMATION

A simplified procedure is presented below for casting a low permeability formation for wellbore simulation testing. The modified mixture design used for casting the low permeability formation is provided in Table A.4.

Table A.4. Mixture quantities for casting a low permeability formation.

Mixture	Water, lb	Type I Cement, lb	Sand, lb	Water reducer, mL	Total weight, lb
4	3.5	8.5	17	0.0	29.5

A.2.1 Casting procedure for low permeability formation

The following are the steps that must be taken when casting a low permeability formation:

Step 1: Repeat Steps 1 to 3 from the high permeability procedure as shown in Section A.1.1.

Step 2: Once mixing is complete, place a 1-in layer of low permeability material into the prepared molds. Vibrate this layer for 1 minute to remove air bubbles. Wait 10 to 15 minutes for this layer to set slightly.

a. Note 1: Allowing the bottom 1-in layer to set slightly will prevent the plastic sheet from greatly deforming when vibrating the remaining 4 in of the formation, and will provide a more uniform and level surface when coring is required.

b. Note 2: Be sure to cover the material remaining in the mixing bowl while waiting for the bottom layer to set slightly.

Step 3: After the bottom layer is placed and has time to set slightly, place the circular plastic sheet on top of the layer and center it within the mold to create a uniformly thick outer edge.

a. Note 1: Remove any trapped air bubbles underneath the plastic sheet by gently sliding your finger from the center of the sheet outward.

b. Note 2: Scratch the outer edge of the bottom layer to prevent debonding between layers.

Step 4: Place remaining mixture material on top of the bottom layer (and plastic sheet) and fill the mold completely. Place the mold onto the vibration table for 2 minutes (or until the air bubbles are mostly removed).

a. Note: Set vibration table to 3/8 turn intensity.

Step 5: Repeat Steps 10 through 14 from the procedure for casting the high permeability formation as described in Section A.1.1.

APPENDIX B

STANDARD PROTOCOL FOR PREPARING THE FORMATION FOR WSC TESTING

The following steps must be performed when preparing the newly cast formation for use when performing a test in the WSC.

Step 1: After adequate curing has taken place (cured for 3 weeks), remove the formation from the curing room. Mark a circle where the core will be taken on the top surface.

Step 2: Once the formation has been marked for coring, stabilize the formation for coring by a coring press.

a. Note: It is important to stabilize the formation to prevent the entire formation from rotating while being coring on the coring press table.

Step 3: Before coring the formation, set up the coring rig with the correct coring bit size (wet 8-in diamond core drill bit), a plum drilling direction, and the proper depth to be drilled (i.e. 1.0 in from the bottom surface of the formation, unless otherwise noted).

Step 4: Core the formation to the proper depth using the lowest drilling speed on the coring press (Level 1).

Step 5: Once the desired depth of coring is reached, retract the coring bit from the formation and remove the formation from the coring press table.

Step 6: Unstrap the stabilization piece and carefully remove the inner core from the formation.

a. Note: Depending on the accuracy in coring depth, the inner core may or may not be completely free to remove. If the inner core cannot simply be removed by hand after coring, gently tap the protective steel pipe to break the weak bond remaining between the second and third layer of the high permeability layer. Be sure not to disturb the copper tubing when removing the inner core.

Step 7: Once the inner core has been removed, rinse the entire formation with water to remove any excess grinding residue.

a. Note: For low permeability formations, once the inner core has been removed from the formation, check the bottom inner surface for any deformations or non-uniformity. If this surface is deemed to be inadequate, grinding is required. Grinding is performed by setting the coring press to the same desired depth (1.0 in bottom layer) as before and installing a smaller coring bit size on the coring press (¼-in carbide drill bit). Bring the bit down to the desired level (i.e. very little material should be in contact with the bit). With one hand on the coring press holding the bit at a constant level, use the other hand to rotate and move the formation on the coring platform to allow for the bit to contact all areas of the bottom inner surface. Repeat/Readjust the coring height until this bottom inner surface is smooth and level.

Step 8: Before sealing the formation, the outer, bottom and top surfaces of the formation must be polished with a hand grinder. See Figure B.1b.

Step 9: Once again, remove coring/grinding residue from all surfaces of the formation by rinsing with water. Allow for formation to dry.

(a) Coring

(b) Grinding

Figure B.1. Formation coring and grinding.

Step 10: Use duct tape to cover inner surface to protect the borehole surface from epoxy. See Figure B.2a.

Step 11: Drill a ¼ in hole 3.0 in up from the bottom of the formation for the thermocouple installation.

Step 12: Place the formation on a plastic sheet so that the bottom base surface is facing up. Apply a very thin layer of epoxy to the outer and bottom base surfaces. Allow for the epoxy to dry for at least 12 hours before handling the formation.

Step 13: Apply epoxy on the outer surface of the formation. In order to reinforce the isolation, fiberglass is wrapped with epoxy on the surface. See Figure B.2b.

a. Note: After applying the first layer of epoxy, formation samples are kept in a vacuum chamber for 5 minutes to extract the air voids on the surface. After slowly release the vacuum pressure, the epoxy will fill the available voids.

Step 14: After the initial application of epoxy has dried and set, flip the formation back over to the correct position and grind the thin top surface once again to remove any epoxy that may have dripped down from the application to the outer surfaces. Remove any epoxy grinding material inside of the formation by rinsing or using pressurized air.

Step 15: Clean the hole with a ¼-in drill bit before inserting the thermocouple. Make sure to fill the hole with epoxy. See Figure B.2c.

Step 16: Apply epoxy on the top interface and vacuum for 5 minutes to ensure no air bubbles are trapped at the interface. Then attach the upper steel ring to the top of the formation. Additional epoxy needs to be applied to the chamfer during epoxy gelation to increase the interfacial bond strength. See Figure B.2d. The epoxy shall then set for 24 hours to reach appropriate hardness.

Step 17: Center the inner casing. Pour the epoxy to the bottom and stir it to ensure the epoxy is well distributed. Vacuum for 5 minutes to ensure no air bubbles are trapped at the bottom interface between the inner casing and the formation bottom surface. Apply petroleum jelly to the upper portion of the inner casing and put the piston in the annulus to guide the inner casing and to keep the inner casing straight. See Figure B.2e. Allow for epoxy to dry for an additional 5 days before testing in the WSC (See Appendix C).

(a) Covering the surface and drilling the hole

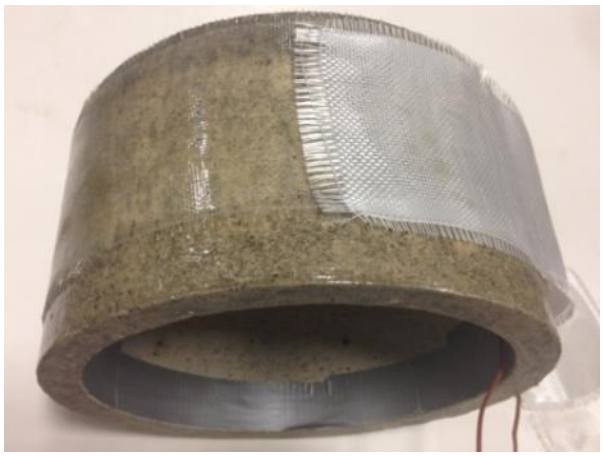

(b) Epoxying outer surface

(c) Thermocouple mounting

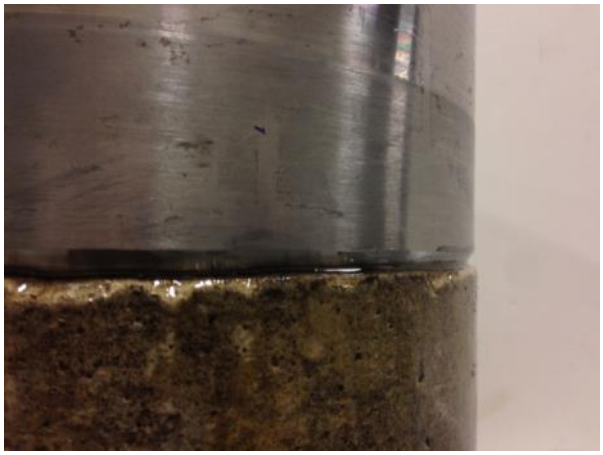

(d) Chamfer at interface

(e) Straightening out inner casing

(f) Sample ready for WSC testing

Figure B.2. Epoxying for formation after casting.

APPENDIX C

STANDARD PROTOCOL FOR WSC TEST SETUP

The following protocol outlines the procedure required to complete a WSC test. This includes preparing the chamber for performing the test, preconditioning the cement slurry, performing the WSC test, and analyzing the test results.

C.1 WSC PREPARATION

Before beginning to blend the cement slurry per API Specification 10A for analyzing in the WSC, various components of the WSC and the artificial formation must be prepared. Outlined below are activities that must be performed prior to performing the actual simulation.

C.1.1 Material list

(1) Slurry design

The slurry design characteristics investigated in this study include cement type, w/c ratio and the use of an accelerator. The w/c ratios considered include 0.4 and 0.46. Table C.1 shows the batch weights for the neat slurries for each of these w/c ratios considered.

Table C.1. Neat slurry mixture designs.

w/c	Cement, lb	water, lb
0.4	7.717	3.087
0.46	7.092	3.261

Note: 1.) Specific gravity of the cement is 3.15. 2.) Weights are based on a 152.6-in^3 (2,500-mL) batch size.

The accelerator included in this study is calcium chloride since this is the type of accelerator commonly used in the petroleum industry. Calcium chloride dihydrate is used instead of calcium chloride anhydrate for this investigation. Although it is typical for calcium chloride anhydrate to be used in industry practices, calcium chloride dihydrate was selected for its high purity. Calcium chloride dihydrate should be dissolved in the mix water and then the solution is set aside so it can equilibrate to room temperature before introducing it into the mix. It is not added as a dry blended admixture because the chemically-bound water molecules within the admixture may cause premature hydration of the cement clinker before calorimetric measurements are ready to be taken of the sample. The primary reasons for dissolving the admixture in the mix water solution include: 1.) to avoid the temperature variation caused by dissolve heat of calcium chloride, 2.) to reduce the variation of the composition of the prepared

cement slurry, and 3.) to accurately estimate the degree of hydration from calorimetric measurement. The combination of w/c ratio and $CaCl_2$ contents considered in this study is in Table C.2 with the corresponding slurry design referenced in Table C.3.

Table C.3 provides the slurry design for each of the cement slurries investigated in this study. A detailed description on how the slurry should be mixed is provided below.

Table C.2. Combination of w/c ratio and CaCl2-based accelerator considered and the corresponding slurry design referenced in Table C.3.

$CaCl_2$, % BWOC	W/c ratio	
	0.40	0.46
0.0	1	2
1.0	3	4
2.0	5	6

Table C.3. Slurry designs.

Slurry	W/c ratio	$CaCl_2$, %BWOC	Cement, lb	Net $CaCl_2$, oz	$CaCl_2*2H_2O$ (99.0 to 105.0% purity), oz	Water, lb	Solution or water, lb
1	0.40	0.0	7.717	0.0	0.0	3.087	3.087
2	0.46	0.0	7.092	0.0	0.0	3.261	3.261
3	0.40	1.0	7.717	1.235	1.635	3.062	3.164
4	0.46	1.0	7.092	1.135	1.503	3.239	3.333
5	0.40	2.0	7.717	2.469	3.270	3.037	3.241
6	0.46	2.0	7.092	2.269	3.005	3.216	3.404

Note: The specified masses are based on a total slurry volume of approximately 152.6 in^3 (2,500 mL).

(2) Material preparation

Deionized water is used to avoid any effect from unpurified water. If calcium chloride is used in the design, the solution of calcium chloride will be prepared according to Table C.3. Use dye and deionized water to prepare 1.5-gallon dye water for filling the WSC before assembling the

chamber. The cement, water and/or solution, and dye water should all be kept at the same ambient room temperature (70 ℉) that will be used for the WSC testing for a minimum of 24 hours prior to mixing the slurry.

C.1.2 Preparation of the WSC

The WSC should be prepared by following the steps presented below prior to mixing of the slurry.

Step 1: Formation saturation

a. Approximately 24 hours before testing, weigh the formation sample (including the upper steel ring and inner steel casing) in a *dry* condition (air dried for a minimum of 120 hours). Record the weight measurement.
b. Fill the formation annulus with deionized water up to the bottom of the upper steel ring, ensuring complete saturation of the formation. Cover the formation with a plastic sheet to limit evaporation.
c. After allowing the formation sample to become fully saturated for 24 hours, pour out all of the deionized water within the annulus and reweigh the *saturated formation*. Record the saturated weight measurement.
d. Calculate the weight of the water absorbed but subtracting the weight obtained in Step 1c with that obtained in Step 1a.

Step 2: Prepare the circular piston to be inserted into the annulus (Figure C.1)

a. Clean off any excess debris from previous testing using a steel-wire brush and paper towel.

b. Cut out ring-shaped geotextile to match the dimensions of the bottom of the piston. Drill/puncture holes in geotextile at every quarter point around the ring where there are holes located in the piston for attachment.
c. Loosely attach geotextile to bottom surface of piston (firm side of geotextile against bottom of piston) using short, small screws.
    i. Note: The use of short, small screws will allow for an easier removal of the piston after testing by allowing the geotextile and piston to separate instead of attempting to break the bond between the hardened cemented annulus and geotextile.
d. Apply a small amount of grease to the exposed heads of the short, small screws to prevent the development of a bond within the annulus and to allow for easier removal after the test is complete. See Figure C.1c.
e. Fit 2 O-rings (1 upper-outer, 1 lower-inner) into pre-fabricated piston grooves and apply a small amount of petroleum jelly to the two fitted O-rings.
f. After the geotextile is loosely attached to the piston, place the piston (geotextile side down) into a bowl of deionized water and allow the geotextile to become saturated. This piston should remain in the bowl until the time in which it will be seated into the steel cylinder attached to the top of the formation.

(a) Piston assembly

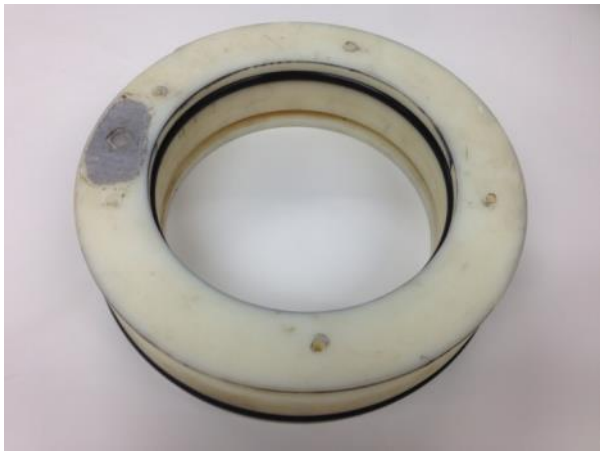

(b) Outlet covered with a 325 mesh

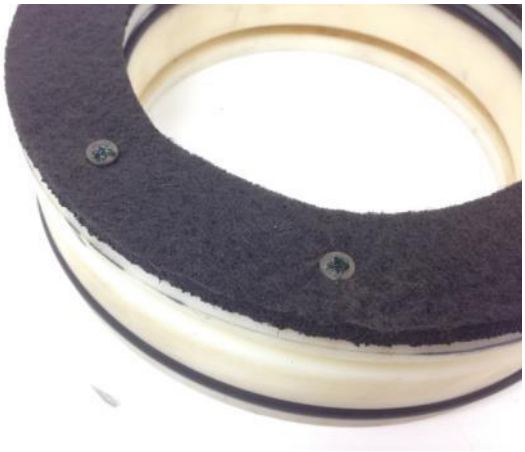

(c) Screws filled with grease

(d) Fluid collection when squeezing the piston in the annulus

Figure C.1. Piston preparation.

Step 3: Prepare inner surface of the WSC for formation insertion/placement

a. Use a paper towel and/or steel wire brush to clean off any excess residue or rust from the bottom and inner surfaces of the WSC.

Step 4: Cut out a circular-shaped geotextile and a plastic sheet with a diameter approximately 7.8 in, which is slightly less than that of the inner WSC diameter. Place both circular pieces at the bottom of the WSC (Figure C.2).

i. Note: The cushioning effect of the geotextile helps distribute the stress from the high pressures applied during testing on to the formation more evenly. This reduces the potential of cracking the formation due to stress concentrations.

Step 5: Prepare pressure and temperature sensors and other fittings on the outside of the WSC (Figure C.2)

a. All pressure and temperature fittings and sensors on the outside of the WSC should be connected 24 hours prior to testing. See Figure C.3.

b. Gas pressure lines should be connected with the outlet valves closed. Adjust the regulators on the tank and make sure that the pressure readings are set at the target pressure levels for 12 hours prior to preformation the test. The purpose for this is to reduce the pressure variation due to the mechanical regulator.

i. Note: Be sure to use thread seal (PTFE) tape to wrap the threads of all of the ports that need to be connected and screwed in to ensure a good connection and seal.

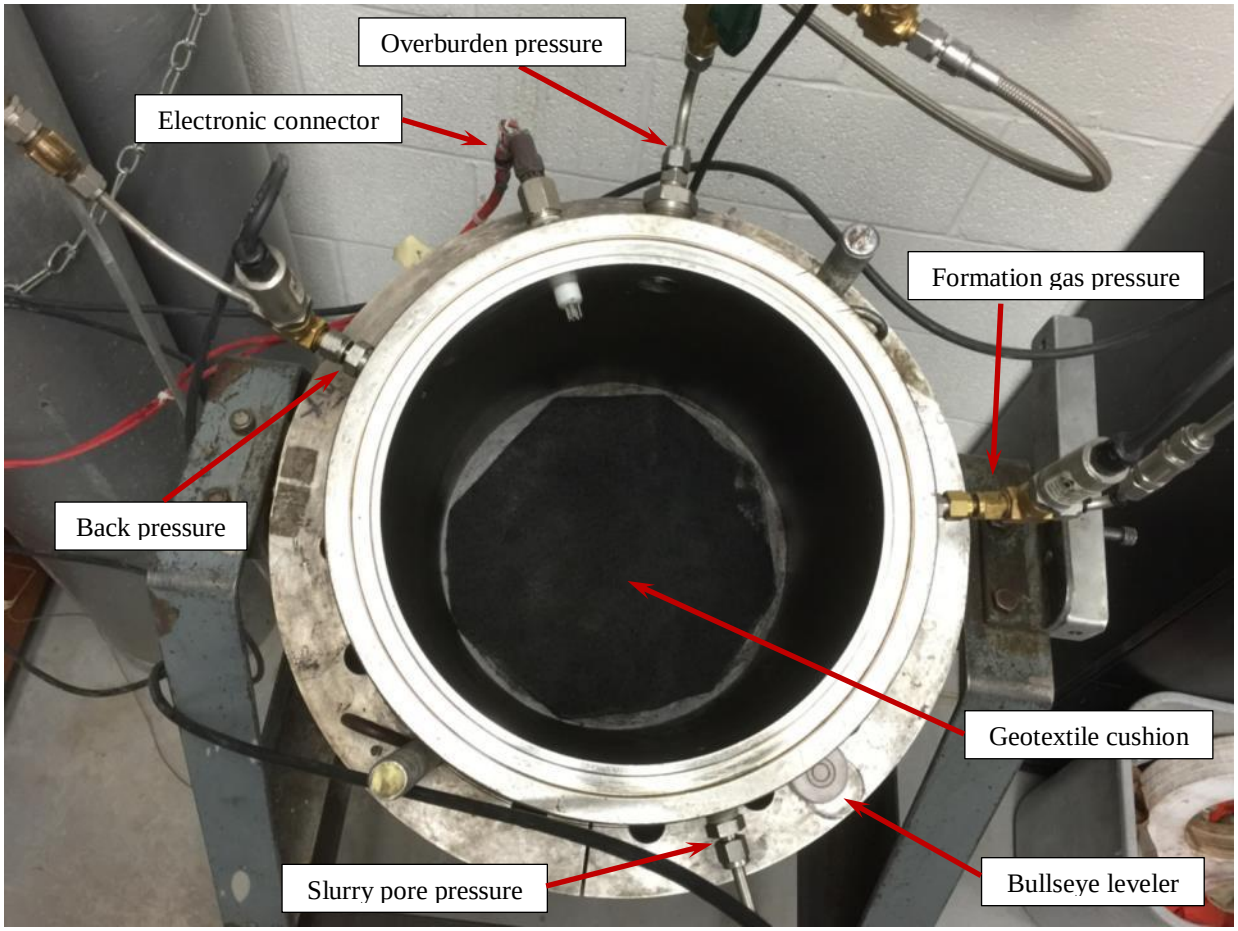

Figure C.2. WSC cleaning.

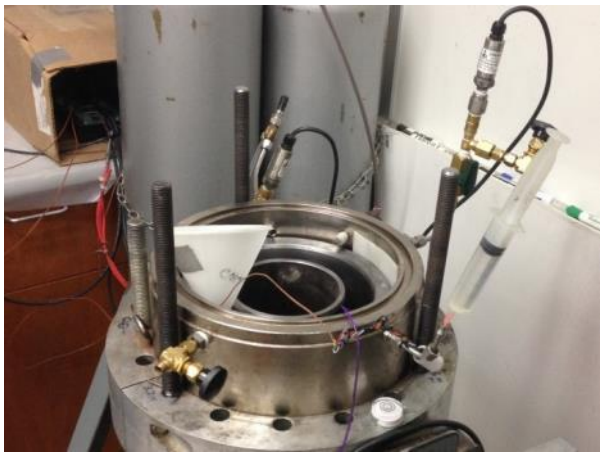

(a) Outside fitting connections

(b) Flexible hose connecting to the regulator on the nitrogen tank

(c) Overburden pressure

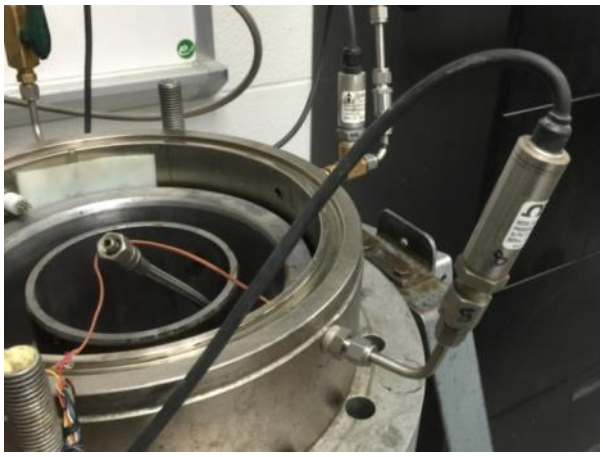

(d) Slurry pore pressure

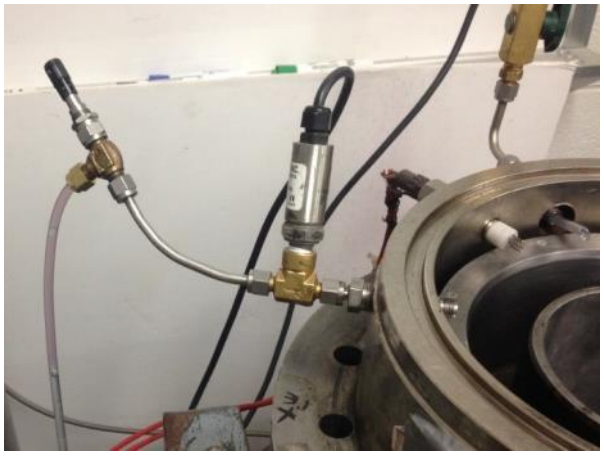

(e) Backpressure

(f) Formation gas pressure

Figure C.3. Connections outside the WSC.

Step 6: Prepare pressure and temperature sensors and other fittings inside the WSC. Figure C.4 provides an overview of the prepared WSC before cementing, and Figure C.5 shows the detail of the setup.)

a. Right before testing (20 minutes), carefully slide the formation into the WSC. Connect a 12-in hose to the slurry pore pressure port on the inner casing wall. Connect a 12-in hose to the formation gas pressure tubing in the formation (Figure C.6).
b. Use 300-grit sand paper to polish and remove any rust from inner surface of upper steel ring and outer surface of inner steel casing.
c. Apply a thin layer of petroleum jelly to the inner surface of the upper steel ring and upper surface of the inner steel casing.
d. Attach a piece of short plastic tubing approximately 2 in long to the overburden pressure port inside the WSC. Use a stiff piece of plastic (1/16 in thick) to bend and keep the tubing facing upward (see Figure C.7).
    i. Note: This step will allow the WSC to be filled to its maximum capacity with dye water, ultimately leading to optimum thermal and pressure stability after the overburden pressure is applied to WSC.
e. The lines connected to each pressure sensors inside the WSC (i.e. back pressure and slurry pore pressure) should be capped at the ends with grease, while the remaining volume is filled with vegetable oil inside the body of the line (Figure C.8).
    i. Note: As will be explained later in the protocol, it is important to disconnect the pressure line from the overburden pressure outside port in

order to allow for the WSC to be filled with the maximum amount of water and improve thermal stability of the apparatus. This will allow the air in the chamber to be pushed out through the plastic tubing when placing the top lid on the WSC.

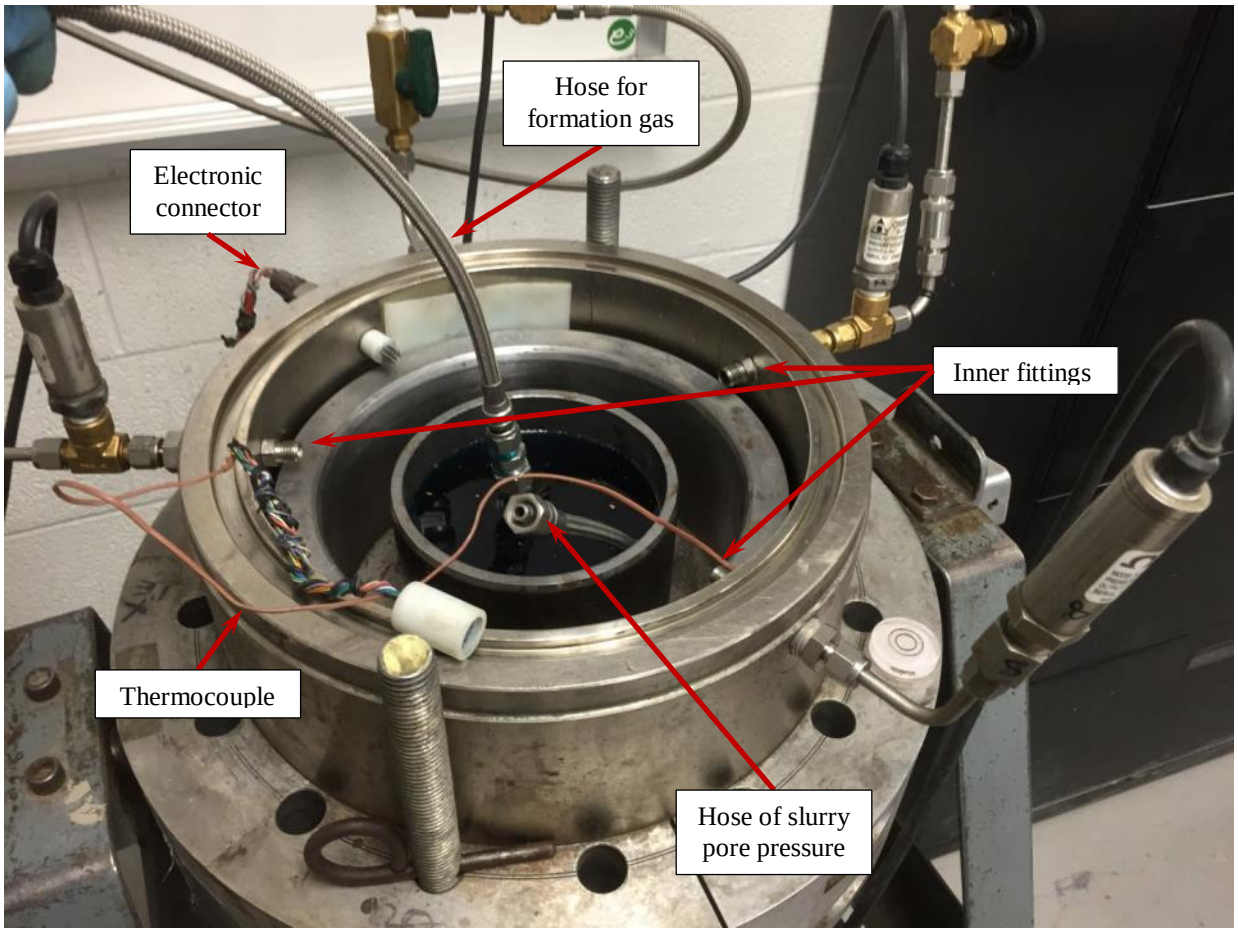

Figure C.4. View of inner connection of the WSC before cementing.

(a) Plastic tubing to the overburden pressure port

(b) Thermocouple connection and electrical connector

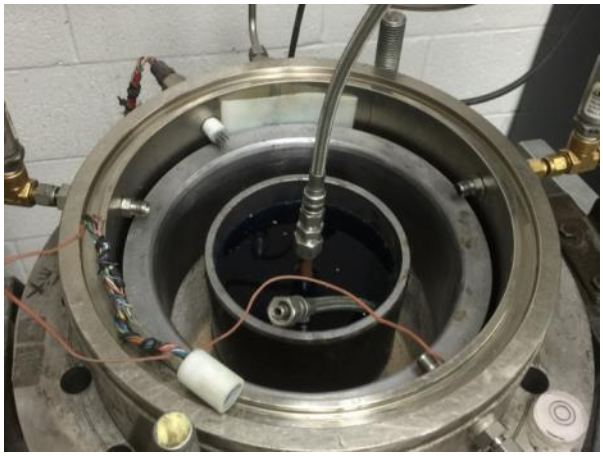

(c) Fill the insider of the casing with dye water

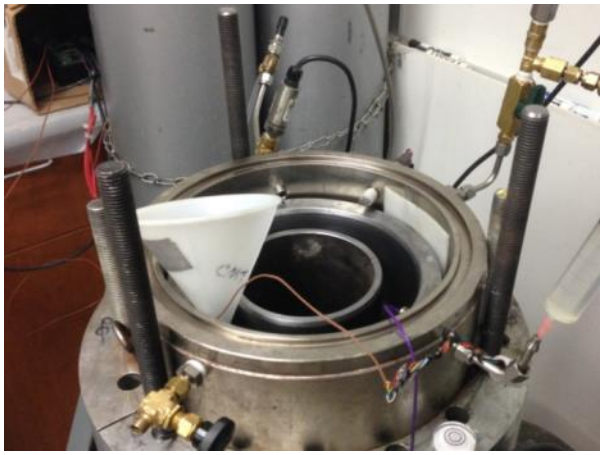

(d) Three bars for squeezing piston

Figure C.5. Detail of inner connections of the WSC.

(a) Fitting on the inner casing wall

(b) Filling flexible hose with oil

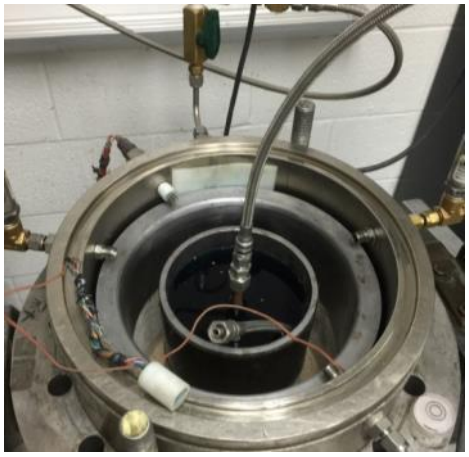

(c) Hoses for formation gas pressure and slurry pore pressure in the formation

(d) Adaptor for formation gas tubing

Figure C.6. Connecting hoses before cementing.

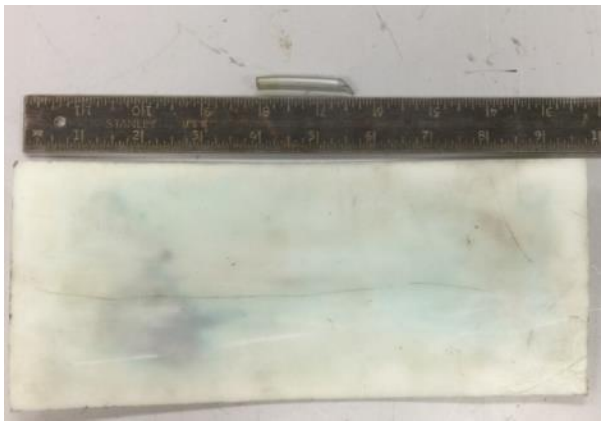

(a) Plastic tubing and flexible plastic sheet to secure hose

(b) Inserting the plastic tubing in the overburden pressure port

(c) Force and hold the plastic tubing upward using the flexible plastic sheet

(d) View of the overburden pressure port from inside the chamber

Figure C.7. Preparing the overburden pressure port insider the chamber.

(a) Thermal wiring (red to red, purple to yellow)

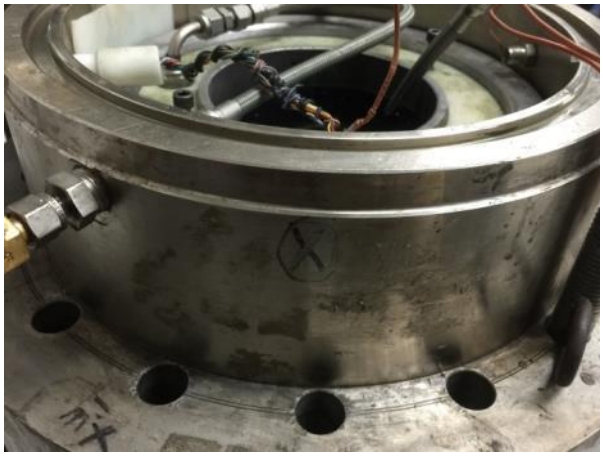

(b) Spot mark for thermocouple outside the chamber

(c) Spot mark for thermocouple inside the chamber

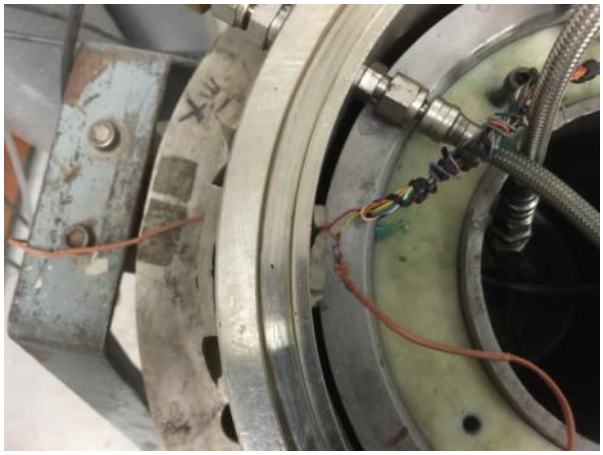

(d) thermocouples inside and outside the chamber at the same spot

Figure C.8. Connecting thermocouple for measuring the slurry temperature.

C.2 WSC TEST SETUP

This section describes the operation of WSC Test, including 1.) slurry blending and conditioning, and 2.) assembly of the WSC.

C.2.1 Slurry blending and conditioning

To obtain a completely-mixed cement slurry to be placed in the annulus of the WSC, a slightly modified mixing procedure, still in accordance with API Specification 10A is required. A 4-liter constant speed blender is used for mixing the slurry. See Figure C.9.

Step 1: As seen in the table above, each constituent of the slurry mixture design must be properly weighed and measured before mixing.

a. Note: It is important that all materials required for mixing (i.e. cement and water) be placed in the room where the mixing process will occur (a representative environment of thermal mixing conditions) in order to ensure minimal temperature variation for 24 hours prior to mixing and testing.

Step 2: After all materials are properly weighed and measured, pour the corresponding amount of water/solution into the blender container and place the blender container onto the blender base.

Step 3: Turn the blender on and simultaneously load the cement into the blender bucket while selecting the low-rpm (4,000 rpm) blending setting ("P1" - preset for 15 seconds).

a. Note: Be sure that all of the cement is loaded into the blender before the first low-rpm blending interval ends. It is most efficient to have one person hold the

blender bucket in place and control the mixing setting, while the other person carefully loads the cement into the blender.

Step 4: Within 15 seconds, add the cement to the blender bucket within the first 15 seconds. Cover the blender bucket with the lid. Immediately after the first blending interval is complete (first 15 seconds), select the high-rpm (12,000 rpm) setting for another 35-second blending ("P4" - preset for 35 seconds).

Step 5: After 35 seconds of high-rpm blending, remove the blender bucket lid to investigate the quality of blended cement slurry. Record the observation for further use.

(a) Slurry blender (b) "P1" - 4,000 rpm (c) "P4" - 12,000 rpm

Figure C.9. Mixing the slurry according to API Specification.

Step 6: Once the mixing is deemed adequate, the slurry should be transferred to a secondary mixer to pre-condition the cement slurry, which simulates the pumping process in the field. Turn on the secondary blender and operate at the lowest rpm (stirring) setting to conduct slurry conditioning. See Figure C.10.

a. Note: The pre-conditioning time interval (i.e. from the start of mixing to the time the pressure is applied) will vary depending upon the field pumping time that is being replicated. In this research, a 20-minute conditioning period is selected to provide a 55-minute duration before the overburden pressure is applied.

(a) Mixer for conditioning

(b) Air bubbles before stirring

(c) Conditioning at stirring level

Figure C.10. Slurry conditioning.

C.2.2 WSC assembly

After the cement slurry has been properly mixed and conditioned, the following steps must be followed to have the WSC setup within 25 to 30 minutes so that the overburden pressure can be applied.

Step 1: Pour the slurry into the formation annulus to 2.25 in below the top surface of the upper steel ring. Use a funnel to limit the cement slurry that may stick to the surfaces of the upper steel ring and inner steel casing, as shown in Figure C.11b.

Step 2: Use a depth indicator to properly level cement slurry to desired height/depth within the annulus (2.25 in below the top surface of the upper steel ring). See Figure C.11c.

Step 3: After cement slurry is leveled off at the correct height/depth, clean the top and inner face of the upper steel ring and the outer face of the steel casing with a paper towel and re-apply petroleum jelly to the ring and casing where needed.

Step 4: Remove the piston and saturated geotextile from the bowl of deionized water and loosely place it in the annulus of the formation in the WSC. Manually push (and twist, if necessary) the piston into the annulus until the geotextile ring clears the top surface of the inner steel casing and upper steel ring.

a. Note: It is important to use a small screw driver to ensure that the geotextile does not get caught and/or pinched between the annulus-casing and/or annulus-steel ring interfaces by pushing the geotextile further into the annulus during the initial twisting process.

Step 5: After the piston has been manually placed into the annulus, place the clear plastic ring on top of the piston followed by the top lid for the WSC. Squeeze the piston in the annulus and then remove the top lid. See Figures C.11e and C.11f.

a. Note: It is important to tap the piston down as evenly as possible in order to keep the epoxy bond between inner steel casing and the inner-bottom surface of the formation intact. To properly complete this step, perform 1 to 2 taps at a given location on top of the piston and continue this process incrementally around the perimeter of the piston.

b. Depending on the cement height/level within the annulus, bleeding water may be ejected from the backflow port on top of the piston. Collect the bleeding water

flowing through the back pressure pot and measure the volume using a graduated cylinder (100-mL range). Continue tapping until the top surfaces of the piston and upper steel ring are even or until the bleeding water reaches the targeted volume (Figure C.11d).

Step 6: Measure the initial piston location after the placement of piston ring. See Figure C.11g.

Step 7: Finish connecting all fittings, pressure lines, and thermocouples to the correct locations within the WSC to ensure proper test recordings (Figure C.11h). Detail for the connection is shown in Figure C.12.

Step 8: Fill the inside of the WSC (with formation inside) up to the top surface of the WSC with dye water. See Figure C.11i.

a. Note: Ensure that the WSC is level so that the maximum amount of water can be placed into the WSC.

Step 9: Stretch out the large O-ring and insert it into the top groove around the perimeter of the WSC.

Step 10: Place the chamber lid on top of the open WSC.

a. Note: release the overburden pressure port so that dye water will be forced out when lid is first placed on and after each incremental tightening/fastening.

Step 11: Insert and fasten steel bars/rods from the bottom of the chamber up through and around the entire perimeter of the chamber to secure the WSC lid. See Figure C.11j.

a. Note: It is important to *hand-tighten* all bars/rods around the perimeter with corresponding nuts on top before the lid can be fully tightened. When tightening the nuts to further secure the WSC lid, Always follow the proper torque sequence.

It is important to tighten nuts opposite the preceding nut and rotate this process around the entire perimeter of the chamber until a maximum hand-tightened level is reached.

Step 12: After all bars/rods have been hand-fastened, remove the initial 2 bars/rods that held up the bottom lid in place before the top lid is bolted onto the WSC. Replace these 2 diametric bars with the same bars used for securing the lid in place.

a. Note: Fasten all the nuts with a socket and *always* follow the same torque value (150 lb-in) for all the nuts and torque sequence as described in the previous step. At this point, the WSC lid is secure and all internal connections should be made.

Step 13: Connect the pressure line to the external overburden pressure port.

a. Note: When making connections, be sure to always use 2 wrenches to fasten connecting lines, ports, and pieces in line with one another to limit possible bending or damage.

Step 14: Before testing may begin, it is important to check for any leaks within the gas system (i.e. poor/loose connections in hydrostatic and formation pressure lines). Both the overburden pressure and formation gas pressure lines must be checked because of the direct connection with the supply gas tank.

a. Ensure that each gas tank supply knob and outlet valve and all exterior valves leading into the WSC are closed to prevent any gas input into the system.

b. Apply the desired pressure to the overburden pressure line/sensor and formation gas pressure (for high permeability formations only) by turning the gas supply knob counter-clockwise followed by the gradual clockwise turn of the outlet valve. Continue turning outlet valve clockwise until the outlet pressure gauge (different

than tank supply pressure gauge) and pressure sensor reading on the laptop are approximately equivalent.

c. After stabilizing the applied pressure from the nitrogen tank with the outlet valve, turn the nitrogen tank supply knob clockwise to stop the continuous supply to the external sensor. The initially applied pressure is still in the line. If either the outlet pressure gauge or pressure sensor show a significant drop in pressure, a leak is present and all connections between the outlet of the gas tank and the closed valve between the WSC and pressure sensor must be checked and tightened. Repeat Steps 14.a to 14.c until the outlet pressure gauge does not show a drop in pressure after closing the gas tank supply knob.

    i. Note: If this important step is not completed, a leak may exist without any indication and may slowly waste the gas as it steeps into the testing room.

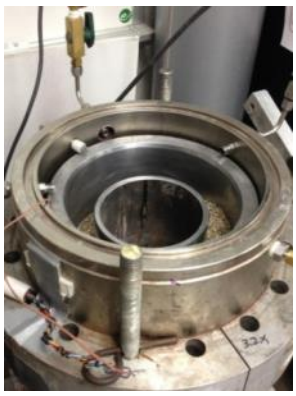

(a) WSC before cementing

(b) Cementing the annulus

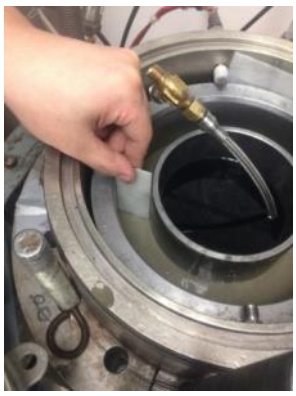

(c) Depth indicator

(d) Measurement from squeezing the piston

(e) Piston installation

(f) Piston squeezing

(g) Initial position measurement

(h) Fitting and electronic connections

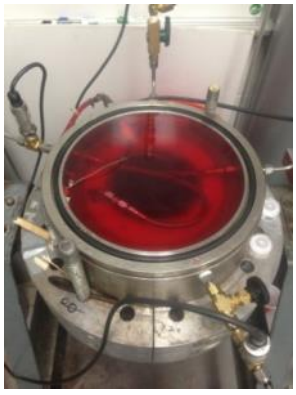

(i) Filled with dye water

(j) Chamber assembling

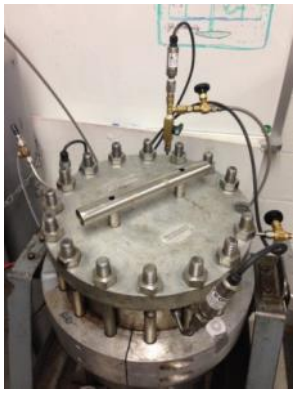

(k) WSC setup

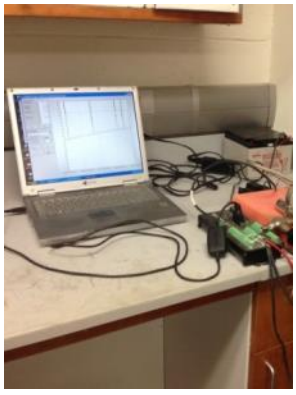

(l) Monitoring

Figure C.11. WSC testing operation.

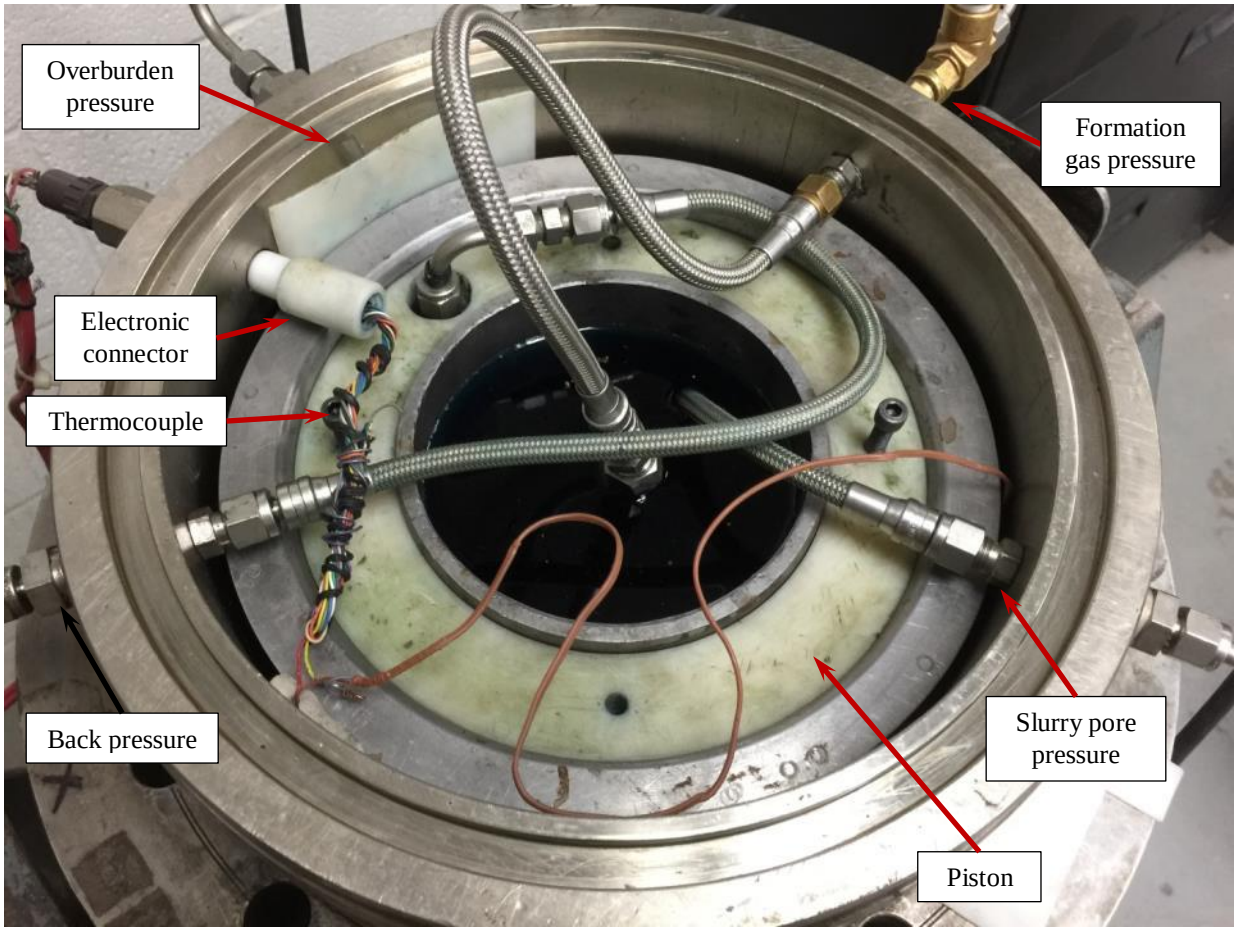

Figure C.12. Connecting hoses after placing the piston.

APPENDIX D

MATERIAL AND EQUIPMENT

Materials and equipment used in developing the WSC are listed in detail below.

D.1 CEMENT

Mill data and physical properties of cements used in this project are presented in Table D.1.

Table D.1. Cement property data sheet.

Cement type			API Class A	ASTM Type I	ASTM Type III
Standard chemical requirements (ASTM 114)	Silicon Dioxide (SiO_2), %		21.2	19.1	19.4
	Aluminum Oxide (Al_2O_3), %		3.7	4.7	4.6
	Ferric Oxide (Fe_2O_3), %		4	3.1	3.2
	Calcium Oxide (CaO), %		63.6	62	6.21
	Magnesium Oxide (MgO), %		2.7	4.3	4.3
	Sulfur Trioxide (SO_3), % A		2.7	3.2	3.9
	Loss on Ignition (LOI), %		1.03	2.1	1.6
	Insoluble Residue, %		0.08	0.31	0.49
	Alkalies (Na_2O equivalent), %		0.37	0.82	0.81
	Tricalcium Silicate (C_3S), Potential %		60	59	58
	Dicalcium Silicate (C_2S), Potential %			9	12
	Tricalcium Aluminate (C_3A), Potential %		3	7	7
	Tetracalcium Aluminoferrite (C_4AF), Potential %		12.06	9	10
Physical requirements	(ASTM C 204) Blaine Fineness, m^2/kg		362	399	619
	(ASTM C 191) Time of Setting (Vicat), minutes	Initial Set		91	69
		Final Set		186	145
	(ASTM C 185) Air Content, %			7	7.6
	(ASTM C 151) Autoclave Expansion, %			0.23	0.17
	(ASTM C 1038) Expansion in Water, %			0.01	0.006
	(ASTM C 187) Normal Consistency, %			26	28
	(ASTM C 109) Compressive Strength, psi	1 Day		2842	4520
		3 Day		4133	5160
		7 Day		4857	5850
		28 Day		5786	6410
	API Compressive Strength (slurry cubes), psi	8 Hour, 100 ℉	813		
		24 Hour, 100 ℉	2944		

D.2 OTHER MATERIAL AND EQUIPMENT

Other important material and equipment used in this project are presented in Table D.2.

Table D.2. Other material and equipment.

Item	Description	Company	Part number
Pressure chamber	100-bar special 1020 with 10 in cylinder and 2 tops	Soilmoisture Equipment Corp.	Y1020S2
Constant speed blender	4-liter mixing vessel	Ametek, Inc.	Model 3260
Mixer for slurry conditioning	KitchenAid professional 5 qt mixer	Whirlpool Corp.	KV25G0X
Vibrator	Electromagnetic vibrating table	FMC Technologies, Inc.	
Mixer for formation cast	20 qt mixer	The Hobart MFG. Co.	A-200
Calcium chloride dihydrate	99% pure $CaCl_2$ dihydrate	Thermo Fisher Scientific, Inc.	C79-3
Epoxy resin	General purpose epoxy resin	System Three Resins, Inc.	SKU:0100A24
Hardener	General purpose hardener 2	System Three Resins, Inc.	SKU:0102B24
Fiberglass cloth tape	Fiberglass cloth tape rolls 6 oz woven roving		
Wire cloth mesh	325 x 325 mesh	W. W. Grainger, Inc.	3DLR6
O-rings	Buna-N, round	W. W. Grainger, Inc.	
Carbon steel casing	5.5 in. outer diameter		
Copper tube	Streamline 3/8 in soft copper coiled pipe		
Geotextile	Carton, brown corrugated	Propex Operating Company, LLC.	S-4476
Pressure transducer	Rugged all stainless steel construction, 0 to 5 Vdc output	OMEGA Engineering, Inc.	PX309-2KG5V
Pressure sensor	1000 psia high accuracy transducer, 0 to 5 Vdc output	OMEGA Engineering, Inc.	PX409-1.0KA5V
Data logger	CR1000 data logger	Campbell Scientific Ltd.	
Check valve	C series check valves, fixed cracking pressures = 1/3 psi	Swagelok Co.	SS-4C-1/3
Adjustable check valve	SS poppet check valve, adjustable pressure, 150 to 350 psig	Swagelok Co.	SS-4CA-150
PVC pipe for the mold	10-in PVC-80 pipe	Pena-Plas Co.	800100
Water reducer	CATEXOL 1000N	Axim Concrete Technologies, Inc.	1000N

D.3 DIMENSION OF PISTON AND UPPER STEEL RING

Figure D.1 shows the dimensions needed for machining the piston, the upper steel ring and the inner casing. The inner surface of the upper steel ring and the top section of the inner casing should be well polished. This is required to reduce the friction and to maintain a good seal.

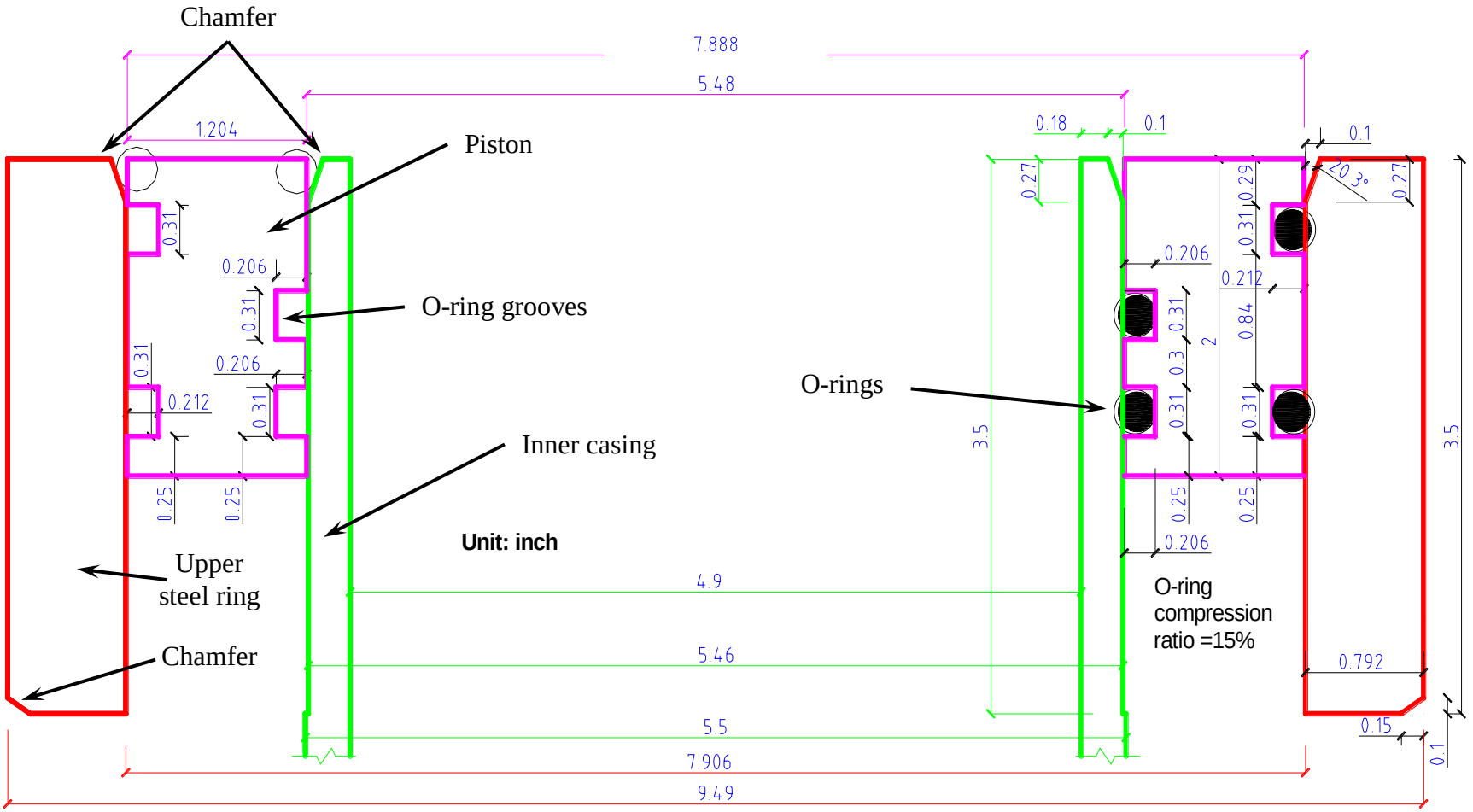

Figure D.1. Machining dimensions of piston, upper steel ring and inner casing.

BIBLIOGRAPHY

API Specification 10A, Specification for Cements and Materials for Well Cementing. 23rd edition. ANSI/API 10A/ISO 10426-1-2001. Effective date: October 1, 2002. Washington, DC: API.

API Std 65-2, Isolating Potential Flow Zones during Well Construction. Second Edition, 2010a. Washington, DC: API.

API RP 10B-6, Recommended Practice on Determining the Static Gel Strength of Cement Formulations. First Edition, 2010b. Washington, DC: API.

API RP10B-2, Recommended Practice for Testing Well Cements. Second Edition, 2013. Washington, DC: API.

ASTM C948-81, Standard Test Method for Dry and Wet Bulk Density, Water Absorption, and Apparent Porosity of Thin Sections of Glass-Fiber Reinforced Concrete. 1981. West Conshohocken, PA: ASTM International.

ASTM C305-06, Standard Practice for Mechanical Mixing of Hydraulic Cement Pastes and Mortars of Plastic Consistency. 2006. West Conshohocken, PA: ASTM International.

ASTM D4638-11, Standard Guide for Preparation of Biological Samples for Inorganic Chemical Analysis. 2011a. West Conshohocken, PA: ASTM International.

ASTM D4944-11, Standard Test Method for Field Determination of Water (Moisture) Content of Soil by the Calcium Carbide Gas Pressure Tester. 2011b. West Conshohocken, PA: ASTM International.

ASTM C1074-11, Standard Practice for Estimating Concrete Strength by the Maturity Method. 2011c. West Conshohocken, PA: ASTM International.

ASTM C109/C109M-13, Standard Test Method for Compressive Strength of Hydraulic Cement Mortars (Using 2-in. or [50-mm] Cube Specimens). 2013a. West Conshohocken, PA: ASTM International.

ASTM C191-13, Standard Test Methods for Time of Setting of Hydraulic Cement by Vicat Needle. 2013b. West Conshohocken, PA: ASTM International.

Banniser, C.E., Shuster, G.E., Wooldridge, L.A., Jones, M.J., and Birch, A.G. 1983. *Critical Design Parameters to Prevent Gas Invasion during Cementing Operations*. SPE Annual Technical Conference and Exhibition, San Francisco, California, 5-8 October. SPE-11982-MS. http://dx.doi.org/10.2118/84-35-106.

Bannister, C.E. and Lawson, V.M. 1985. *Role of Cement Fluid Loss in Wellbore Completion*. SPE Annual Technical Conference and Exhibition, Las Vegas, Nevada, 22-26 September. SPE-14433-MS. http://dx.doi.org/10.2118/14433-MS.

Beirute, R.M. and Cheung, P.R. 1990. *Method for Selection of Cement Recipes to Control Fluid Invasion after Cementing*. *SPE Prod Eng* 5(4): 433-440. SPE-19522-PA. http://dx.doi.org/10.2118/19522-PA.

Bellabarba, M., Bulte-Loyer, H., Froelich, B., Le Roy-Delage, S., van Kuijk, R., Zeroug, S., Guillot, D., Moroni, N., Pastor, S., and Zanchi, A. 2008. Ensuring Zonal Isolation beyond the Life of the Well. *Oilfield Review* 20(01): 18-31.

Boisnault, J.M., Bourahla, A., Dahl, T., Holmes, C., Maroy, P., Moffett, C., Mejia, G.P., Revil, P., and Roemer, R. 1999. Concrete Developments in Cementing Technology. *Oilfield Review* 11(1): 16-29.

Bonett, A. and Pafitis, D. 1996. Getting to the Root of Gas Migration. *Oilfield Review* 8(1): 36-49.

Brandt, W. Dang, A.S., Magne, E., Crowley, D., Houston, K., Rennie, A., Hodder, M., Stringer, R., Juiniti, R., Ohara, S., and Rushton, S. 1998. Deepening the Search for Offshore Hydrocarbons. *Oilfield Review* 10(1): 1-21.

Brufatto, C., Cochram, J., Conn, L., Abd, S.Z., EI-Zeghaty, A., Fraboulet, B., Griffin, T., James, S., Munk, T., Justus, F., Levine, J.R., Montgonery, C., Murphy, D., Pfeiffer, J., Pornpoch, T., and Rishmani, L. 2003. From Mud to Cement - Building Gas Wells. *Oilfield Review* 15(1): 62-76.

Carino, N.J. 1991. *Handbook on Nondestructive Testing Concrete*. Boca Raton, FL: CRC Press Inc.

Carino, N.J. and Lew, H.S. 2001. *The Maturity Method: From Theory to Application*. Building and Fire Research Laboratory, National Institute of Standards and Technology. Gaithersburg, MD 20899-8611 USA. Available from: http://fire.nist.gov/bfrlpubs/build01/PDF/b01006.pdf [Accessed 5 December, 2014]

Carter, L.G., Cook, C., and Snelson, L. 1973. *Cementing Research in Directional Gas Well Completions.* SPE European Meeting, London, United Kingdom, 2-3 April. SPE-4313-MS. http://dx.doi.org/10.2118/4313-MS.

Carter, G., and Slagle, K. 1972. A Study of Completion Practices to Minimize Gas Communication. *J Pet Technol* 24(9): 1170-1174. SPE-3164-PA. http://dx.doi.org/10.2118/3164-PA.

Cement Test Equipment, Inc. 2014a. Rotating Paddle Consistometer / Static Gel Strength Analyzer. Available from: http://www.ctetulsa.com//products/rotating-paddle-consistometer [Accessed 10 November, 2014].

Cement Test Equipment, Inc. 2014b. *CTE Model 300 Gas Migration Apparatus (M300)*. Available from: http://www.ctetulsa.com/products/gas-migration-apparatus/m300 [Accessed 29 November, 2014].

Chandler Engineering, Inc. 2014a. Model 5265 SGSA Static Gel Strength Analyzer. *Chandlerengineering.* Available from: http://www.chandlereng.com/Products/OilWellCementing/Model5265.aspx [Accessed 10 November, 2014].

Chandler Engineering, Inc. 2014b. *Model 7200 Cement Hydration Analyzer*. Available from: http://www.chandlerengineering.com/Products/OilWellCementing/Model7200.aspx [Accessed 19 November, 2014].

Chandler Engineering, Inc. 2014c. *Instruction Manual for Model 7200 Cement Hydration Analyzer*. Part Number 7200-1050. Revision F – October 2014. 2001 N. Indianwood Ave. Broken Arrow, OK 74012 U.S.A.

Chenevert, M.E. and Jin, L. 1989. *Model for Predicting Wellbore Pressures in Cement Columns*. SPE Annual Technical Conference and Exhibition, San Antonio, Texas, 8-11 October. SPE-19521-MS. http://dx.doi.org/10.2118/19521-MS.

Cheung, P.R. and Beirute, R.M. 1985. Gas Flow in Cements. *J Pet Technol* 37(6): 1041-1048. SPE-11207-PA. http://dx.doi.org/10.2118/11207-PA.

Cooke, C.E. Jr., Kluck, M.P., and Medrano, R. 1983. Field Measurements of Annular Pressure and Temperature during Primary Cementing. *J Pet Technol* 35(8): 1429-1438. SPE-11206-PA. http://dx.doi.org/10.2118/11206-PA.

Copeland, L.E., Kantro, D.L., and Verbeck, G. 1960. *Part IV-3 Chemistry of Hydration of Portland Cement*. 4th International Symposium of the Chemistry of Cement, Washington, D.C.: 429-465.

Crook, R. and Heathman, J. 1998. Predicting Potential Gas-Flow Rates to Help Determine Best Cementing Practices. Halliburton Energy Services, Inc., *iadc*, November/December, 1998. Available from: http://www.iadc.org/dcpi/dc-novdec98/n-halliburton.pdf [Accessed 18 November, 2014].

Drecq, P. and Parcevaux, P. A. 1988. *A Single Technique Solves Gas Migration Problems across a Wide Range of Conditions.* International Meeting on Petroleum Engineering, Tianjin, China, 1-4 November. SPE-17629-MS. ttp://dx.doi.org/10.2118/17629-MS.

Dusseault, M.B., Jackson, R.E., and Macdonald, D. 2014. *Towards a Road Map for Mitigating the Rates and Occurences of Long-Term Wellbore Leakage*. University of Waterloo and Geofirma Engineering Ltd. *Catskillcitizens*, May 2014. Availeble from:

http://catskillcitizens.org/learnmore/Wellbore_Leakage_Study%20compressed.pdf [Accessed 18 November, 2014].

EIA. 2014. *Nature Gas: U.S. Nominal Cost per Natural Gas Well Drilled*. Available from: http://www.eia.gov/dnav/ng/hist/e_ertwg_xwwn_nus_mdwa.htm [Accessed 11 November, 2014].

Fann Instrument Company. 2011. *Multiple Analysis Cement System (MACS II)*. Available from: http://www.fann.com/public1/pubsdata/Manuals/MACS%202.pdf [Accessed 18 November, 2014].

Freiesleben-Hansen, P., and Pedersen, E.J. 1977. Maturity computer for controllingcuring and hardening of concrete. *Nordisk Betong* 1(19): 21-25.

Garcia, J.A., and Clark, C.R. 1976. *An Investigation of Annular Gas Flow Following Cement Operations.* SPE Symposium on Formation Damage Control, Houston, Texas, 29-30 January. SPE-5701-MS. http://dx.doi.org/10.2118/5701-MS.

Gomes, C.E.M., Ferreira, O.P., and Fernandes, M.R. 2005. *Influence of Vinyl Acetate-versatic Vinylester Copolymer on the Microstructural Characteristics of Cement Pastes*. Mat. Res. [online]. ISSN 1516-1439, 8(1): 51-56, http://www.scielo.br/pdf/mr/v8n1/a10v8n1.pdf [Accessed 18 November, 2014].

Gonzalo, V., Aiskely, B., and Alicia, C. 2001. *A Methodology to Evaluate the Gas Migration in Cement Slurries*. SPE Latin American and Caribbean Petroleum Engineering Conference, Rio de Janeiro, Brazil. 20-23 June. SPE-94901-MS. http://dx.doi.org/10.2118/94901-MS.

Goodwin, K.J. and Crook, R.J. 1992. Cement Sheath Stress Failure. *SPE Drill Eng* 7(4): 291-296. SPE-20453-PA. http://dx.doi.org/10.2118/20453-PA.

Harris, K.L. Ravi, K.M., King, D.S., Wilkinson, J.G., and Faul, R.R. 1990. *Verification of Slurry Response Number Evaluation Method for Gas Migration Control*. SPE Annual Technical Conference and Exhibition, New Orleans, Louisiana, 23-26 September. SPE-20450-MS. http://dx.doi.org/10.2118/20450-MS.

Harrison, S.S. 1985. Contamination of Aquifers by Overpressuring the Annulus of Oil and Gas Wells. *Ground Water* 23(3): 317-324.

Harton, J.J., Davies, D.R., and Stweart, R.B. 1983. An Integrated Approach for Successful Primary Cementations. *J Pet Technol* 35(9): 1600-1610. SPE-9599-PA. http://dx.doi.org/10.2118/9599-PA.

Hefley, W.E., Seydor, S.M., et al. 2011. *The Economic Impact of the Value Chain of a Marcellus Shale Well*. Katz Graduate School of Business, University of Pittsburgh. August. Available from: http://www.business.pitt.edu/faculty/papers/pittmarcellusshaleeconomics2011.pdf [Accessed 11 November, 2014].

Jackson, P.B. and Murphey, C.E. 1993. *Effect of Casing Pressure on Gas Flow through a Sheath of Set Cement*. 1993 SPE/IADC Drilling Conference, Amsterdam, 23-25 February. SPE/IADC 25698. http://dx.doi.org/10.2118/25698-MS.

Jones, R.R. and Carpenter, R.B. 1991. *New Latex, Expanding Thixotropic Cement Systems Improve Job Performance and Reduce Costs*. SPE International Symposium on Oilfield Chemistry, Anaheim, California, 20-22 February. SPE-21010-MS. http://dx.doi.org/10.2118/21010-MS.

Kada-Benameur, H., Wirquin, E., and Duthoit, B., 2000. Determination of Apparent Activation Energy of Concrete by Isothermal Calorimetry. *Cement and Concrete Research* 30(2): 301-305.

Kellingray, D. 2007. *Cementing Planning for success to ensure isolation for the life of the well*. SPE Distinguished Lecturer Series, *spe*. Available from: http://www.spe.org/dl/docs/2007/Kellingray.pdf [Accessed 18 November 2014].

Kolstad, E., Mozill, G., and Flores, J.C. 2004. Deepwater isolation, shallow-water flow hazards test cement in Marco Polo. *Offshore* 64(1): 76-80.

Kutchko, B.G. 2008. *Effect of CO_2 on the Integrity of Well Cement under Geologic Sequestration Conditions*. Ph.D. Dissertation, Carnegie Mallon University, Pittsburgh.

Labibzadeh, M., Zahabizadeh, B., and Khajehdezfuly, A. 2010. Early-age compressive strength assessment of oil well class G cement due to borehole pressure and temperature changes. *Journal of American Science* 6(7):38-47.

Levine, D.C., Thomas, E.W., Bezner, H.P., and Tolle, G.C. 1979. *Annular Gas Flow after Cementing: A Look at Practical Solutions*. SPE Annual Technical Conference and Exhibition, Las Vegas, Nevada, 23-26 September. SPE-8255-MS. http://dx.doi.org/10.2118/8255-MS.

McIntosh, J.D. 1949. Electric Curing of Concrete. *Magazine of Concrete Research* 1(1): 21-28.

Mindess, S., Young, J.F., and Darwin, D. 2003. *Concrete*. Edition: 2nd. ISBN10: 0130646326, ISBN13: 9780130646323. Prentice Hall, Pearson Education, Inc. Upper Saddle River, NJ 07458, USA.

Muehlenbachs, K. 2012. *Using Stable Isotope Geochemistry to Fingerprint Fugitive Gases from Hydraulically Fractured Wells.* Presented at Hydraulic Fracture Stimulation, Society & Environment, Canadian Society of Petroleum Geologists' Gussow Conference, Banff, Alberta, Canada, 7 November.

Mueller, D.T. 2002. *Redefining the Static Gel Strength Requirements for Cements Employed in SWF Mitigation*. Presented at Offshore Technology Conference, Houston, Texas, 6 May. OTC-14282-MS. http://dx.doi.org/10.4043/14282-MS.

Nelson, E.B. 1990. *Well Cementing*. First edition. Schlumberger Educational Services. ISBN 0-444-88751-2. Elsevier Science Publishers.

Newman, K., Wojtanowicz, A., and Gahan, B. 2001. Cement Pulsation Improves Gas Well Cementing. *World Oil* (July): 89-94.

Nixon, J.M., Schindler, A.K., Barnes, R.W., and Wade, S.A. 2008. *Evaluation of the Maturity Method to Estimate Concrete Strength in Field Applications*. ALDOT Research Project 930-590. February.

Nurse, R.W. 1949. Steam Curing of Concrete. *Magazine of Concrete Research* 1(2): 79-88.

OFI Testing Equipment, Inc. 2014a. *Static Gel Strength Measurement Device: Instruction Manual*. Ver.1.1, *ofite*, June 2014, Available from: http://www.ofite.com/instructions/120-53.pdf [Accessed 10 November 2014].

OFI Testing Equipment, Inc. 2014b. *Fluid Gas Migration Analyzer (#120-57)*. Available from: http://www.ofite.com/products/120-57.asp [Accessed 17 November, 2014].

Pane, I., and Hansen, W. 2002. Concrete Hydration and Mechanical Properties under Nonisothermal Conditions. *ACI Materials Journal* 99(6): 534-542.

Parcevaux, P. 1984. *Mechanisms of Gas Channeling During Primary Cementation-Methods for Prevention and Repair*. Chemische Produkte in der Erdolgewinnung, Clausthal-Zellerfeld, September 6.

Rapp P. 1935. *Effect of Calcium Chloride on Portland Cements and Concrete*. Reseach Paper 782. U.S. Depeartement of Commerce and National Bureau of Standards. Vol. 14: 499-517.

Richardson, N., Gottlieb, M., Krupnick, A., and Wiseman, H. 2013. *The State of State Shale Gas Regulation.* RFF Report. Resources for the Future. Available from: http://www.rff.org/rff/documents/RFF-Rpt-StateofStateRegs_Report.pdf [Accessed 5 April, 2015]

Pennsylvania Department of Environmental Protection. 2009. Stray Natural Gas Migration Associated with Oil and Gas Wells. Report-TAB10/28/2009, *PA DEP*, 28 October 2009. Available from: http://www.dep.state.pa.us/dep/subject/advcoun/oil_gas/2009/Stray%20Gas%20Migration%20Cases.pdf [Accessed 18 November, 2014].

Plank, J. 2014. Latex Dispersions. Personal page, *bauchemie-tum*. Available from: http://www.bauchemie-tum.de/master-framework/index.php?p=late&i=12&m=1&lang=en [Accessed 18 November, 2014].

Poole, J.L. 2007. *Modeling Temperature Sensitivity and Heat Evolution of Concrete*. Ph.D. Dissertation. The University of Texas at Austin. Austin, Texas, May.

Prohaska, M., Ogbe, D.O., and Economides, M.J. 1993. *Determining Wellbore Pressures in Cement Slurry Columns*. SPE Western Regional Meeting, Anchorage, Alaska, 26-28 May. SPE-26070-MS. http://dx.doi.org/10.2118/26070-MS.

Rae, P., Wilkins, D., and Free, D. 1989. *A New Approach to the Prediction of Gas Flow after Cementing*. SPE/IADC Drilling Conference held in New Orleans, Louisiana, 28 February- 3 March. SPE-18622-MS. http://dx.doi.org/10.2118/18622-MS.

Reese, S.O. Neboga, V.V., Pelepko, S., Kosmer, W.J., and Beattie, S. 2014. *Groundwater and petroleum resources of Sullivan County, Pennsylvania: Pennsylvania Geological Survey, 4th ser*. Water Resource Report 71, *PA DEP*, 2014. Available from: http://www.dcnr.state.pa.us/cs/groups/public/documents/document/dcnr_20029443.zip [Accessed 26 November, 2014].

Rößler, C. Eberhardt, A., Kučerová, H., and Möser, B. 2008. Influence of Hydration on the Fluidity of Normal Portland Cement Pastes. *Cement and Concrete Research* 38(7): 897-906.

Rocha, J.S., Calado, V., and Tavares, F. 2013. *Study of the Influence of Cement Slurry Composition in the Gas Migration*. OTC, Brasil, Rio de Janeiro, Brazil, 29-31 October. OTC-24420-MS. http://dx.doi.org/10.4043/24420-MS.

Roges, M.J., Dillenbeck, R.L., and Eid, R.N. 2004. *Transition Time of Cement Slurries, Definitions and Misconceptions, Related to Annular Fluid Migration*. SPE Annual Technical Conference and Exhibition, Houston, Texas, 26-29 September. SPE-90829-MS. http://dx.doi.org/10.2118/90829-MS.

Rowe, D. and Muehlenbachs, K. 1999. Isotopic Fingerprints of Shallow Gases in the Western Canadian Sedimentary Basin: Tools for Remediation of Leaking Heavy Oil Wells. *Organic Geochemistry* 30(8): 861-871.

Sabins, F.L., Tinsley, J.M., and Sutton, D.L. 1982. Transition Time of Cement Slurries between the Fluid and Set States. *SPE J.* 22(6): 875-882. SPE-9285-PA. http://dx.doi.org/10.2118/9285-PA.

Sabins, F.L. and Maki, V. 1999. *Acoustic Method for Determining the Static Gel Strength of a Cement Slurry*. US Patent No. US5992223A; International (PCT) Patent No. WO/1999/004254.

Sanjel Corporation. 2014. Fluid Migration Analyzer (FMA). Available from: http://www.sanjel.com/technologyinnovation/professionalpark/professionalpark-specialequipment.cfm [Accessed 19 November, 2014].

Saul, A.G.A. 1951. Principles Underlying of the Steam Curing of Concrete at Atmospheric Pressure. *Magazine of Concrete Research* 2(6): 127-140.

Schindler, A.K., and Folliard, K.J., 2005. Heat of Hydration Models for Cementitious Materials. *ACI Materials Journal* 102(1): 24-33.

Shenyang Taige Oil Equipment Co.Ltd. 2014. *Fluid (Gas) Migration Analyzer TG-7150*. Available from: http://www.everychina.com/buy/c-zba1e69/p-24117100-fluid_gas_migration_analyzer_tg_7150.html [Accessed 19 November, 2014].

Shiflet, N., Dion, M.O., and Flores, D.P. 2005. *A Practical Solution to Control Gas Migration*. AADE 2005 National Technical Conference and Exhibition, Houston, Texas, 5-7 April. AADE-05-NTCE-71.

Stewart, R.B. and Schouten, F.C. 1988. Gas Invasion and Migration in Cemented Annuli: Causes and Cures. *SPE Drill Eng* 3(1): 77-82. SPE-14779-PA. http://dx.doi.org/10.2118/14779-PA.

Stiles, D.A. 1997. *Successful Cementing in Areas Prone to Shallow Saltwater Flows in Deep-Water Gulf of Mexico.* Offshore Technology Conference, Houston, Texas, 5-8 May. OTC-8305-MS. http://dx.doi.org/10.4043/8305-MS.

Sutton, D.L., Sabins, F., and Faul, R. 1984a. Annular Gas Flow Theory and Prevention Methods Described. *Oil and Gas Journal* 82 (10 December): 84-92.

Sutton, D.L., Sabins, F., and Faul, R. 1984b. New Evaluation for Annular Gas-flow Potential. *Oil and Gas Journal* 82(51) (17 December): 109-112.

Sutton, D.L. and Ravi, K.M. 1989. *New Method for Determining Downhole Properties That Affect Gas Migration and Annular Sealing*. SPE Annual Technical Conference and Exhibition, San Antonio, Texas, 8-11 October. SPE-19520-MS. http://dx.doi.org/10.2118/19520-MS.

Sykes, R.L. and Logan, J.L. 1987. *New Technology in Gas Migration Control*. SPE Annual Technical Conference and Exhibition, Dallas, Texas, 27-30 September. SPE-16653-MS. http://dx.doi.org/10.2118/16653-MS.

Tilley, B. and Muehlenbachs, K. 2013. Isotope Reversals and Universal Stages and Trends of Gas Maturation in Sealed, Self-contained Petroleum Systems. *Chemical Geology* 339: 194-204.

Tinsley, J.M., Miller, E.C., Sabins, F.L., and Sutton, D.L. 1980. Study of Factors Causing Annular Gas Flow Following Primary Cementing. *J Pet Technol* 32(8):1427-1437. SPE-8257-PA. http://dx.doi.org/10.2118/8257-PA.

U.S. Environmental Protection Agency. 2011. *Investigation of Ground Water Contamination near Pavilion, Wyoming*. EPA600/R-00/000, December 2011. Available from: http://www2.epa.gov/sites/production/files/documents/EPA_ReportOnPavillion_Dec-8-2011.pdf [Accessed 18 November, 2014].

Willianms, H., Keese, R., Roy-Delage, S., Roye, J., Leach, D., Rottler, P., and Porcherie, O. 2012. *Flexible Technology*. Reprinted from July 2012. Oilfield Technology. Available from:

https://www.slb.com/~/media/Files/cementing/industry_articles/201208_ot_flexible_technology.pdf [Accessed 13 March, 2015]

Wojtanowicz, A.K., Nishikawa, S., and Rong, X. 2001. *Diagnosis and Remediation of Sustained Casing Pressing in Wells*. Final Report, Louisiana State University, Baton Rouge, Louisiana (July 31).

Wojtanowicz, A.K., Smith, J.R., Novakovic, D., Chimmalgi, V.S., Newman, K.R., Dusterhoft, D., and Gahan, B. 2002. *Cement Pulsation Treatment in Wells*. SPE Annual Technical Conference and Exhibition, San Antonio, Texas, 29 September-2 October. SPE-77752-MS. http://dx.doi.org/10.2118/77752-MS.

Zhang, J., Weissinger, E.A., Peethamparan, S., and Scherer, G.W. 2010. Early hydration and setting of oil well cement. *Cement and Concrete Research* 40(7): 1023-1033.

Zhang, X. 2002. *Study on Weightlessness Mechanisms of Slurry Suspension during Cement Gelation*. Ph.D. Dissertation. Southwest Petroleum University, Sichuan, China.

Zhou, D. and Wojtanowicz, A.K. 2000. *New Model of Pressure Reduction to Annulus During Primary Cementing*. IADC/SPE Drilling Conference, New Orleans, Louisiana, 23-25 February. SPE-59137-MS. http://dx.doi.org/10.2118/59137-MS.

Zhu, H. Lv, G., Liu, A., Xie C., and An, S. 2012. *Research on a New Method to Evaluate the Hydrostatic Pressure of Cement Slurries*. IADE/SPE Asia Pacific Drilling Technology Conference and Exhibition. Tianjin, China, 9-11 July. SPE-155923-MS. http://dx.doi.org/10.2118/155923-MS.